EXPERIMENTAL AND COMPUTATIONAL INVESTIGATIONS OF FORCE PREDICTION METHODOLOGY FROM FORCE BALANCES FOR SHORT DURATION APPLICATIONS

A Thesis Submitted in Partial Fulfillment of The Requirements for the Award of the Degree of

DOCTOR OF PHILOSOPHY

By

PALLEKONDA RAMESH BABU

(11610317)

DEPARTMENT OF MECHANICAL ENGINEERING

INDIAN INSTITUTE OF TECHNOLOGY GUWAHATI

GUWAHATI-781039, INDIA

JULY 2015

CERTIFICATE

This is to certify that the Thesis entitled **"Experimental and Computational Investigations of Force Prediction Methodology from Force Balances for Short Duration Applications**" submitted by **Pallekonda Ramesh Babu** (Roll No: 11610317), a research scholar in the Department of Mechanical Engineering, Indian Institute of Technology Guwahati, for the award of degree **Doctor of Philosophy** in Mechanical Engineering has been carried out under our supervision. The results embodied in this thesis are original and have not been submitted for the award of any other degree.

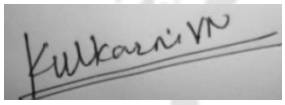

Dr. Vinayak N. Kulkarni
Associate Professor,
Department of Mechanical Engineering,
Indian Institute of Technology Guwahati,
India.

Dr. S.K Dwivedy
Professor,
Department of Mechanical Engineering,
Indian Institute of Technology Guwahati,
India.

July 2015

ACKNOWLEDGEMENTS

First and foremost of all I thank my Lord and Savior Jesus Christ for giving me eternal life and for his love and sacrifice and the Holy Spirit guidance throughout my course of time. I would like to make my sincere gratitude to my dear thesis supervisors and mentors, Dr. Vinayak N. Kulkarni and Dr. S. K. Dwivedy for their invaluable guidance, encouragement, support and their patience towards me during the tenure of my thesis work. I am blessed to have them as my supervisors.

My sincere acknowledgement goes to Prof. Anoop K. Dass and Prof. P. Mahanta and Prof. D. Chakraborty present and former Heads of Mechanical Engineering Department, IIT Guwahati. I thank them for their support from the initial to the final stages of my PhD work and for providing the facilities to carry out the same.

I am also indebted to the members of Doctoral Committee Dr. K. S. R. K. Murthy, Prof. Niranjan Sahoo, and Prof. H. B. Nemade for giving their valuable time and precious suggestions about critical issues related to my work.

I am also thankful to Dr. D.K Sharma and Prof. P.S Robi, and Dr. Pankaj Biswas for their cooperation during the fabrication of experimental models. I also thank technical superintend Mr. N.K Das and Jr. Technical superintend Mr. Chandan Banikya for their help during workshop related issues. I also thank workshop technicians especially Mr. U. Guhain, Mr. M. Sharma and Mr. D. Chetri for their help and patience in fabrication of the experimental models. Great full acknowledgement is made to all my well-wishers both faculty and students of Indian Institute of Technology Guwahati for their support, encouragement and critique.

I also express my gratitude to Dr. Viren Menezes, associate professor in Aerospace Engineering Department of Indian Institute of Technology Bombay for allowing me to conduct the experiments related to my thesis work in IITB-Shock tunnel and I also express my sincere thanks to Mr. Kiran Joy, Mr. Jadavji, Mr. Amol and Mr. Raghavendra for their help during my stay at IIT Bombay. I am thankful to Bro. Dinesh for providing accommodation and food during my stay at IITB. I also express my heartfelt thanks to Mr. Soumy Ranjan Nanda, for his help in the implementation of soft computing techniques and also in correction and proof reading of the thesis. I would also like to extend my sincere thanks to all my beloved seniors Dr. Ravi anna, Dr. Nagesh anna, Mr. Rajendra anna, Dr. Shekar anna, Dr. Agile brother for their support, encouragement and prayers which helped

me to work hard and to complete my PhD. I also express my thanks to juniors Mr. Divakar Bommana, Mr. Shivdayal, Mr. Ankit Dave, Mr. Rakesh Mr. Shuvayan, Mr. Sumith, Mr. Makhand Vyas, Nikhil Sharma, Siddesh Desai and Rohit Priyaul for their help during the tenure of my PhD. I also thank my dear brothers Mr. Gnana Praveen, Mr. Suresh, Mr. Srinu, Mr. Tharun, Mr. Bala Subramani, Mr. venu, Mr. Suresh anna, Mr. Arun, Mr. P.C. Lal, Mr. Kiran, Mr. Pradeep, Mr. Raja Shekar, Mr. Ravi and Mr. Joseph for their fellowship and help. I also express my sincere thanks to Sister G. Rajyalakshmi for her patience in proof reading and correction of the thesis.

I am in debited to Mr. Ravi and Mrs. Manemma my dear brother, sister and Maranatha for their open home during my health problem and always.

A special thanks to Daniel Brother, Haokip sir, Roy Sir, Pamu sir, Teiborlang L. Ryntathiang Sir and Bithiah madam for their support and prayers in the times of troubles and hardships.

My heartfelt thanks to my spiritual mother Mrs. Lidia Rajendraprasad for her daily prayers for me along with all the women fellowship in Andhra Evangelical Lutheran Church Patha Reddy Palem (Sthreela Samajam) members. I also thank my sisters Raji akka, Chinnakka, Vinodini akka, Aruna Jyothi akka, for all their guidance support and prayers. I also thank my home friends Koti, Murali, Kantha Rao, Subbarao, Nani and many other.

A special thanks to all my family members. Words cannot express how grateful I am to my Grandmother Pallekonda Samadhanam, Father Pallekonda Rajendra Prasad, and Mother Jyoti Kumari. I am in debited to my loving and caring brother Pallekonda Mahesh and Sister Nattala Sunitha and Mama Gera Samuel whose love and affection motivated and helped me this far. I am very much privileged to have loving and caring grandparents, Ammamma Gera Sampurnamma, Tathayya Gera Yesuratnam. Also Peddamma, Nattala Chinnimma, Akka Rekha and all my other family members for all of the sacrifices that you've made on my behalf. Your prayers for me was what sustained me thus far. I especially thank my Pedananna, Pallekonda Yesus Dasu, Pallekonda Babu Rao, Pallekonda Aseervadam, Pallekonda.Sunil Kumar (AGM, Vijaya Bank), Aruna Attai, Bhushanam Mamaiah, Vasanta Atattai, Ravi Mamaih Suman, Sushmitha, Kiran Anna and all other brothers and sisters for their support love and caring till this time.

I am indebted to my Sunil Pedananna and Suhasini Peddmma for their love and care in all my necessities and especially at the time of Gate coaching at Hyderabad. Finally I thank all my near and dear and whomever I missed by any chance.

I also convey my deepest gratitude to many other individuals with whom I have come into contact during my stay in IIT Guwahati. The friendship and unforgettable attachments shared with them has made my life pleasant. I extend my indebted gratitude towards the church, with whom I cherished my good times, for their support and encouraged in all my tough times and most of all their prayers for me and my project.

IIT Guwahati **PALLEKONDA RAMESH BABU**

July 13, 2015

Dedicated to My Lord and Savior **JESUS CHRIST**

For God loved the world so much that he gave his only Son (Jesus Christ), so that everyone who believes in Him may not die but have Eternal life.

(John: 3-16)

ABSTRACT

Force measurement is one of the vital areas of research, which is essential in the design of any mechanical or electromechanical systems. Due to lack of sophisticated testing and force prediction on the scaled models in the design phase, a lot of failures are encountered over the decades for various vehicles such as ships, rockets, airplanes, internal combustion engines etc. However in recent years, rate of failures of such kind were reduced due to the development in force measurement facilities and force measurement techniques. Force measurement in impulse facilities such as shock tunnel is one of the specialized area useful for the design of hypersonic vehicles. These measurements are sophisticated due to their short test duration. Computational techniques like Finite Element Method (FEM) and Computational Fluid Dynamics (CFD) are generally used before actual design of the system. Recently evolved fluid structure interaction (FSI) is one of the emerging computational tools for the analysis of fluid and solid domains simultaneously. Here, the surface forces obtained from the fluid simulations are transferred to the fluid solid interface for obtaining the response from the structural simulation. Since increasing mission complexities and advanced technologies demand more accurate assessments, the experimental force prediction strategies are preferred since they provide golden mean between the accuracy and the cost effectiveness. Therefore, ground based facilities are essential for the purpose of proper understanding of the physics of the flow and the associated aerodynamic parameters. Encouraging developments in the short duration facilities like conventional shock tunnel free piston shock tunnel etc. has posed challenges in measuring forces and moments during the experiments.

Two different techniques viz., accelerometer and stress wave based force balances are generally used for measurement of forces and moments in the high speed impulse (short duration) facilities. Therefore in the present work initial investigations deal with establishment of a non-intrusive force measurement technique using laser and development of the associated experimental set-up. This technique is then assessed with the well-established contemporary techniques for the step and impulse loading.

Accelerometer force balance has been used by various researchers for force measurement in shock tunnel testing with the assumption of free-flying condition. Finite element modeling is carried out for one of the literature reported test model to evaluate the

resistance offered by the rubber during the experimental test time. These studies show that the effective test time decreases with increase in the angle of attack due to increase in resistance of the rubber. These studies are also found useful to demonstrate the use of computational techniques in developing the force balance for a given test model.

Accelerometer based force balances are seen to be directly used for force measurement as seen in the literatures. At the same time stress wave force balances are involved with detailed calibration procedure based on de-convolution technique. Therefore, present investigations are carried out to assess the use of soft computing techniques viz. Neural Network (NN) and Artificial Neuro-Fuzzy Inference System (ANFIS). An ANFIS based methodology is found to be more precise to predict the forces and moments in comparison with the NN based methodology. In view of this parametric studies are initiated to explore the use of best algorithm in ANFIS for prediction of forces and moments.

Shock tunnel tests are then performed on a hemispherical test model for force measurement using accelerometer balance. These experiments are carried out in the Shock Tunnel at Indian Institute of Technology, Bombay, India (IITB-ST) in order to justify the use of soft computing techniques for actual experiments in impulse facilities. In view of this calibration tests are carried out to train the ANFIS based algorithm using known impulse force and accelerations signals. Acceleration signals obtained from the shock tunnel tests are then used to recover the force. It has been observed that the ANFIS based prediction of aerodynamic coefficients has encouraging match with the prediction of same using accelerometer force balance theory.

LIST OF FIGURES

LIST OF TABLES

ABBREVIATIONS

ALE	Arbitrary Lagrangian-Eulerian
AGARD	Advisory Group for Aeronautical Research and Development
ANFIS	Artificial Neuro Fuzzy Inference System.
BPNN	Back Propagation Neural Network
CFD	Computational Fluid Dynamics
DSMC-IP	Direct Simulation Monte Carlo-Information Preservation
FE or FEM	Finite Element Method
FSI	Fluid Structure Interaction
FIS	Fuzzy Inference System
FL	Fuzzy Logic
GA	Genetic Algorithm
ANFIS-GRID	Grid Partition Based ANFIS
HST 2	Hypersonic Shock Tunnel -2, at Indian institute of Science (IISC), Bangalore, India
IITB-ST	Indian Institute of Technology Bombay, Shock Tunnel
IMT	Interval Modelling Technique
NASA	National Aeronautics and Space Administration
NN	Neural Network
RBFN	Radial Basis Function Network
SWFVS- NS	Steger-Warming Flux Vector Splitting Navier Stokes solver
ANFIS-SUB	Sub Clustering Based ANFIS
TCR	Temperature coefficient of resistance

NOMENCLATURE

α	Angle of attack
θ_2	Final angle of the string with reference axis after impacting with the model
θ_1	Initial angle of string with reference axis
w	Weights in the layers of neural network
*	Convolution Operator
C	Coefficient
D	Diameter (m)
E	Center of pressure
E	Young's modulus (GPa)
F	Force (N)
G	Gain
L	Length (m)
M	Mach Number
M	Mass (kg)
P	Pressure (Pa)
R	Resistance (ohm)
r^2	Goodness of fit
Re	Reynolds Number
T	Temperature (K)
X,Y,Z	Cartesian coordinate system
P	Density (kg/m^3)
Y	Poisson's Ratio

SUB SCRIPT

d	Drag
l	Lift
m	Moment
∞	Free stream quantities
0	Stagnation quantities

TABLE OF CONTENTS

CHAPTER 1

INTRODUCTION

Overview

Hypersonic speed range is generally marked above five times the local speed of sound. While traveling with such high speed, space re-entry or launch vehicles experience high drag force and high surface temperatures. Therefore precautionary measures must be taken while designing the shape of the hypersonic vehicles in order to sustain it in that environment. In view of this, ground based tests are conducted on the scaled models before the actual flight tests. Various measurement techniques are established to measure the aerodynamic coefficients among which stress wave force balance and accelerometer force balance are most prominently used. Therefore, the present investigation deals with the development of a non-intrusive force measurement technique and assessment of the same with contemporary force balance for its use in the short duration impulse test facilities. Apart from this, use of computational techniques for the design of a force balance is also a part of the present study. Application of soft computing techniques for the recovery of short duration forces and implementation of the same for the actual shock tunnel tests is also explored herein. Therefore, present chapter provides detailed literature review about various force measurement techniques, calibration methods of force balances and soft computing techniques. The motivation and the objectives of the present research work are reported based on the reviewed literature and the thesis organization is also highlighted at the end of this chapter.

1.1 History of Flight Design

The desire of flying was conceived mainly from the bird and the insect flights. In the initial attempt some researchers tried to fly by using wings attached to the human hands which lead to many failures. Flapping wings were then attempted to generate the lift. Such vehicles are called as ornithopers and drawing of these vehicles made by Leonardo da Vinci are also available. Later in 1782 Montgolfier brothers viz. Joseph and Etienne observed fire and thought of hot air entrapped can be used to lift the structure carrying man. Several trials of flights are carried out using balloon carrying a cock, sheep and duck. On November 20th of 1783, Montgolfier brothers succeeded in lifting a human out of the ground using a balloon for a considerable amount of time in the sky. Later French Physicist J.A.C Charles used balloons filled with hydrogen from Tuileries Gardens in Paris on 1st December 1783. All these things are discussed in Anderson (2005).

Sir George Cayley is considered as the father of modern airplane. After many helicopter tests for about 10 years, he introduced the concept of fixed wing for creating the low pressure below the wing for lift generation. Discretization of components for generation of lift and thrust is the major achievement. He had put separate components for the thrust, lift and stability. In 1799 Sir Cayley inscribed the idea of fixed wing on a silver coin. In 1804 he designed a whirling arm for testing of the airfoil, which consists of a lifting airfoil mounted at the end of long rod. The rod was rotated at high speed to generate the lift. It was an important contribution to the airplane industry in those early years of development for measurement of the force and the center of pressure. Cayley's experimental results are available in one of the best documents titled as "On Aerial Navigation" by Cayley (1810). Here the principle of flight, separation of propulsion, lift and the uses of a fixed wing have been explained. In the same time, another person named W.L. Heanson designed a flight based on the same concept of fixed wing running with the steam engine with two propellers, named as aerial steam turbine. Finally in 1903 a great leap in the airplane design had been noticed when Wright brothers demonstrated the first heavier than air flight (Anderson (2005)). This was the first human transport airplane in the history and the dream of the man to fly high in the sky became true. Rapid progress in the flight vehicle design has made possible to cross the sound barrier and enter in to the hypersonic or hypervelocity flow regime. This advancement is integrated with the safety of the flight and hence prior

measurement of aerodynamic coefficients has always been done. Albeit the challenges ahead the researchers working in the flow regime, successful designs of hypersonic vehicles and associated design data are available in the literature.

1.2 Introduction to Hypersonic Test Facilities

Reusable space planes, launch vehicles and the missiles encounter very high speed flow regime. Different analytical solutions and empirical correlations were developed for the estimation of different aerodynamic coefficients or parameters during the early stages of space missions of these space vehicles. However, increasing mission complexities and advanced technologies demand more accurate assessments. Computational techniques can be used to get the estimation of these flight parameters. Moreover, further development or advancement is required in these techniques for implementation in actual flight simulations. Therefore, ground based facilities are essential for the purpose of proper understanding of the physics of the flow and associated aerodynamic parameters.

One of the commonly used facilities for subsonic and supersonic applications is the wind tunnel. Different wind tunnels have been established all over the world for the simulation of fluid flow in the regime of subsonic or supersonic flow. However the associated cost for the experimentation increases with increase in velocity of the flow. Therefore, use of conventional wind tunnels is impossible for the simulation of flow over missile or launch vehicle.

Encouraging developments in short duration facilities in recent decades have opened a new option for simulation of hypersonic flows. The shock tunnel, an impulse facility, may be used to create steady hypersonic flow of high energy content. Typical conventional shock tunnel is comprised of a driver and driven section along with the nozzle, test section and dump tank. Experimental simulation test time for the presently considered shock tunnel is in the range of 1-5 milliseconds. Hence this is called as an impulse facility. Development of free piston driven shock tunnel is the recent advancement in the field of shock tunnels. This test facility can be used to test external or internal flows at orbital speeds to assist the space programs. Required heating of the driver gas for obtaining high energy flows is achieved here through momentum of the piston. Typical free piston driven shock tunnel is comprised of a high pressure reservoir, piston, compression tube, driven tube, nozzle, test section and dump tank. Experimental duration in a standard free piston driven shock tunnel is in the same range as that of the conventional shock tunnel.

Assembled photograph of a conventional type shock tunnel operating on the reflected mode established in the Aerospace Engineering Department of Indian Institute of Technology, Bombay, India (IITB) with all the components is shown in Fig.1.1.

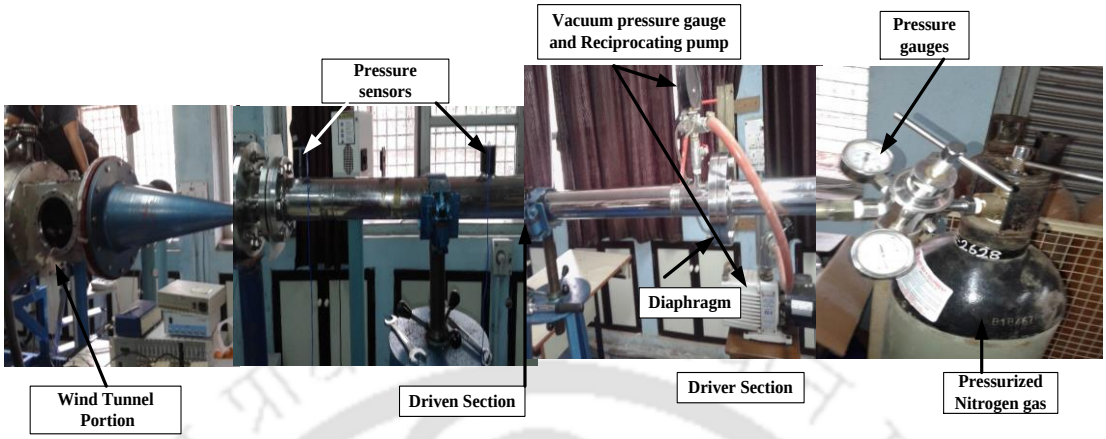

Figure 1.1: Photograph of a conventional type reflected mode Shock Tunnel (Shock tunnel laboratory, IIT Bombay, India).

Various measurements like pressure, heat transfer rate, force etc. are possible in these short duration test facilities. Very low test time is the constraint in devising the allied instrumentation. Hence fast response sensors along with the sophisticated instrumentation define the need of shock tunnel testing.

1.3 Force Balances for Impulse Facilities

Force measurements in ground-based test facilities are of major interest to the designers of hypersonic flight vehicles. Accurate experimental results of fundamental aerodynamic forces are essential for predicting the vehicle performance (stability and control). Force measurements in impulse hypersonic facilities is a challenging task and was very difficult in the past because of the unavailability of the proper fast responsive sensors. Due to availability of the fast response gauges in the present times it became easy to conduct impulse tests. The general sensors or instruments used in the force and moment measurements are the strain gauges, foil gauges, accelerometers and pizo-film sensors. The measurement of aerodynamic forces on models in hypersonic impulse facilities has been restricted in the past because of the time it takes for the test model to reach a state of force equilibrium with its support mechanisms. Researchers have proposed various force measurement techniques for the short duration test facilities which are classified based on

the principle of operation of the technique such as inertia dominated and the stiffness dominated techniques.

1.3.1 Stress wave force balance

Stress wave force balance technique was first proposed by Simmons and Sanderson (1991) in University of Queensland, Australia. This principle accepts the fact that no steady state is achieved during the test flow duration. When the aerodynamic load is suddenly applied to the model, stress waves are initiated within the model. These waves propagate along a stress bar attached to its end, called sting and reflect within the model and its support structure. Using system identifications and inverse convolution techniques in the system dynamic analysis, it is possible to determine time history of aerodynamic forces.

The linear mathematical model is considered as a simple open control system, with force applied being the input and strain response being the output. The function that converts input (force) to output (strain) is called transfer function of the given model. One dimensional wave theory is used to estimate the response times of the model to the stress wave. The schematic diagram of the typical stress wave force balance is shown Fig 1.3. It consists of the conical model, attached with a support structure on which sensors are mounted and this whole structure is suspended freely using the flexible wires from a rigid support.

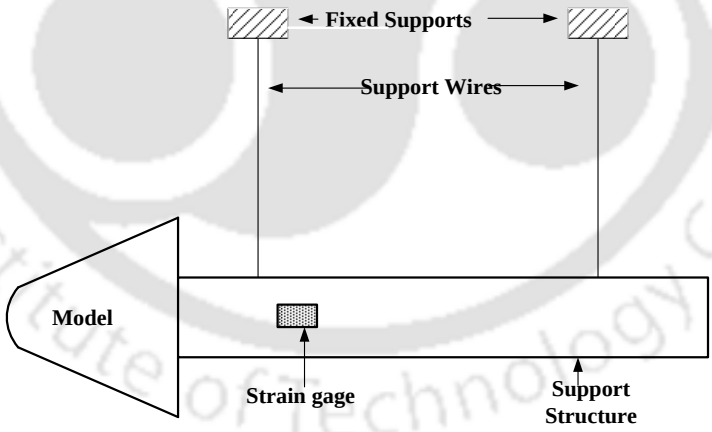

Figure 1.2: Schematic diagram of a stress wave force balance.

1.3.2 Stress wave force balance vs strain gage balance

The basic principle in a stress wave force balance, which is used in the short duration impulse facilities, is that the steady state is never achieved in the test duration. Measurements are to be taken in the transient time period itself. A strain gage balance is used in cases where the test time durations are higher, and the measurements are taken only after the steady state has been achieved. Though strain gages are used in both types of force

balances, it is the duration of test time and the measurement technique differentiate the class of the balances. Strain gages used in the stress wave force balance should have a very short response time of the order of a few microseconds, as the entire testing get over in a few milliseconds. From the literature by Tuttle and Simmons (1992) it is confirmed that for the full sized models stiffness dominated balance test times are greater than 200 ms and in the case of the inertia dominated balance the test times are less than 10 ms. In general, metal foil gages are used in strain gauge balance which measures the steady state strain. In case of stress wave force balance, the semiconductor strain gages are mostly preferred due to their sharp response time as discussed by Kozub and Tinyakov (1970).

1.3.3 Literature review on stress wave force balances

In case of stiffness dominated force balance for impulse facilities, the model is attached to the balance system through the beam elements where strain gauges are located, due to the applied forces on the model, stress waves are initiated and propagate through the model and beam elements as discussed by Strokmann et al. (1998) and Carbonara (1993). Depending on the intensity of force applied on the model, strain gages pasted on the beam delivers strain signal through the wheat-stone bridge circuit integrated with the strain gages. Jessen and Gronig (1989) designed a combined high stiffness and low inertia balance and strain gauges were used for measuring the strains on a six component balance.

A single component stress wave force balance was designed and tested for short duration test facilities by Tuttle et al. (1995), using a long axisymmetric model with semi cone angle of 5^0, the length of the model is 425 mm and the mass of the model is 1.71 kg. The model was checked for the feasibility of the configuration with the theoretical values and are found satisfactory for a time duration of 1 ms. From this analysis it was confirmed that the model length has no significance on drag measurement and the model can be used without prior knowledge of type of load application and an accuracy of 95% was observed from the comparison of theoretical and experimental results. It is also proposed that more than one millisecond time duration tests can be conducted by decreasing the number of reflections of the stress waves from the model to the strain gauge location. Better results are obtained in the experiment when the impulse response is obtained by differentiating the output response due to step load.

Abdel-Jawad et al. (2007) designed a calibration technique for a multi-component force balance and tested it for three component stress wave force balance. The impulse response has been obtained from the load distribution on the configuration using tensorial superposition of the impulse response which is similar to the vectorial superposition of the

impulse load. The tests were carried out on a small scaled model of Mars pathfinder and the responses are found out using the de-convolution technique from the experiment. Impulse response sub matrices for axial force, normal force and pure moment are obtained and assembled as a matrix to obtain the input force or moments at any location on the configuration using the impulse response matrix and the output response.

Porter et al. (1994) carried out experimental analysis for checking the effect of bluntness by conducting the shock tunnel test on a blunt cone model of 5^0 semi cone angle with base radius of 50 mm. They used eleven different tips of impact hammer with different radii varying from 0.2 to 18 mm in steps of 1.8 mm and the bluntness ratio (ratio of nose radius to the base cone radius) vary from 4 mm to 360 mm in steps of 36 mm. The length of the model with pointed tip is 517.5 mm, a stress bar of length 2.3 m made of brass is attached to the model and the configuration is suspended horizontally to test in the shock tunnel. Strain gauges are attached to the stress bar to measure transient strain. These tests were conducted and the theoretical calculations have been made to find the system response using de-convolution technique.

Simmons and Sanderson (1991) proposed a technique for drag measurement on a hypervelocity impulse facility having 100 μs rise time on a non-lifting model in a free piston shock tunnel. Interpretation of stress wave propagation in the model and stress bar attached to it is also carried-out and the mean square estimate of the aerodynamic load history on the model is predicted by using finite element and spectral methods. These tests have been conducted on a blunt cone model with 15^0 semi cone angle in a flow of 5.6 Mach number and stagnation enthalpies of 2.6 to 33 MJ/kg. Strain-gauges are used to measure the response of the stress waves travelled from the model till the end of the stress bar, forces are predicted from the strain gauge response. The impulse response function $g(t)$ is computed to predict the unknown drag force applied on the model.

Sahoo et al. (2005) used two force measuring techniques viz. accelerometer balance and stress wave force balance and compared simultaneously during the force measurement on a 30^0 blunt cone model with base diameter 70 mm, the model was fabricated by aluminum material and is attached with the brass stress bar of length 555 mm. It was tested in a hypersonic shock tunnel HST-2 shock tunnel in IISC Bangalore, India, to measure the drag force on the model with test duration of 450 μs and the obtained experimental values are compared with theoretical values and Newton's second law is also satisfied during the experiment.

Robinson et al. (2006) used three component stress wave force balance to measure drag, lift and pitching-moment on a supersonic combustion ramjet in the T4 free-piston shock tunnel. The length of the scramjet model is 567 mm, the mass of the model is 5 kg, and the combustion takes place at the enthalpy of 3.3 MJ/kg at nozzle supply pressure of 32 MPa. At Mach 6.6 for equivalence ratio of 1.4, the force coefficients varies linearly with the equivalence ratio. Lift and pitching moments are constant when the nozzle-supply enthalpy increased to 4.9 MJ/kg at equivalence ratio of 0.8, the drag coefficient is reduced drastically when nozzle supply pressure was reduced and at the enthalpy of 3.3 MJ/kg. The lift and drag force are predicted from the known output responses by using de-convolution techniques and the results are found to be in good agreement but the pitching moment was not predicted correctly.

Robinson et al. (2004) performed transient finite element analysis to compare the performance of a stress wave force balance for measuring the thrust, lift and pitching moment on a large scramjet model. The model indicates good decoupling of the output signal and low sensitivity of the model to signal. The load distribution on the model can be obtained through a three-bar balance. The balance was calibrated by applying number of point loads on the model. Experimental and finite element results are obtained nearly same. Force measurements was made on the model with and without fuel injection and the predicted loads are compared with the measured loads using simple models of the scramjet and combustion but the signals obtained are with low magnitude and low frequency disturbance because of the vibration. Hence from this analysis it is suggested that the vibration isolation is necessary for obtaining the accurate results.

Smith and Mee (1996) used piezoelectric polymers to measure the intensity of stress wave travel or transient strain in the Split-Hopkinson pressure bar which consists of an incident bar and a striker bar. The striker bar is made of steel material and the incident bar with aluminum. Here Polyvinylidene fluoride piezoelectric material which is useful particularly for dynamic strain sensing is used. These are also having the properties like light weight, flexible, high sensitivity, low dependence on the temperature and can be mounted easily on any material (electrically conductive or non-conductive). The piezo film was mounted on the incident bar and the surface of the stressed component and the piezo film form the electrodes of the gauge.

Stalker et al. (2005) performed the measurements of the drag and thrust force on a scramjet model which is mounted in a shock tunnel at various stagnation enthalpies. The thrust on the model decreased with increase of the stagnation enthalpy above 3 MJ/kg, this

happened because of the increase of the pre-combustion temperature with increase of the stagnation enthalpy. Experiments are conducted to increase the thrust by increasing the fuel supply or by reducing the stagnation enthalpy.

Robinson et al (2011) designed and implemented an internal stress wave force balance in a shock tunnel. The forces are measured in the order of milliseconds for the blunt cone model of 303 mm height and 10^0 semi cone angle with an accuracy of ± 6%. CFD predictions for the above experiments indicated the success of the three component force balance.

Mee (2003) proposed four different dynamic calibration techniques for the stress wave force balances for impulse hypersonic facilities. Here de-convolution technique has been used for predicting the unknown aerodynamic forces. It is shown that the response derived from the force balance test, in which the model and the stress bar are suspended from a fine wire-cut, agree with impulse response derived from calibration made using an impact hammer. The suitability of the balance for measuring the dynamic forces is demonstrated by showing the drag force on a model that follows the history of Pitot pressure in the test section.

Kozub and Tinyakov (1970) also explained the importance of measurement and recording of small linear and angular displacements using semiconductor strain gauges at higher degree accuracy for applications like fundamental studies of mechanical properties of materials.

Anderson (1997) studied the importance of Wheatstone bridge in the current and the voltage measurements using strain gauge for diagnosing the circuit connections with its merits and demerits has been discussed in NASA's new current loop. This method of instrumentation provides larger and linear output and can be simply implemented using measurement circuit topology. Abramchuk et al. (1977) explained the characteristics of semiconductor strain gauges in strain measurement and the advantages of strain gauges over the foil gauges.

Two multichannel sequential automated systems for strain gauge data readings were examined by Cappa (1990). Different techniques for measuring and recording of the strain are explained with different components in the automated monitoring system. It is concluded that a simple and low-cost automated strain measurement based on non-specialized scanner units, can be used for long term strain measurements when temperature variations are within 40^0C.

Dem'yan et al. (2000) created a resistance strain gauge on the basis of thread like semiconductor mono crystals of selenium and tellurium. They investigated their deformation characteristics under tension and compression in uniaxial direction (up to $\pm\ 2.6\times10^{-3}$). They developed electric contacts for selenium crystals and concluded that the resistance strain gauges are promising for investigation of composite materials under uniaxial tension.

A strain gauge designed by Grogery and Quing (2001), consists of a thin film made of ceramic material for measurement up to 1400^0C. These thin film sensors are very much useful in situ strain measurement in harsh environment such as gas turbines engines. The large band gap semiconductor used as active strain elements in these devices exhibited a large temperature coefficient of resistance (TCR) for reducing the apparent strain or thermally induced strain.

1.3.4 Accelerometer force balance

In accelerometer force balance system transient acceleration of the model during the test time of the impulse facility is measured using an accelerometer. The force applied on the free flying model is obtained directly from the measurement of acceleration. The spring-mass system based analysis is carried out for the recovery of force signal from the experimentally obtained acceleration. Different type of Accelerometer force balance exists viz. single component and multi component. The schematic of the single component accelerometer force balance is shown in Fig. 1.3. It consists of a model attached with a stress bar suspended freely from the fixed support using the flexible wires. The axial acceleration is measured along the longitudinal axis of the model.

The three component accelerometer force balance is useful for the force measurement in axial and normal direction along with the moment about azimuthal axis using the accelerometer balances. It can be used in the shock tunnel test for force measurement, using stiff springs or rubber bushes for supporting the model. However, free flying condition is generally achieved using rubbers as a distributed flexible support. The resistance offered by the rubber during the test time is assumed to be negligible during the short test time. The rubber material is chosen in such a way that it is flexible enough to support the model in the test section of the shock tunnel at the same time it does not decrease the mean amplitude of the acceleration. Typical arrangement of three component accelerometer force balance is as shown in Fig. 1.4.

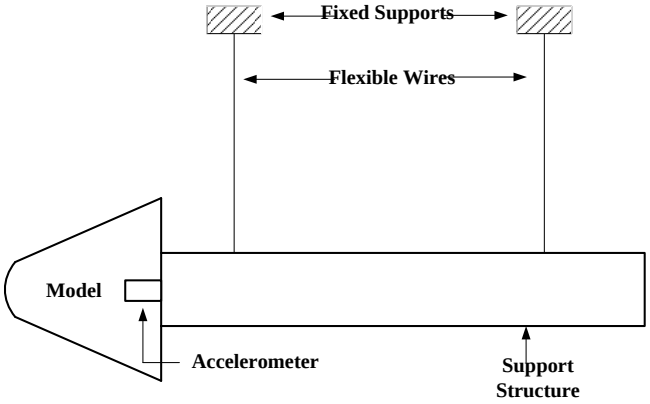

Figure 1.3: Schematic diagram of a single component accelerometer force balance (Mee (2003)).

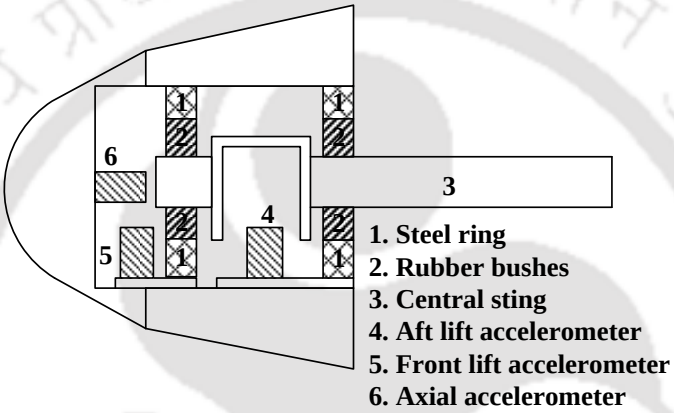

Figure 1.4: A 60^0 apex-angle blunt cone model with 15^0 flare fitted with a three-component accelerometer balance system. Sahoo et al. (2003).

1.3.5 Literature on non-contact type force measurement

The force measurement in the wind tunnel has been implemented and tested using a non-contact type force measurement method using a image tracking based cinematography technique by Laurenece and Karl (2010), where the motion of a free flying model has been tracked. The accuracy of this technique has been analyzed using experimental, artificially generated images. These images are analyzed by using the lease square technique resulted in the improvement of the accuracy of the method.

Experimentally the surface displacement has been measured by Chen et al. (2007) using the laser vibrmeter. Calibration has been performed with the help of a known amplitude and frequency of the sound wave and the laser was able to represent the wave characteristics well. It showed that the laser can be used as one of the measuring instrument for obtaining the characteristics of the system under the force application.

High speed shadowgraph has been used by Laurence et al. (2007) for the measurement of the force and moments on a capsule body tested in a high speed shock

tunnel Gottingen (HEG) in which the results showed good agreement. The model is attached with a weak strings which allows it to have free flying motion. Also the accelerometers and the visualization based techniques are used for the measurement of the forces and moments on the model. While measuring the pitching moment the visualization based techniques are better compared with the accelerometer based measurement.

A complex hypersonic ram jet engine has been modelled and fabricated by Hannemann et al. (2015) to increase the combustion performance in a 1.5 m long supersonic combustion ramjet (scramjet) (scram jet) engine is used and tested for the force measurement in a shock tunnel. The tests are performed at Mach 7.4 at an altitude of 28 km along with the simulations. The experimental displacements measured using the non-contact type optical tracking technique are compared with the simulated one and the results are found to be accurate using both the methods.

1.3.6 Literature review on accelerometer force balance

Vidal (1956) first designed and implemented accelerometer balance in a shock tunnel test and obtained the force from the acceleration measured on the model which is suspended with the help of flexible wires. This configuration is considered as the unrestrained configuration in the flow passing time and it was tested with accelerometers of different sensitivities.

A free flying technique is developed by Naumann et al. (1991) and Naumann et al. (1993) for measuring the acceleration directly by releasing the model during test flow. In this both free flying and fixed configuration techniques are involved, a fast acting mounting support releases the model just before onset of the flow and grips it again after free flying signal is obtained (1-2 ms test time).

Holden (1985), and Ioth et al. (2001) studied the effects of vibration on a model subjected to forces in different orientations like bending moment and pitching moment are compensated by measuring acceleration at different locations on the model.

Sahoo et al. (2007) carried out three dimensional FE analysis on a accelerometer based balance system which used rubber bushes to support the model during the test flow duration. In this case a blunt nosed triangle plate model comprising of rubber bushes and steel rings has been considered for analysis. Study of effect of rubber stiffness on axial acceleration showed that the rubber with Young's modulus (E) of 0.3 to 30 MPa is ideal for 1 ms test duration. Measured acceleration in axial direction is compared with FE results.

A free flying accelerometer balance mounted internally on frictionless rollers, is designed to measure the drag force on a blunt nosed flat plate in Indian Institute of Science,

Bangalore, India (IISc Bangalore) hyper shock tunnel by Joarder and Jagadeesh (2004). The roller and the model moves on one another and there is point contact between model and the slide, the slide is fixed at the top and the model moves on the rollers during the flow duration, accelerometer is mounted along the axis to measure the axial acceleration and three dimensional finite element method was used to compare the performance of the accelerometer balance system with the experiment.

Measurement of shock events by means of strain gauges and accelerometers were performed by Knapp et al. (1998). The investigation concerned about different kinds of strain gauges and accelerometers available for high frequency shock environment application. The Hopkinson bar was designed for two different types of waves; one for longitudinal mono mode pulse wave (mainly for calibration) and the other with a longitudinal/radial multimode (for operational tests). It was concluded that strain gauges were well suited as versatile sensors for shock tests compared to that of accelerometers.

A new three component accelerometer balance was designed and tested in the hypersonic shock tunnel (HST2) of Indian Institute of Science. The configuration measures the aerodynamic forces on the model for 1 millisecond, the model is tested with the angle of attack from 0 to 12^0 by Saravanan et al. (2009). Two models viz. one with blunt cone model with after body and blunt cone with after body and frustum are used for the calibration of the sensors with a constant Mach number of 8 and the enthalpy of 2MJ/kg.

The flow fields around model are obtained using a 3D-axisymmetric Navier-Stoke solver and the simulated results are compared with the experimental results. The accuracy of the balance was estimated with the Newtonian theory and the values are ± 10% for the axial component and ± 8 for normal and pitching moments.

Trivedi and Menezes (2011) demonstrated the shock tunnel experimental analysis at a free stream Mach number of 8 to quantify lift, drag, and yawing moment using accelerometer balance on a blunt nosed triangular plate model attached with flaps. The model was tested under different angle of attack (AOA) by considering air as test gas and nitrogen as driver gas, the test time duration is about 1.2 ms. Coefficient of drag, lift and yawing moment for less AOA are found to be in good agreement with the theoretical value but marginal deviation is found for higher AOA due to the viscous effect and flow separation.

Later a similar investigation has been performed by Menezes and Trivedy (2011) for six component force balance in two steps, a blunt-nosed, triangular lifting body with soft suspension system is tested in a hypersonic shock tunnel (IITB-ST) at free stream Mach

number of 8 in the first case with different angle of attack to measure drag, lift, and roll using an accelerometer force balance. The results obtained for coefficient of drag, roll, and lift from Newtonian theory is in good match with the experimental result till an AOA of 10^0 and slightly deviated for increased AOA because of flow separation for coefficient of lift, viscous effect enhancement for coefficient of drag, and detached shock effect for coefficient of roll.

An accelerometer force balance was investigated by Trivedi and Menezes (2012) on a blunt triangular model in a hypersonic shock tunnel, IITB-ST at Mach 8 for an average test time of 800-1000 μs. Yawing moment, pitching moment, and side force are measured in the present analysis. Rubber bushes are used to ensure free flying condition of the model. Newtonian theory along with pressure measurements by the high frequency pressure transducers are used for moments and the force calculations theoretically to validate the experimental results at different angle of attack. It has been observed that the experimental coefficient of yawing moment and side force deviate in magnitude from theoretical results at higher angle of attack as the theoretical approach does not consider flow physics like flow separation and strong shock effect which results during larger angle of attack.

1.4 Calibration Methods of Force Balances

In transient force measurement, initial set-up of stress waves in the test model leads to unsteady state force equilibrium. Hence calibration of the force balance becomes essential for deriving the system characteristics through impulse response function or transfer function. The system dynamics can be understood by conducting the calibration tests using the model and the stress bar suspended freely using the flexible steel wires. The unknown impulse load applied on the model can be predicted by measuring the strain or accelerometer response. These calibration tests can be conducted for stress wave as well as accelerometer force balance.

Two different types of stress wave force balance calibration tests viz., cut-wire test and pulse test are proposed and implemented by Mee (2003). The transfer function was obtained by applying the step load and impulse load.

1. Cut wire test (for step load): An approximate step load can be applied on the model in two ways viz. horizontal and vertical calibration. Model with stress bar arrangement, using a fine wire hung over a pulley for horizontal calibration is as shown in Fig. 1.5. The load gets applied when the fine wire is cut instantaneously. In this case, the end of the model needs to be supported, so that free body motion of the body does not occur when the load is applied

via the fine wire. There are two possible arrangements for vertical calibration, which are as shown in Fig. 1.6.

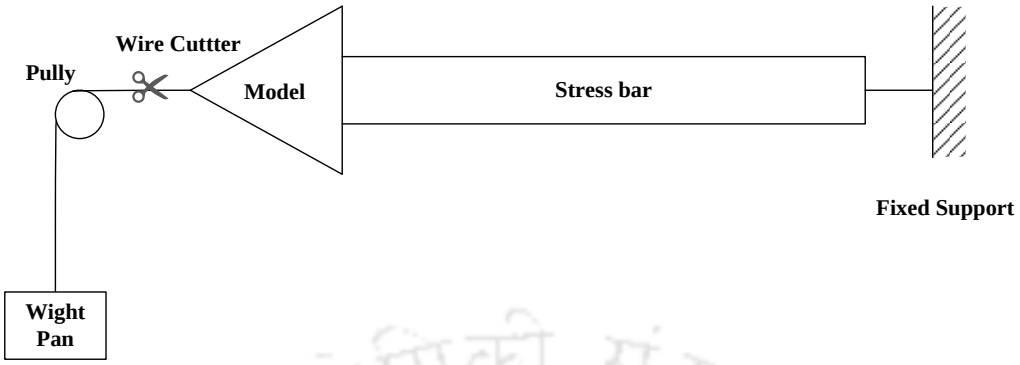

Figure 1.5: Schematic diagram of horizontal calibration for step load.

In the first case as shown in Fig. 1.5, a known mass is suspended by a wire from the model which is held axially. The wire has to be cut close to the model. The effectiveness of the applied load depends on closeness of the cutting location to the model and also on sharpness of the cut. In the second case shown in Fig 1.6 (a), the model is suspended vertically, with the end of the stress bar suspended by a fine wire with a known mass attached to the end of the model.

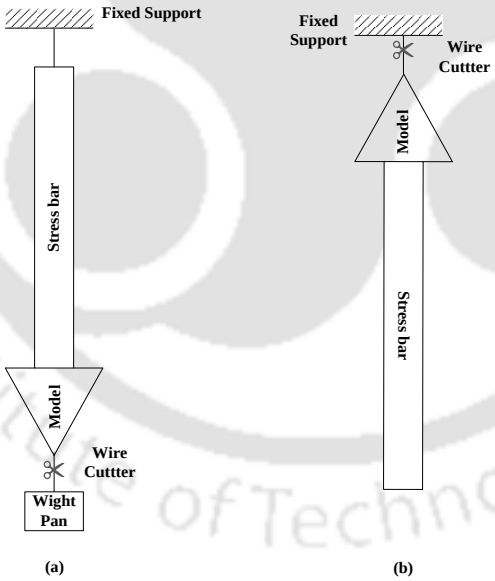

Figure 1.6: Schematic diagram of (a) Vertical calibration (b) Free end Calibration.

In both the horizontal and vertical calibration test, the stress bar has to be suspended from its end. This limits the signal collection time and the time taken by the stress wave to travel from the model tip, through the stress bar and reflect back to the point of strain

measurement. For a typical 300 mm long aluminum model and a 2 m brass stress bar, this time was found to be around 1.15 ms. This can be avoided with an arrangement as shown in Fig 1.6 (b). This type of arrangement is known as free end calibration where the model is suspended vertically from a rigid support by attaching the wire at the tip of the model. However the load applied on the model is fixed in this case.

2. Pulse test (for impulse load): Obtaining a perfect impulse load is not possible in practice. However, a short or a sharp impulse can be applied to produce essentially the same response as that of a perfect impulse. Here, the shape of the applied impulse is important. If the time period of application of impulse is small in comparison with the characteristic time of the system, then the shape of the impulse does not affect the impulse response. If the area under the impulse curve is large, then the shape of the pulse also affects the impulse response.

   One method of obtaining a true impulse function is by striking the model with an impactor. In Fig. 1.7, the impactor is shown as a hammer. It is programmed to record the time history of the applied impulse loading.

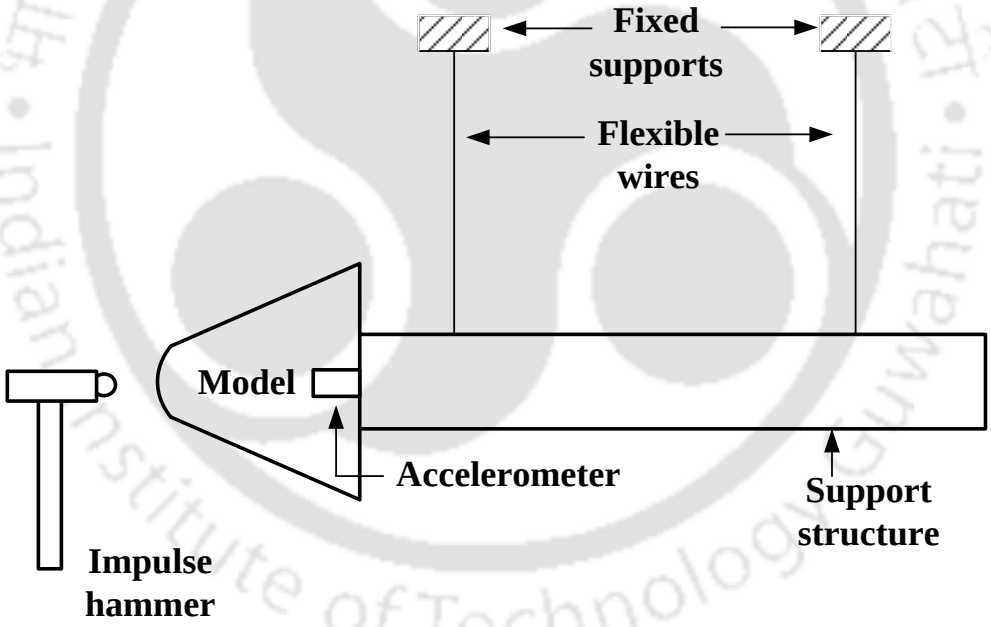

Figure 1.7: Schematic diagram of impact hammer calibration.

Another method as shown in Fig. 1.8 is to impact the model with the help of a pendulum as shown. In this case, the main disadvantage is that the time history of loading cannot be determined directly from the impactor (pendulum). However, by calculating the potential energies before and after impact, it is possible to determine the magnitude of impact force upon the model.

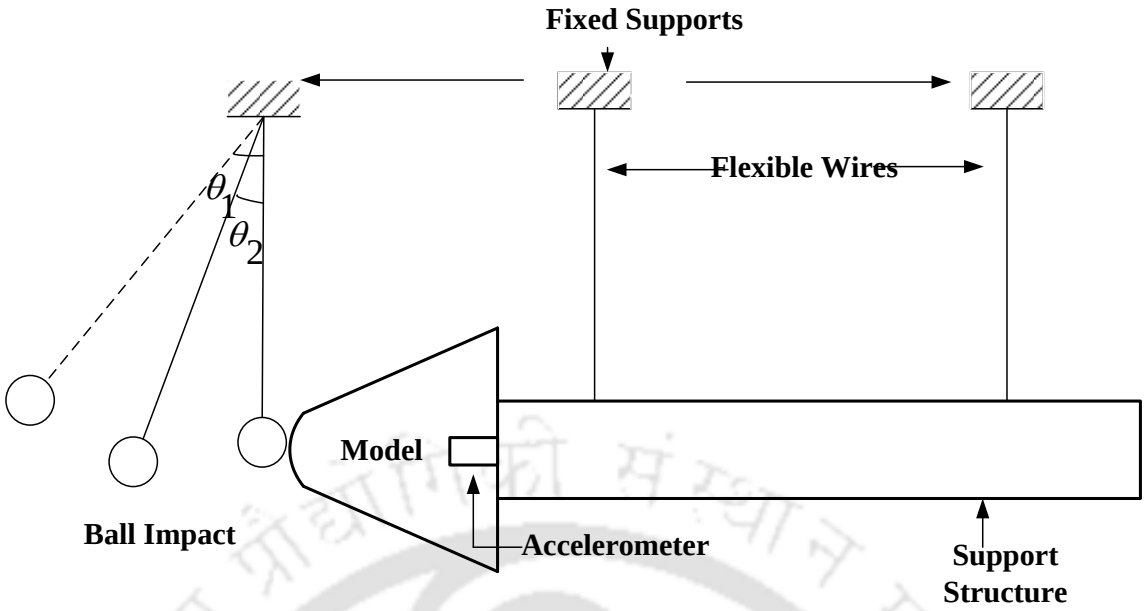

Figure 1.8: Schematic diagram of ball pendulum impact calibration.

1.5 Force Prediction Using Soft Computing Techniques

Generally input and output signals obtained during calibration tests are used to evaluate the impulse response function (transfer function) of the system by using convolution technique. Using the transfer function and a known acceleration or strain response, actual force and moments can be predicted through deconvolution technique. In case of aerodynamic structures the applied short duration forces or aerodynamic force coefficients can be predicted in this manner. It is observed that though the deconvolution technique can be applied for the single component force balance accurately, it is not able to handle the multi component force balance systems accurately. Hence there is a need to explore other methods for the prediction of force and moments. Studies on dynamical systems show that the soft computing techniques are applied to many reverse engineering problems. But this technique has not been used in the prediction of forces in hypersonic impulse facilities. The following section deals with the most appreciated soft computing techniques applied in various fields.

1.5.1 Neural network

Soft computing was introduced by Prof. Zadeh (1998), different soft computing techniques such as Neural Networks (NN), Fuzzy Logic (FL) and the Genetic Algorithm (GA) are widely used in many engineering application. These techniques are also used in their combined form such as GA-NN, NN-FL (ANFIS), and GA-FL-NN which uses the

combined advantages of these techniques without conflicting each other. The major advantage of these soft computing techniques is that they don't require the complex dynamics of the system. Neural network is usually employed in unknown parameter estimation for a system. Training of the network involved in finding the optimum model weights, network type, training method, number of hidden layers input and output membership function which will be used further during testing. Neural network also can be applied to unsorted data, so it is a universal data adopting technique.

1.5.2 Artificial neuro fuzzy inference system (ANFIS)

ANFIS is the combined structure of neural network and fuzzy logic. It is very much useful for the prediction of the unknown parameters. During the training it constructs the fuzzy inference system (FIS), assigns the model weights there by using the training algorithms such as (a) back propagation or (b) hybrid algorithm, it optimizes the model weights in such a way that the error in the output is minimum during the training. Henceforth the optimized ANFIS structure is used for the testing. The output accuracy also depends on the various input and output membership functions. These functions are chosen based on the type of the input data and output data. Few literatures related to application of ANFIS in mechanical engineering are cited in the following paragraphs.

1.5.3 Literature review on neural network and ANFIS

Rolling force prediction is very much essential for automation of the hot rolling process using model based optimization techniques. Rath et al. (2010) designed a neural network model to predict the force during the hot rolling process. The inputs used for the training of the NN model is gap between the two rollers in the previous pass, gap between the two rollers in the present pass, thickness of the sheet in the present pass, rolling feed, rolling temperature, pass number, and width of the sheet. The neural network model gives good accuracy in the prediction of the rolling force with (goodness of fit) $r^2 = 0.94$.

Tool wear is one of the important parameter in the machining process. The timely prediction of the tool wear increases the precision of the machining. Neural network and ANFIS based methods along with statistical parameter analysis method (I-kaz) method are used for the prediction of the tool wear during the turning process. The parameters used for the flank wear prediction are cutting speed, depth of cut, feed rate and the I-kaz coefficient for the turning process. Rizal et al. (2013) proposed a method for the prediction of the flank

wear with a higher accuracy. The proposed model has the optimum result with the correlation coefficient of 0.989-0.995 and the average error is about 2.30-5.08%.

An ANFIS model was designed for measuring the force components of the copy (end) milling process by Cus et al. (2006) The details of the modelling of the ANFIS for a linguistic rule is discussed in detail by considering ten influential parameters. Back propagation method has been used for the training of the model and it showed a good accuracy in predicting the 3-dimensional forces with an error of about 2%. Sigmoidal and Gaussian membership functions are used for prediction and the error is about 3%. In case of triangular membership function the error is 12%.

The cutting force prediction in the machining process is an important aspect for understanding the performance of the automated machines in the present times. The ANFIS model was designed for predicting the cutting force components (F_x and Fz) in the conventional milling process by Nayak et al. (2014). Three input parameters such as speed, feed and the depth of cut are considered as the prime parameters for the training. The cutting force is the test parameter. The results with the Gaussian type of training method show minimum error during the prediction.

Azari et al. (2014) used finite element method along with the soft computing technique for the prediction of the force in radial forging processes. The radial forging process is one of the essential processes useful for the manufacturing of the precision components such as tubular components with or without internal profiles. Since the maximum die force per pass is constant, the precision can be achieved during the forging. The prediction of these forces is very much essential for the design of the forging process without damage of the work piece or the machine components. Various parameters such as die inlet angle, billet temperature, area of cross section reduction and feed rate are used as the input parameters and the radial forging force is used as the output parameter. Two artificial intelligence methods viz. NN, ANFIS are used for the prediction and these results are compared with the multiple regression technique. It is observed that the ANFIS model gives the highest accurate prediction.

The damage detection of the machine component due to the excessive vibration is very important task in any mechanical system. Jhu and Wu (2014) performed the rapid damage detection using ANFIS and Interval Modelling Technique (IMT). Structural dynamic vibration data of the machine is used for the training of the model. ANFIS predicted accurate response of the model and the IMT method uses the response to find out the damage detection parameters.

Drilling is one of the important machining operation and the force analysis of the drilling process is very essential for the optimum parameter identification. Panda et al. (2008) used two neural network models namely back propagation neural network (BPNN) and radial basis function network (RBFN) for the prediction of the flank wear in the drilling process with the help of the training parameters such as speed, feed, and diameter of the drill bit. Also the derived parameters such as the torque, thrust force are used for the training of the networks. It has been observed that by increasing the input parameters the flank wear of the drill bit is well predicted.

Accurate determination of the injection profiles of the oil fields is very much essential during its development. It is difficult to use the conventional methods for obtaining the accurate profile shape. Hence Wei et al. (2007) compared two adaptive soft computing techniques for the profile determination viz. ANFIS-GRID (grid partition based fuzzy inference system (FIS)) and ANFIS –SUB subtractive clustering based FIS. The results from two models are compared with each other which showed that the two models are having the effect of low magnitude and low frequency disturbance but the low magnitude and low frequency disturbance free data gives good results for the experiments but the ANFIS-GRID is more accurate compared to the ANFIS-SUB due to its simplicity of structure.

Loganathan and Girija (2013) used an ANFIS model for system identification for a given trained data. The optimum parameters such as training type and the number of layers during the training are analyzed. Also the combinations of various training algorithms viz. back propagation, gradient descent and Runge-Kutta learning method are used for the training. The main aim was to find out the best combination of the training method and optimum training parameters. The performance analysis among these methods revealed that the combination of ANFIS with RKLM training algorithm yield accurate results.

1.6 Computational Methods for Force Prediction

1.6.1 Computational fluid dynamics (CFD)

Computational fluid dynamics (CFD) is one of the powerful tools for solving the numerical problems which are complicated to solve analytically and also beneficial for estimation of the coefficients of the forces and moment. The thermal properties such as heat transfer rate and chemical reactions can also be modeled using the simulation setup. This method is emerging and preferred in many areas such as industrial as well as the non-

industrial areas like aerospace industry, automobile industry, chemical processing industry, I.C. engines, gas turbines, modelling of ship. CFD analysis is useful to visualize the flow in micro-channel and also in chemical process industries, external and internal environment modelling, wind loading and the ventilation of the building. This computational tool has been used extensively for prediction of forces and moments at hypersonic speeds.

1.6.2 Literature review on computational fluid dynamics (CFD)

Silton (2011) found the static and dynamic coefficients of a standard 0.50-cal army projectile using computational analysis. In this analysis cubic k-ε turbulent model, realizable k-ε turbulence model are used and showed good accuracy compared with the k-ε-R turbulence model.

A hybrid particle continuum method has generally high accuracy and precision. Wang and Boyd (2003) proposed the hypersonic non-equilibrium flow over a 2-D axisymmetric configuration. Two different techniques such as direct simulation Monte Carlo-Information Preservation (DSMC-IP) technique for the particle domain while a finite volume second-order accurate, Steger-Warming flux vector splitting NS solver was opted in the continuum domain. Numerical analysis of the hypersonic flow over a blunt cone and a cylinder are carried out. It has been observed that the hybrid methods are able to analyze the hypersonic flow characteristics with highest accuracy as that of experiment. However the performance of the hybrid method is not very much accurate near the shock regions which is due to the equilibrium assumption while solving the problem using DSMC-IP.

Roveda (2009) compared the capabilities of three commercial CFD solvers such as Fluent (Ansys, Inc.), Cobalt (Cobalt solutions, LLC) and CFD++ (Metacomp, Technologies, Inc.,) to obtain the flow parameters around the aero spiked model with cylindrical and hemispherical configurations. The flow considered is a supersonic flow and the steady state results are in good agreement with the experimental results. All the main flow features such as pressure temperature, density are captured with high accuracy using the CFD.

A compressible Navier-Stokes solver was used for finding the flow structure over a spherical nose with cylindrical aft body by Roychowdhary and Unnakrishnann (2013). Various Mach number flow conditions varying from 5 to 30 are analyzed using the solver with constant free stream pressure and temperature. The initial velocity of the flow along with the enthalpy conditions are varied from 1.5 to 48 MJ/Kg. k to obtain the corresponding

Mach number of the flow. The heat flux and the pressure and temperature contours are plotted around the surface of the body. The variation of the graphs between the real gas and the perfect gas are also presented along with the comparison of the experimental data.

Two different methods such as direct Simulation Monte Carlo (DSMC) and Navier-Stokes (NS) CFD solver are used for the analysis of the helium flow over a supersonic blunt body for finding the aero thermodynamic properties by Nilifard and Ahmadikia (2010). The density contours of two methods are compared, and showed a good match with each other which is clear from the shock layer contours. However at the surface of the shock layer the DSMC seems to give a higher density value in comparison to the CFD. Also the surface temperature contours at the nose has maximum value which is seen to be 850 K from the DSMC method but in case of the CFD the value is 805 K. The comparisons showed that the two methods can be used interchangeably because the deviation of the results are within10% .

1.6.3 Introduction to fluid structure interaction (FSI)

All the moving bodies or the rigid structures interacting with the moving fluid encounters various forces which causes stresses and deformation in the body. The analytical solution of the physical interaction of the solid model with the fluid is very complex. Hence numerical simulations are performed to understand the interaction between the fluid flow and the solid structure. The combined analysis of the fluid properties and interface properties with a solid structure simultaneously is referred as fluid structure interaction. There are two different approaches to solve these kind of problems, (a). One way FSI, (b). Two way FSI. In case of one way FSI, the CFD solver solves the governing equations till the specified residue is achieved. The results obtained from the CFD solver (pressure, temperature etc.) at the interface of the solid and fluid are given as input for the structural analysis. Where the fluid solid interface pressure is applied on structural solid model and the results from the solid structure are taken as the output from the simulation. This is also called as one way coupling and in this type of coupling there is no interaction between the CFD solver and structural solver during the simulation. Once the CFD solver completes the solution, the interface pressure is given as load input to the structural model but the interface displacement due to applied force or temperature are not sent back to the fluid solver for updating the solution of the CFD. Since there is no feedback of the structural component to the CFD it is called one way coupling. One way coupling is useful for the

small displacement simulations where there is no large deformation in the model due to the applied pressure on the surface of the structural solid.

In two way FSI the CFD solver solves one time step, it sends the interface pressure on to the structural model and the FEM solver sends back the deformation or the displacement of the structure due to the applied pressure. Then the CFD solver adjusts itself accordingly and re-meshes the fluid domain and again solves the next iteration. This will continue till the both structural and fluid simulations comes to equilibrium state with each other. The two way coupling is useful when the interface pressure applied on the structural body leads to large displacement in the structural surface which influences the CFD solution very much. In the following paragraphs literature related to fluid structure interactions are presented.

1.6.3 Literature review on Fluid Structure Interaction

Zhang et al. (2014) measured wind shear effect (WSE) on vibration of geometrically nonlinear wind turbine blade. The blade is made of glass reinforced plastics because of their light weight, high strength and good rigidity. The fluid structure interaction has been carried out on the blade model. The experimental and FSI results are in well agreement with each other, with an error of 1.94 %while finding the Mises stress at the root of the blade. It has been observed that WSE on displacement increases along the span direction whereas the contribution of FSI on Mises stress decreases from central region to the two ends of the blade model.

Fluid Structure Interaction (FSI) can be performed in two ways viz. monolithic and partition approach. Michler at el. (2004) compared these two approaches in terms of stability, accuracy and computational cost by analyzing a one dimensional piston interacting with the fluid. It has been observed that partition scheme requires less computational cost for time step compared to monolithic approach. However in this case numerical instability is observed. It also observed in the study that same level of accuracy can be obtained in the monolithic approach with larger time step.

Lee et al. (2012) performed fluid structure interaction analysis of turbine blades with the fluid flow. Also the structural analysis of FRP wind turbine blade has been performed to analyze the aero elastic effect. It has been observed that the FSI results in actual response of the blade structure subjected to pressure loading condition. Also, the power capacity of the turbine is effected due to rotation in the foil section and flap wise deformation of the blade.

Zhu et al. (2014) used three dimensional Reynolds-Averaged-Navier-Stokes (RANS) equation and k-ε turbulence model to investigate the flow erosion and flow induce deformation of a three-limb pipe and the characteristics of oil flow is calculated. Various flow and structural parameters are changed during the FSI analysis to understand the effect and it has been observed from the results that the flow erosion in the downstream junction is more than the upstream of the junction. Also the higher inlet mass flow rate with 90^0 merging angle leads to severe deformation.

The study of inflation of a folded parachute using simplified arbitrary Lagrangian-Eulerian fluid structure interaction (SALE/FSI) is carried out by Yu et al. (2014) and it is found that the experimental results from the wind tunnel and the numerical results are in well agreement with each other. The FSI analysis also helped to obtain the information about material selection, to predict the stability and also swinging of the payload-parachute system.

The FSI analysis with arbitrary Lagrangian-Eulerian (ALE) framework and Dirichlet-Neumann approach using coupling for blood flow application was carried out by Chabannes et al. (2013). This method is validated by using flow over a cylinder with elastic beam clamped to it. The obtained results showed good match for drag but some fluctuations are observed in case of lift force. This technique is also used to simulate the propagation of pressure wave through a pipe in 2D and 3D. The results showed a good agreement for various flow rate and pressure at various cross sections of the flow.

Gerdroodbary and Hosseinalipour (2010) studied the effect of presence of aero spikes with different lengths and shapes for the drag, heat transfer reduction in hypersonic vehicles flying at Mach number 5.75 for different angles of attack. The compressible 3D Navier-Stokes equation with k-ω turbulence model has been used for the estimation of drag in comparison to the experiment. Also the effect of modification of the tip of the spike on the type of shock formation and condition to avoid coincidence of impingement location of bow shock was carried out.

Analysis of aero-elastic process induced during initial phase of rocket engine was carried out by Garelli et al. (2010). Euler's equation was solved by Arbitrary Lagrangian-Eulerian formulation for fluid domain also constitutive structural relations with rotation was used for solving solid domain. The flutter phenomena which occur during supersonic fluid flow over flat plate was studied along with the validation of code where Crank-Nicholson scheme with variable time step was used. Identification of Eigen frequencies of characteristic mode of nozzle are also analyzed using developed code.

A numerical study has been carried out using fluid-structure interaction for an elastic cylinder clamped at both ends subjected to tubular fluid flow by Liu et al.(2012). The Arbitrary Lagrangian-Eulerian Formulation with large eddy simulation model was applied for fluid flow solver and Euler-Bernoulli beam dynamic equation was used for structural solver for solving elastic cylinder vibration due to application various magnitude of dimensionless flow velocity. It was observed that the large displacement of the cylinder is damped into weak oscillation at low dimensionless flow velocity and buckling phenomena evolve when dimensionless flow velocity is very high.

Fluid-structure interaction in supersonic fluid flow over 2D and 3D-fin profiles are numerically analyzed by Kroyer (2003) to determine the stiffness effect and chances of aero elastic instability. It is evident from the results that for higher Mach number possibility of instability cannot be avoided and relationship exists between sensitivity of torque moment behavior and structure flexibility.

1.7 Computational Methods for the Design of Force Balances

1.7.1 Finite element (FE) analysis

Computational facilities are part and parcel of the modern world, these sophisticated facilities can be useful for the different fields of research such as solving physically complex problems involved in more cost and safety. The force measurement is also one of the important research area where the calibration techniques, experiments and the computational methods are used for the analysis of the different force measurement techniques and also useful for the design of the force balances. It is less expensive and also the things which cannot be possible with the experiments can be tested using FE analysis. These analysis are useful for the force prediction in the short duration facilities also useful for finding the locations of the sensors and for finding the optimum shapes of the bodies to be tested in the experiment, it also clarifies many doubts of the researchers and complexities in the analysis. The dynamic analysis of the model can be performed to see the effects of the shape and size variation and the proportionality of the responses to the applied loads. In the following paragraphs, literatures related to the finite element analysis are briefly presented.

1.7.2 Literature review on Finite Element Analysis

A three component force balance has been designed and analyzed to measure the drag force, lift force and pitching moment by Daniel and Mee (1995) using finite element method. The difficulties in designing three dimensional FEM models and during the response measurement are also discussed. The limitation of FEM simulations to recover the input forces using the output strain signals is also presented. From the simulations one can obtain type of strain signals required to predict the applied force and the sensitivity of the method to the applied load time history accurately. For measuring the lift component on the model, the model is attached to the sting by means of symmetrical triangulated bars and the axial strains are measured in that bars. The experimental results on the support model are compared with the FEM simulation results.

Smith et al. (2001) used stress wave force balance method has been used for obtaining the impulse response of a model tested in hypersonic shock tunnel The system transfer function has been derived from the obtained response using the de-convolution technique. Finite element analysis has been carried out for obtaining the response of the model for predicting the drag lift and moments in the flight condition. Also the load distribution on the model is obtained using the FE analysis which helps during the design of the balance.

Exhaustive transient finite element analysis has been carried out on a hemispherical model with 60^0 semi apex angle by Sahoo et al. (2007). The three component accelerometer balance performance was also analyzed using various methods for achieving the free flight conditions. Different rubber properties are checked for the analysis and it is found that the rubber with Young's modulus between 0.3 to 30 MPa is suitable for creating the free flight condition during the experiments.

1.8 Summary of Literature Review

Aerodynamic force measurements techniques for impulse facilities developed by various researchers are discussed in detail. It can be seen from the open literature that the accelerometer force balance technique is very much suitable for ground testing to measure forces and moments incurred in the hypersonic flow regime. However, calibration of accelerometer force balance for multi-component force measurement is still a topic of research. Moreover, stress wave force balance has been calibrated for forces and moment measurements with three degrees of freedom. Hence, investigations are still required for

extension of stress wave force balance for six degrees of freedom measurements. All the techniques reported in the literature are intrusive techniques like accelerometer and stress wave based force balances. Therefore explorations are required for design, development and implementation of a non-intrusive force measurement technique.

1.9 Motivation and Objectives

In view of the literature reported investigation for the measurement of various kind of forces and moments, following objectives are set for the present studies.

1. It can be seen that the force measurement techniques presently used by researchers are contact type or intrusive measurement techniques where acceleration or strain are measured to predict the applied load. As there are many issues related to the mounting of the sensor and accuracy of the predicting response, in the present work effort has been made to use laser based non-contact or non- intrusive technique to measure the velocity and then predict the applied forces. Also the results are reported herewith to assess the applicability of a non-intrusive technique for the force measurement along with the established methodologies.

2. Accelerometer has been considered for the force measurement either with complex mounting system or with the rubber to achieve free-flying condition. But the quantification of resistance offered by the rubber during the experiment is essential to justify the associated free-flying condition. Therefore computational studies are planned to evaluate the reaction force and the moment by the rubber based support. Importance of computational studies would thus be demonstrated for designing the force balance by predicting the expected acceleration signal.

3. Calibration of the force balances has always been given the prime importance before actual prediction of forces. In one side, accelerometer force balance excludes such calibration by incorporating simplified assumptions while the detailed mathematical inputs are required to devise calibration methodology for stress wave force balance. Therefore it is essential to formulate a simpler calibration methodology based on the soft computing techniques which are invariantly used for building the relation between the input and output data.

4. Detailed parametric study of Neural Network (NN) and Artificial Neuro-Fuzzy Inference System (ANFIS) based multi-component force prediction strategy using finite

element based acceleration signals and the implementation of the same for actual shock tunnel experiments has also been planned.

Following milestones are proposed to achieve the present objectives of the thesis

- Design of an experimental set up for calibration of force balance.
- Design and calibration of a stress wave force balance for single component force measurement.
- Design and calibration of accelerometer force balance for single component force measurement.
- Development of de-convolution technique for prediction of force in a single component force balance.
- Design and calibration of a laser based non-intrusive force balance for single component force measurement.
- Finite element analysis of an accelerometer balance for the quantification of the reaction forces, moments and the sensor requirement with optimum location.
- Fluid Structure Interaction (FSI) of AGARD model for finding the drag, lift and moment coefficients in the hypersonic flow.
- Parametric analysis for obtaining the optimum ANFIS structure useful for the short duration force prediction.
- Development of a soft computing based technique for the prediction of the three dimensional forces and moments using neural network and ANFIS.
- Extension of the single component force balance for three component force balance using accelerometer based force balances.
- Experimental analysis of the three component force balances using hypersonic shock tunnel experiments.
- Prediction of the three components of experimental forces and moment using ANFIS

Different force measurement methods, parameters, models and analysis techniques carried out in this work are shown in the Fig. 1.9.

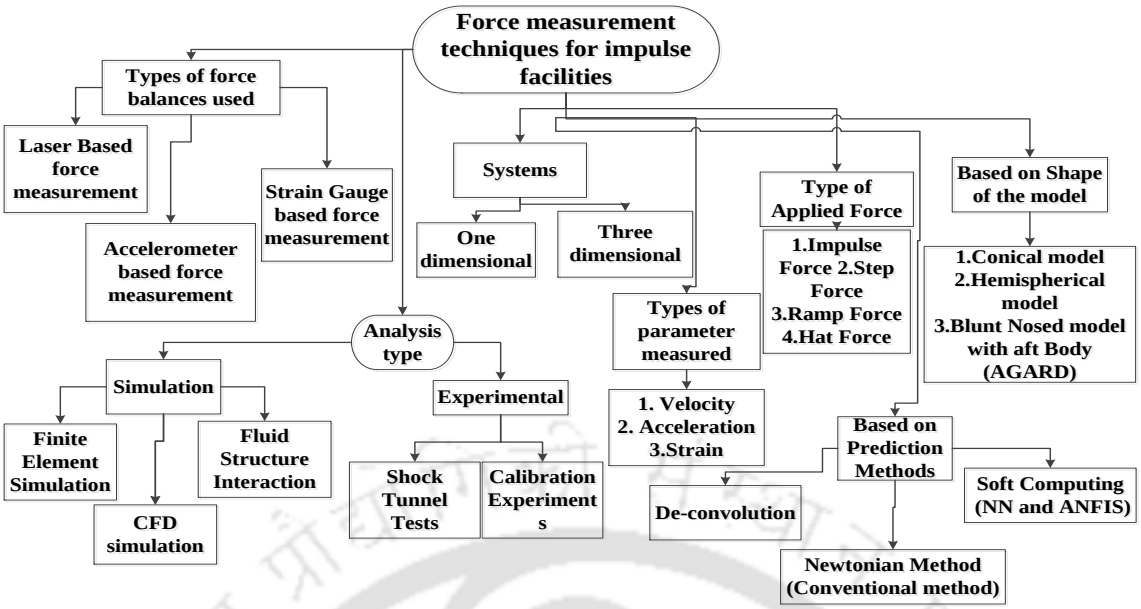

Figure 1.9: Methodology to be used for the fulfillment of the proposed objectives.

1.10 Organization of the Thesis

This thesis is organized in seven chapters. First chapter gives the brief introduction and updated literature review of various force measurement techniques under consideration in the hypersonic flow regime. Development of the laser based force measurement technique and associated experimental set-up are discussed in second chapter. Assessment of this novel technique with the conventional accelerometer and the stress wave force balances are the topics of discussion of third chapter. Use of computational tools like CFD and FEM for effective designing of force balance has been demonstrated for accelerometer force balance system in chapter four. Presentation in chapter five is about consideration of soft computing techniques for recovery of forces and moment. This chapter provides the detailed parametric studies in the process of development of ANFIS based force recovery method. Chapter six is comprised of the discussion about shock tunnel experimental set-up, force measurement during experiments and force recovery using ANFIS and conventional method. Finally all the efforts and associated results are concluded in chapter seven.

CHAPTER 2

DEVELOPMENT AND ASSESSMENT OF NON-CONTACT TYPE LASER BASED FORCE MEASUREMENT TECHNIQUE

Overview

Force measurement is an essential element in design of system or process. Choice of a particular technique, among the numerous available measurement techniques, depends on various parameters within which nature of force is an important one. Hence, measurement of the impulse force is considered in present investigations using two techniques namely accelerometer force balance and laser vibrometer based force balance. In view of this, an experimental set up has been developed to perform the force measurement for assessment of the laser based extrusive technique along with the established intrusive accelerometer based technique using a small conical model. Finite element based simulations are also performed on the same model to understand the system behavior under the same experimentally applied impulse forces. The de-convolution technique has been used for the prediction of the unknown force.

2.1 Introduction

Knowledge of the applied or incurred force is a foremost prerequisite for design of any mechanical or non-mechanical system. Various practical examples provide the evidence for the same, viz. force applied by the tool on the work piece, drag force offered by the water to the sheep, force incurred by the road and space vehicles due to their motion etc. Hence, measurement of force is an integral part of design of a robust system or smooth process. Various measurement techniques are reported in the literature for measurement of force. However, suitability of a particular technique, in a given situation, mainly depends on the nature of the force. Impulsive nature of the force is one such exceptional requirement where fast response sensors and acquisition system along with the special data reduction technique are required for accurate estimate of temporal nature and magnitude of the force. Such a high frequency force can be routinely encountered in various situations like impact testing, structural loading, high speed experimental testing, detonation prediction etc.

Various techniques for force measurement and choice of sensors are discussed in literature for the realm of impulsive forces through diverse applications. Vidal (1956) developed an accelerometer based force balance system for short duration impulse facilities. This inertia dominated force measurement technique has been then extended for numerous applications (Naumann et al. (1991), Naumann et al. (1993) and Sahoo et al. (2007)). Simmons and Sanderson (1991) developed a stress wave force balance, based on local strain time history, for measurement of suddenly applied aerodynamic load in the high speed test facility. This stiffness dominated force measurement concept has been then considered for various applications. Odeen and Lundberg (1990) experimentally measured acceleration and strain for prediction of the force applied by one object on the other during impact. Three objects (truncated cone of Nylon-6, compound cylinder of Nylon-6 and aluminum and long cylindrical steel rod) were considered for these experiments. Knapp et al. (1998) conducted Hopkinson's bar test and evaluated the applied force through strain and acceleration measurements. Takeo and Yoshinobu (2004) predicted the impulsive force in the Electric Discharge Machining (EDM) using a piezoelectric sensor. Wang and Chen (2007) employed polyvinylidene fluoride (PVDF) film for force measurement during cavitation studies. Development of a two filter technique has also been reported in the literature to measure the impulsive force (Lyon and Zable (1973)). Similarly, use of inverse technique (Benedetti et al. (2011)) and wave propagation responses (Espinosa and lee (2006)) have also been considered to identify the impact load.

In view of the literature reported measurement techniques, it can be seen that the proposed or prevalently implemented techniques are contact type or intrusive measurement techniques. Simplicity and lesser cost are the major attractive points for acceptance of these techniques. However, present studies concentrate on the possibility of implementation and assessment of a non-intrusive technique for force measurement. This technique becomes the lone possibility to understand the system or process in some rare situations where access to the system for sensor mounting becomes impossible or damage to the instrumentation is prevalent during the experiment.

Displacement and velocity are the most commonly considered measurable parameters in such non-contact type measurements to predict the derived quantities like applied or incurred force. Investigations reported by Yusaku (2009) provide the evidence for the same where system analysis has been carried out for step loading through velocity measurement. Therefore, this chapter deals with development and assessment of a non-intrusive technique for force measurement. A laser based experimental set up has been developed to measure velocity of the object set in motion by applying the impulse force. Accelerometer has also been housed inside the test model to monitor its accelerations. Recovery of the force has been obtained from the direct measurement of velocity and direct and indirect measurement of acceleration with the help of FFT method. Critical comments have also been made about the impulse response function obtained from both acceleration and velocity measurements. Details of the experimental technique, data reduction methodology and associated implementation of Finite Element Analysis (FEA) are explained in the following sections.

2.1.1 De-Convolution Technique for Force Recovery

The de-convolution methodology has been used for the recovery of the unknown applied force from the measured responses. The convolution integral is the basis for this technique where the proposed system has been modeled as a linear system. The relation between the input and the output is shown in the following equations.

$$y(t) = \int_0^t u(\tau) \,.\, h\,(t\ -\ \tau)\, d\tau \tag{2.1}$$

$$y(t) = h(t) * u(t) \quad ` \tag{2.2}$$

Here $h(t)$ is the impulse response function, $y(t)$ is the response of the accelerometer or the laser vibrometer, $u(t)$ is the applied input impulse force on the model, '*' represents convolution operator.

Equation 2.1 represents the convolution integral which relates the two signals having the time lag such as applied force and the response due to the force. Here $y(t)$ is the response of the system and $u(t)$ is the applied force and $h(t)$ is the transfer function of the system relating the input and the output of the system. A MATLAB based code using Fast Fourier Transform (FFT) has been developed to obtain the system response function or transfer function or impulse response function. Thus obtained impulse response functions from one force $(F1)$ is used to recover the other force $(F2)$ and vice-versa in the same code.

2.2. Description of Experimental Setup

The experimental setup has been designed and fabricated for conducting the impulse tests which is shown in Fig.2.1. It consists of the rigid cast iron frame to which a wooden block has been attached. Holes are drilled in wooden beam at regular intervals along the length of the beam. Special '*J*' shaped hooks are housed inside the wooden beam at the respective holes. The hook position can be varied as per the requirement, suitable for the length of the model used for the experiment. Hence models with different lengths can be suspended from these hooks for obtaining the free flying condition. During the proposed experiments, care has been taken such that the model is restrained to have free flying motion in axial direction without any obstruction. Also the experimental model axis should be parallel to the plane of ground. In view of this, test model is suspended from the wooden beam through the hooks using flexible wires and proper electrical connections are made for the experiments using (Bayonet Neill-Concelman) BNC connecters. In case of single component experiments, the force should be applied parallel to the direction of the model and should be applied only at the tip of the model. The schematic diagram of the experimental setup with all the connections is shown in Fig.2.3. This setup is useful for conducting the experiments to apply step, impulse loads on the models for measuring the desired responses.

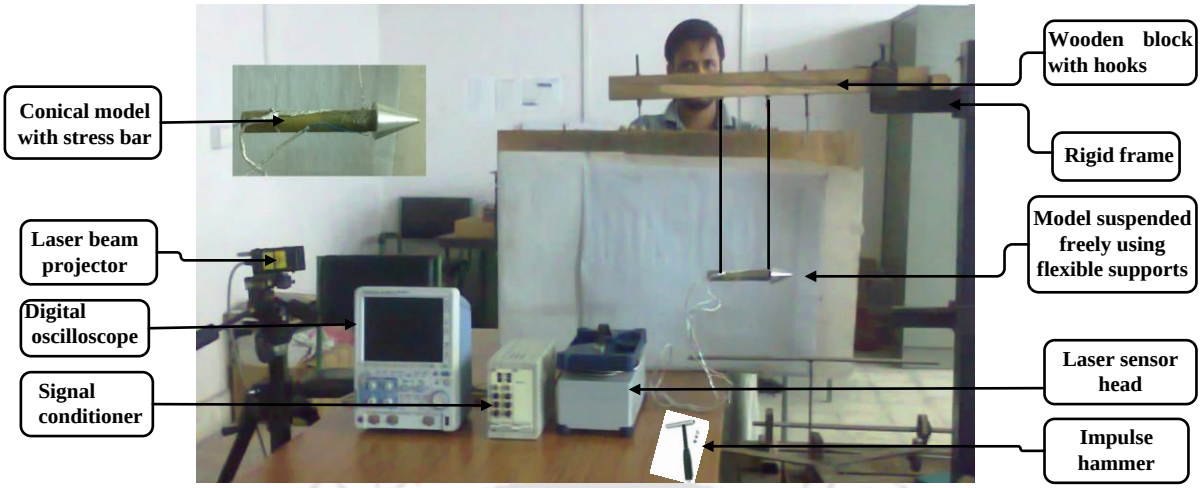

Figure 2.1: Photograph of the experimental setup designed for impulse test.

Present experiments are conducted for velocity and acceleration measurement under the impulsive loading conditions. An aluminum blunt cone attached to a brass rod has been considered for these experimental studies. The 20^0 semi cone angle blunt cone has 40 mm base diameter. The 150 mm long bar, screwed to this cone, has 19 mm inner diameter and 1.5 mm wall thickness. A provision has also been made at the base of the cone part of the model for accelerometer mounting to measure the axial acceleration. Schematic of this model is as shown in Fig. 2.2.

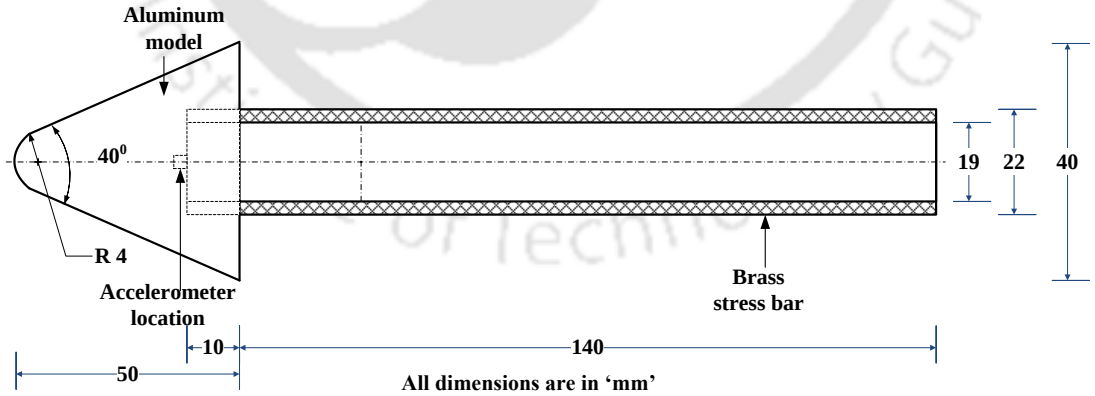

Figure 2.2: Schematic diagram of the test model.

During the experiment, the test model is suspended from a rigid support beam with the help of two flexible strings. The schematic of this experimental set up is as shown in

Figure 2.3. During the experiments, impulse excitation has been given to the test model using an impulse hammer (PCB Piezotronics, Fig. 2.4) at the tip of the cone.

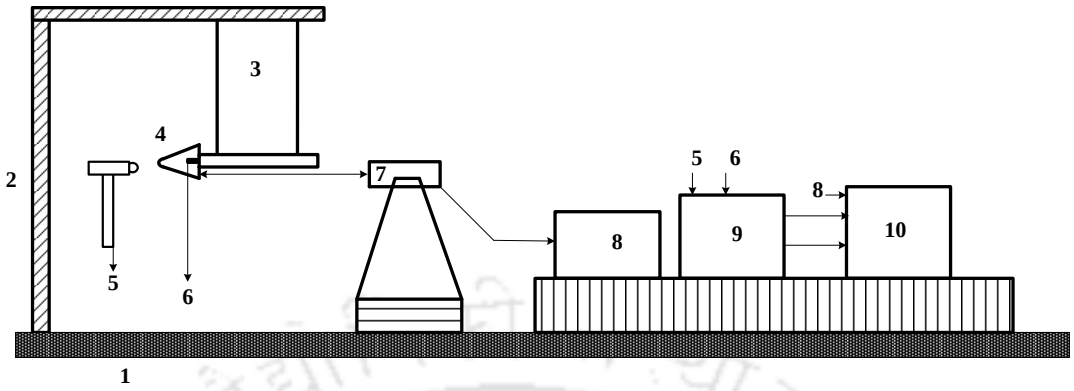

Figure 2.3: Schematic diagram of the experimental setup for laser based force balance.

(Where 1. Concrete Bed, 2. L- Shaped frame, 3. Flexible wires, 4. Aluminum model with stress bar, 5. PCB Impact hammer, 6. PCB piezo-electric accelerometer. 7. Laser vibrometer sensor head, 8. Controller, 9. Signal conditioner, 10. Digital oscilloscope.)

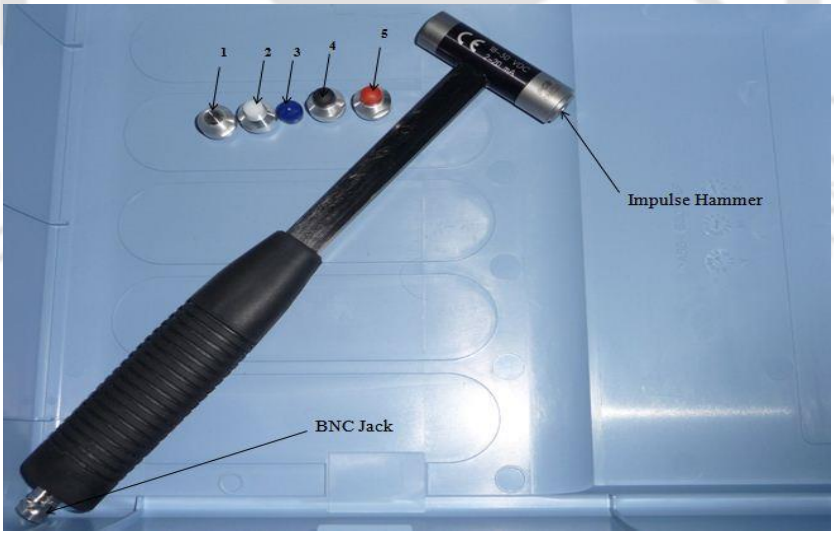

Figure 2.4: Impact hammer with different tips.

The hammer specifications are given in Table 2.1. Rotational Laser Vibrometer (RLV-5500) is employed in the present studies to measure linear velocity of the test model. Details of this Vibrometer are given in Table 2.2.

Table 2.1: Specification of an ICP impulse hammer

Model	086C01
Manufacturer	PCB Piezotronics
Sensitivity	11.2 mV/N
Measurement Range	440N peak
Non Linearity	≤1%

Laser vibrometers are advanced non-contact type sophisticated instruments with no added mass to the system. These are mainly useful for the measurement of the angular velocity and it can also be useful for the linear velocity measurement for short test time.

Table 2.2: Specifications of Plytec laser vibrometer.

Manufacturer	Polytec, Inc.
Amplitude Range (peak)	$2\frac{\mu m}{s}$ *to* $2\frac{m}{s}$
Sensitivity	$2\frac{mm}{s}/\ V$ *to* $200\frac{mm}{s}/\ V$
Frequency Range	0.5 *Hz to* 20 *kHz*
Measurement error	± 1.5% of RMS reading at Frequency 1 kHz, Amplitude > 1% of full scale

As RLV-A-TRANS enables translatory vibration measurements from 0.5 Hz to 20 kHz for velocities up to 2 m/s, it is a perfect velocity and displacement sensor for measuring structural dynamics. The RLV-5500 Rotational Laser Vibrometer consists of the RLV-500 Rotation Sensor Head and the RLV-5000 Controller. The sensor head also consists of two functional sections: the Laser Unit and the Compact Sensor. The Laser Unit includes a Helium-Neon laser and two high-precision interferometers for converting minute frequency changes of the reflected laser light into electrical signals. These signals are then decoded in the RLV-5000 controller shown in the Fig. 2.5.

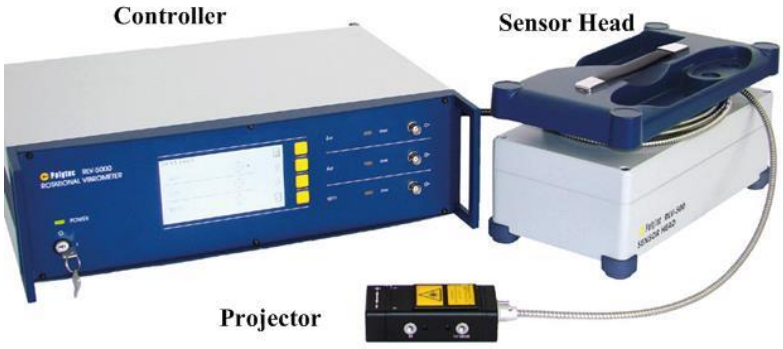

Figure 2.5: Rotational laser vibrometer (RLV 5000 and RLV 500).

It operates on the principle of interferometry. Improved signal to low frequency low magnitude disturbance ratio is obtained from the digital decoding techniques. The standoff distance of 20 to 600 mm can be maintained while performing the experiment. The laser projector can focus two beams separated by distance of 7.5 mm at a time on a body for the maximum speed case and also the distance between the beams can be adjusted to 25 mm for the case of high sensitivity measurement. The laser beam can be adjusted in minute time using level indicator which can be removed. The setup can be used in the harsh environments where the high temperature, oil, dirt and moisture exist. A PCB Piezotronics accelerometer (Model: 352C66) is also mounted inside the model to measure the axial acceleration. The output of the accelerometer is also connected to the signal conditioner. Specifications of this accelerometer and its signal conditioner are given in Table 2.3 and Table 2.4 respectively.

Table 2.3: Specifications of an ICP Accelerometer.

Model	352C67
Serial No.	127894
Manufacturer	PCB Piezotronics
Sensitivity	10.15 mV/(m/s^2)
Non Linearity	$\leq$1%
Settling time	< 10sec ($\pm$10%)

The signal conditioner is used as power supplying unit for the accelerometer and impact hammer. The specifications are given in Table 2.4. The projector of laser is placed near the base face of the model for the translational velocity measurement. Output of the accelerometer and the laser vibrometer are connected to the data acquisition i.e. the multi-

channel oscilloscope. The impact hammer is connected to the signal conditioner and then its output is connected to the oscilloscope. It is the trigger source in the present experiment. Specifications of oscilloscope are given in Table 2.5.

Table 2.4: Specifications of an ICP Signal Conditioner

Model	442B104
Manufacturer	PCB Piezotronics.
Channels	4
Gain Settings	x 1, x10, x100
Sensor Excitation Voltage	25.5±1.5 VDC
Sensor Excitation Current	0.5 to 20 mA

Table 2.5: Specifications of YOKOGAWA DLM2022 oscilloscope.

Manufacturer	YOKOGAWA
Model	610105-F-HE
Channels	2
USB Ports	2
Bandwidth	200 MHz
Sampling Rate	5000-125000 k S/s

The experimental results obtain are analyzed and compared by performing the finite element simulations on the same model. The impulse forces of same time history are applied on the FEM model for obtaining the acceleration, velocity response which is discussed in the following section.

2.3 Finite Element (FE) Analysis

Due to the advancement of high performance computers and technology, complex simulations can be handled using computational tools such as Finite Element Analysis (FEA). It is the widely used technique for the analysis of the systems under static and dynamic loading condition. The finite element analysis has been carried out on the same experimental test model with the transient structural analysis using ANSYS.

2.3.1 Design and Modeling

A three dimensional conical model attached with a stress bar has been modeled in ANSYS APDL. The model is made of aluminum and the stress bar is of brass material. The

meshed model along with the boundary conditions and loading condition are shown in Fig. 2.6. The model is considered as an isotropic elastic body, the material properties considered for the analysis are mentioned in the Table 2.6.

Table 2.6: Material properties used in the simulation.

S. No	Material	Young's Modulus (E) GPa	Density(ρ) kg/m^3	Poisson's Ratio(ν)
1	Aluminum	70	2700	0.24
2	Brass	100	8400	0.3

Three dimensional 10-noded tetrahedron elements (Solid-187) have been used for meshing the model which has 3-DOF at each node and is very suitable for meshing the irregular 3-dimensional geometries. Efforts are also carried out to perform the mesh independence studies. The FE model used for present simulations has 15978 elements. Time varying force has been applied on a node at nose of the cone while the cone area and area at the end of the stress bar are fixed in Y and Z-axes directions which can also be seen in Fig. 2.6.

Mass matrix formulation is lumped type and the implicit type standard Newmark time integration method is used. The time step size is 4 microseconds. Highest frequency of the signal is 10 kHz, hence Nyquist frequency of 20 kHz has been considered while choosing the time step and also the accuracy of the simulation has been checked for different element sizes.

Transient finite element analysis has been performed on this test model using the known impulsive force to obtain the acceleration and velocity of the test model. This FEA simulation is carried out for 1 ms test duration which is same as the duration of the impulse applied on the model during the experiment. The experimentally measured force has been applied on the model. Many trials are conducted during the experiments but for the present analysis two different magnitudes of force are considered. Acceleration is obtained at the center of the conical model and the velocity at the base face of the model, which are corresponding to the actual locations of the sensors during the experiments. These results are further analyzed and compared with the experimentally measured values for proper understanding of the accelerometer balance and laser balance which is discussed in the following section.

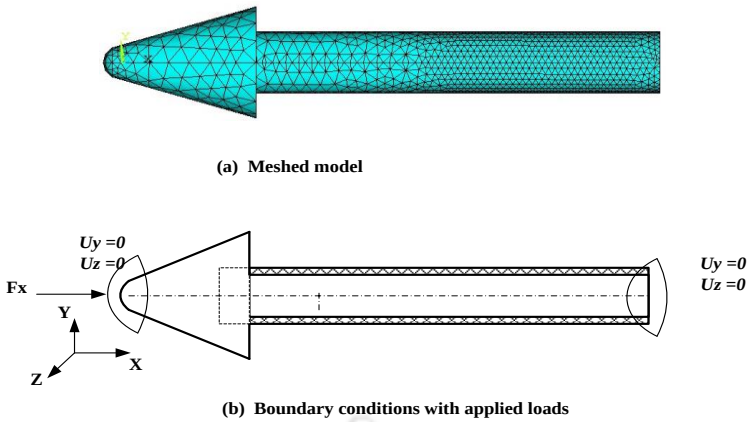

Figure 2.6: Meshed model and associated boundary conditions

2.4. Results and Discussion

Impulse force has been applied using the impact hammer on the test model during the present experimental studies. Resultant acceleration, measured using accelerometer, and velocity, measured using RLV, are recorded in the acquisition system along with the applied impact force. Time trace of two sample impulse forces is shown in Fig. 2.7. Terminologies used in the figures of this chapter are mentioned in Table 2.7.

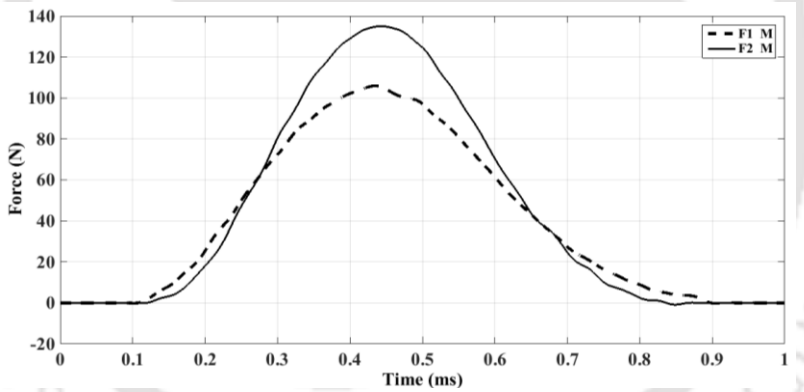

Figure 2.7: Measured force history of two impulse loads applied on the model.

Table 2.7: Terminologies used in the figures of chapter -2.

F1 and F2	Force histories for Case-1 and Case-2
A1 and A2	Acceleration histories for Case-1 and Case-2
V1 and V2	Velocity histories for Case-1 and Case-2
AV1 and AV2	Acceleration histories obtained from measured velocities V1 and V2 for Case-1 and Case-2
F, B, C	Forward, Backward and Central Difference Technique
M, S, R	Measured, Simulated and Recovered signals
Example: F1RAM : Recovered force history for Case-1 from measured acceleration for Case-1	

Experimentally measured velocity time trace in comparison with the simulated ones corresponding to both of the forces are shown in Fig. 2.8. It is clearly seen that the velocity is in proportion with the applied force in terms of time interval and the magnitude.

Encouraging agreement among the experimentally obtained and simulated velocity signals is evident from this figure. Both the signals exhibit initial higher rate of change of velocity followed by the reduced one. This trend of velocity signal can be justified by the force variation shown in Fig. 2.7 and also the acceleration signal shown in Fig. 2.9.

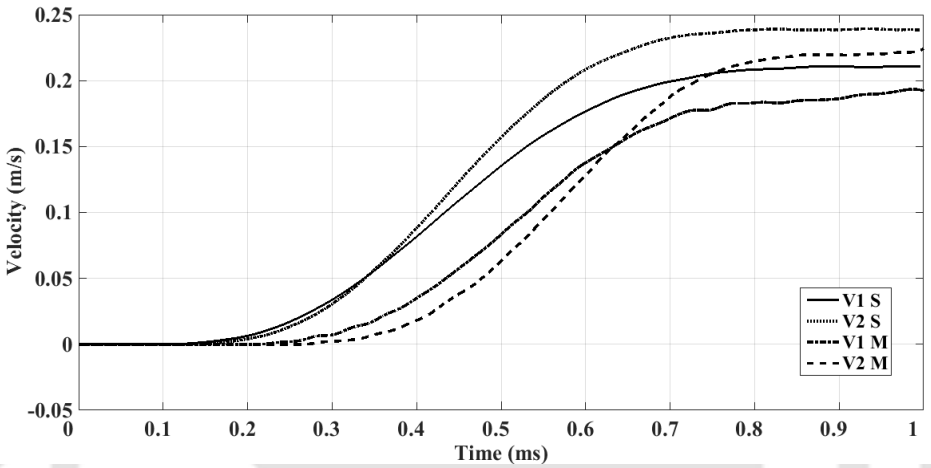

Figure 2.8: Comparison of measured velocity history of two sample experiments with the same obtained from FEA simulations.

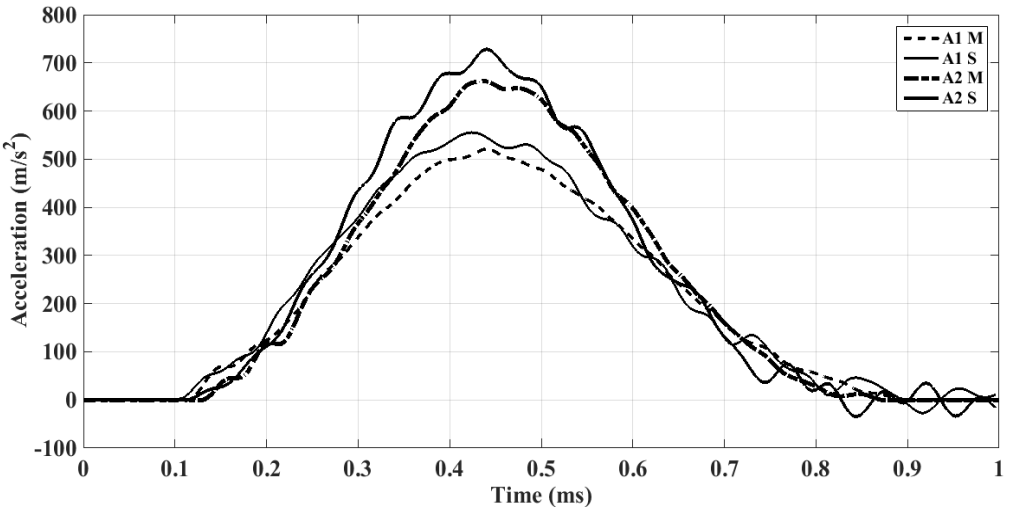

Figure 2.9: Comparison of measured acceleration history of two sample experiments with the same obtained from FEA simulations.

Excellent match, between the simulated and measured acceleration signals, is evident from the above figure. Initial increase in acceleration with increase in force and onwards decrease after reaching the peak value clearly follows the time variation of force signal. Three techniques viz. forward, backward and central finite difference, are used to calculate the acceleration from measured velocity. Thus recovered acceleration, shown in Fig.2.10 (a) and Fig.2.10 (b), seems to exhibit undulations around the measured acceleration and follows similar gross temporal trend.

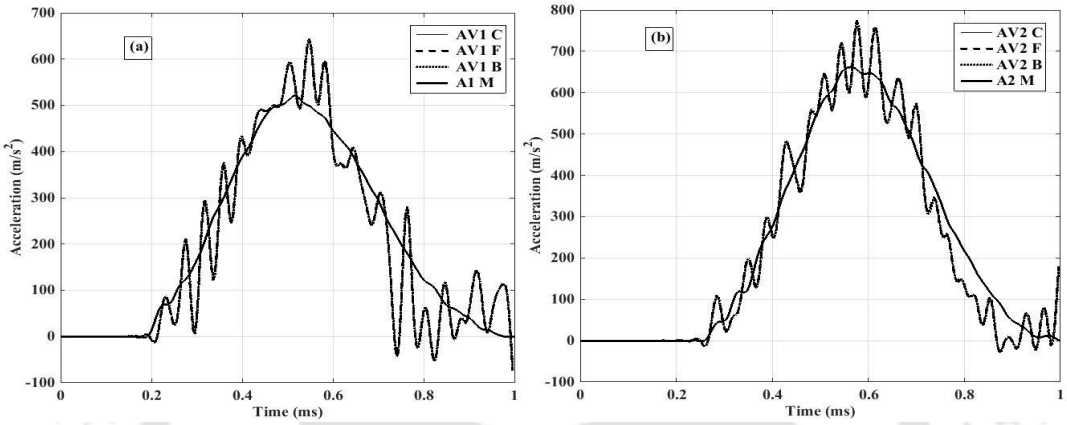

Figure 2.10: Acceleration history obtained from the velocity signal using various techniques. a) Case-1, b) Case-2.

Both the measured, simulated velocity and acceleration signals are then used to recover the force under the assumption of linearity of the system. In view of this assumption, the relationship between input (impulse) and output (velocity or acceleration) can be expressed by using the convolution integral. The impulse response function, representing the characteristics of the system, can be obtained from known input and output using Fast Fourier Transform (FFT) technique as discussed in section 2.1.1.

The force signals recovered from acceleration and velocity based impulse response functions using de-convolution technique along with the measured force are shown in Fig. 2.11 and Fig. 2.12 respectively.

Force and acceleration time window width in case 1 (Fig. 2.11), is approximately equal to $800 \pm 10\ \mu s$. In case-2 it is approximately equal to $850 \pm 10\ \mu s$. Sampling rate of 250 kilo samples per second with a time interval of 4 microseconds.

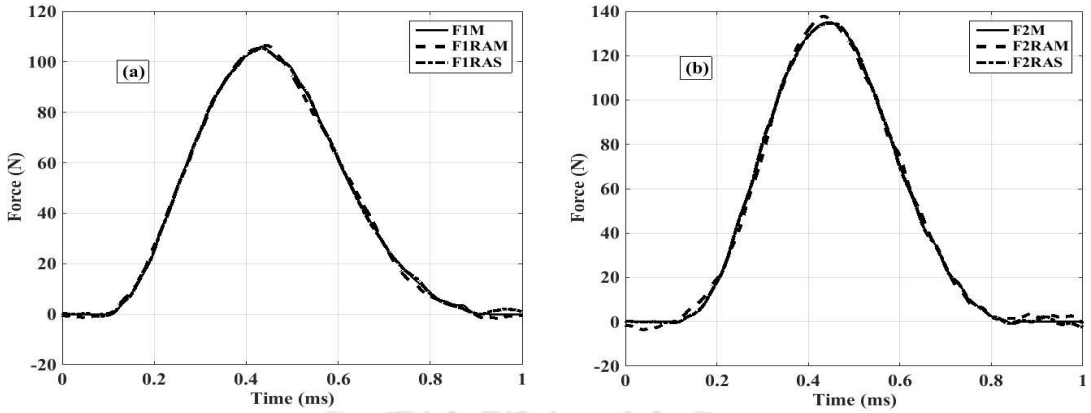

Figure 2.11: Recovery of applied impulse forces using acceleration based impulse response function. a) Case-1, b) Case-2.

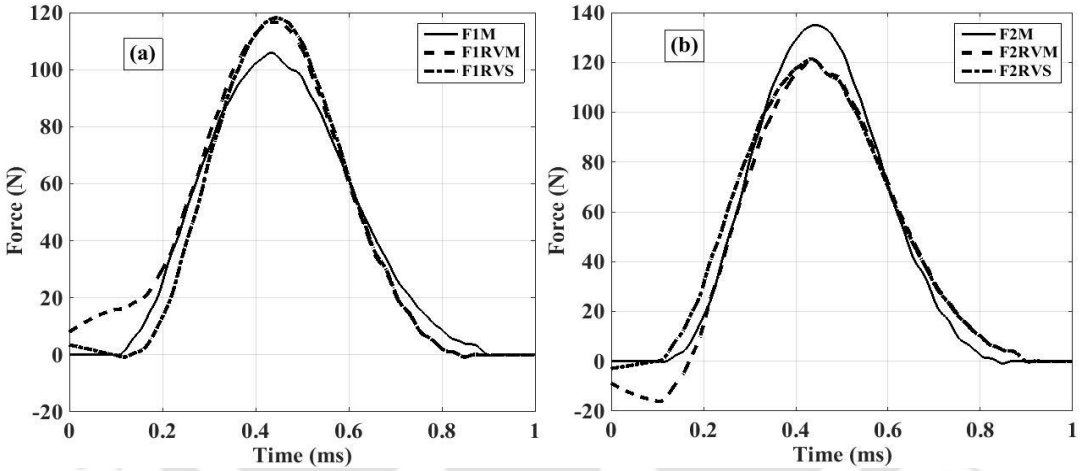

Figure 2.12: Recovery of applied impulse forces using velocity based impulse response function. a) Case-1, b) Case-2.

Excellent recovery of both the forces is clear from Fig. 2.11 where peak value of the impulse and temporal nature of the same are seen to be correctly captured**.** The average uncertainty calculated from all the experiments is $\pm 5\%$ for the prediction of peak force value from the measured acceleration.

In the prediction of the impulse force, the averaged error is calculated as the ratio of the deviation between the upper and the lower limit of the predicted peak force to the applied peak force.

The simulated and measured velocity based force recoveries (Fig. 2.12) are seen to be inconsistent in both the cases. Over-prediction of the peak value by $\sim$ 20% is noticeable in

Fig. 2.12 (a). Under-prediction of peak force by ~ 14% in the second case can also be marked from Fig. 2.12 (b).

Similar inconsistent behavior of the force predicted from velocity based transfer function, in comparison with the measured one, has been noticed for all the experiments. Apart from this, the measured velocity based recovery exhibits disagreement in the temporal variation with the measured force mainly at the point of commencement of the impulse. The probable reason for these discrepancies is the assumption of linearity of the system considered to obtain the impulse response function from measured velocity signal and onwards usage of the same for recovery of the force.

On the other hand, assumption of the linearity between measured acceleration and applied force is found to be persuasive in the present case. This fact can be revisited by recovering the force from the acceleration evaluated from the velocity signal as shown in Fig. 2.13. It is clearly evident from this figure that the force predictions from direct and indirect acceleration measurements are in good agreement with each other in comparison with the same obtained from velocity. Hence it is advisable to predict the acceleration from measured velocity for onwards prediction of the force during non-contact type measurements.

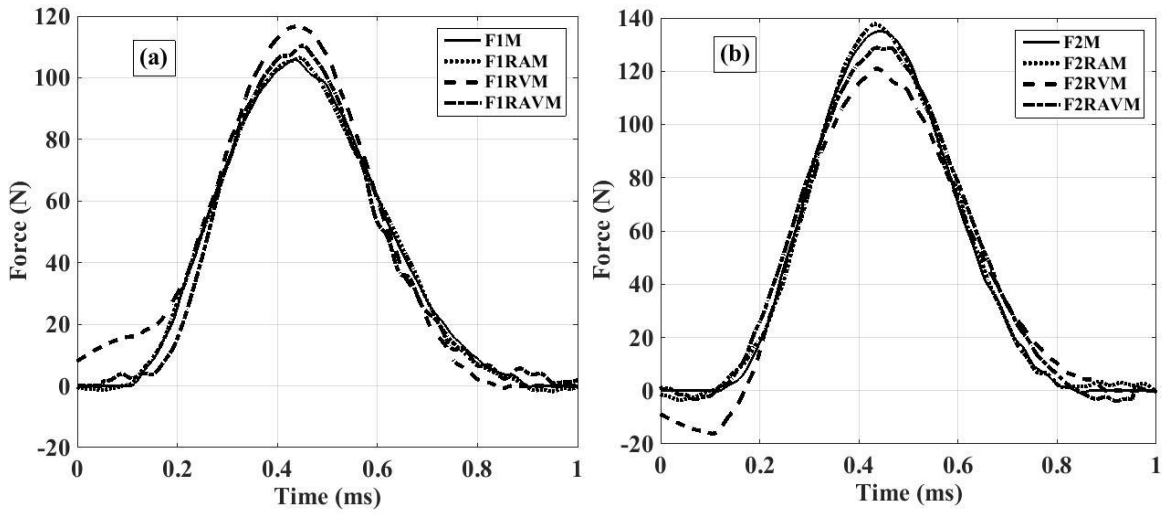

Figure 2.13: Comparison of impulse recovery from direct and indirect acceleration measurement along with the velocity measurement a) Case-1, b) Case-2.

Since the force and velocity are directly proportional to each other, the reconstruction of the force from the acceleration history showed good accuracy. However the force and the velocity are related in the differential form of velocity and hence the accuracy of the force prediction is less accurate in case of velocity based recovery. However the increase in the sampling rate of the velocity history can lead to the high accuracy prediction using the velocity.

2.5. Conclusions

Applied or incurred force is measured by various techniques. Special techniques for measurement and onwards data reduction are employed for impulsive nature of the force. In view of this, present studies are carried out to access the applicability of a non-intrusive force measurement technique with the established one. Therefore the impulse force and associated measurements are carried out on a 20^0 semi cone angle blunt cone. Laser based velocity measurement and onwards indirect acceleration measurements are considered for recovery of impulse force along with the direct acceleration measurement using accelerometer. Impulse response function obtained from direct or indirect measurement of acceleration is seen to represent the system more precisely in comparison with the one represented using velocity measurement. Therefore predicted impulse force using direct or indirect acceleration measurement is found to have excellent agreement with the actual force. Hence it is advisable from present explorations to convalesce the acceleration from the measured velocity for precise prediction of force during non-intrusive measurements.

CHAPTER 3

ASSESSMENT OF LASER BASED FORCE BALANCE WITH ESTABLISHED TECHNIQUES FOR SHORT DURATION STEP LOAD

Overview

Development of force measurement method for the short duration test facilities using step load calibration tests has been the topic of interest in the present chapter. Three different responses viz. acceleration, velocity and strain are measured simultaneously during the application of two magnitudes of step loads on the model. The corresponding results are plotted and analyzed for finding the system transfer function using the Fast Fourier Transform technique. The two step forces are interchangeably predicted using the transfer functions obtained from the other force and the response (acceleration, velocity and the strain) and the accuracy of the force prediction from the three response is discussed in detail.

3.1 Introduction

In order to design an optimum and safe mechanical or non-mechanical systems the measurement of force applied on such type of systems is inevitable. Hence measured response of the system for particular cases such as step and impulse, before the actual design of the system in general considered as the threshold for the testing of the components. Such loads are generally considered in calibration experiments of the force balances used in hypersonic experimental facilities. Force measurement is one of the prominent research areas in this flow regime. These force measurement techniques are carried out either in conventional or free piston driven shock tunnels or in expansion tubes. Very short testing time, of the order of few hundred micro-seconds to few milliseconds, is the major drawback of these test facilities. Before the actual tests on the test model, calibration of force measurement techniques is essential to evaluate the forces and moments on the body flying at higher speeds. The application of aerodynamic load on the test model during the experiments has mathematical similarity with step and ramp functions. Therefore in the present study, step load is used to arrive at the system response function Mee (2003).

The dynamic calibration of the system for obtaining the properties can be performed by applying the step load on the model. In this case the model is suspended from the fixed support and a pulley arrangement is kept for providing the axial motion of the body due to applied force on the model. The loads of known weight are suspended from the tip of the model and the load is suddenly released using wire cutting method. The wire cut should be sharply done such that the response is smooth. In this test, sudden release of the load leads to the step change in the load which causes the model to respond for the transient loading condition. Schematic of this experiment is as shown in Fig. 1.5.

Such calibration tests for the force measurement can also be conducted by using the vertical calibration method where the model is suspended vertically from the fixed support and to the tip of the model the weights are hanged with the help of flexible wires and the wire is cut near the model such that the step change in the force can be applied on the model. Schematic of this experiment is as shown in Fig. 1.6.

In the literature, Simmons and Sanderson (1991) developed a stress wave force balance technique which incorporates the transient nature of the response using the strain gages with fast response capacity for the measuring the steady aerodynamic load in the short duration. Calibration techniques for stress wave balance have been discussed by Sahoo and Reddy (2010). Similar calibration methodology has been used by Kulkarni and

Reddy (2008) for accelerometer force balance with impulse loading. Mee explains in details the strategy for calibration of force balances in specific for stress wave force balance. Sahoo and Reddy (2010) have summarized the recent advances about force measurement in such situations.

In view of the literature for force measurement techniques and their calibration, all the techniques are intrusive type and among those impulse load had been considered for accelerometer force balance calibration. Hence, present chapter concentrates on application of a non-intrusive force measurement technique and its calibration for step load. The laser based force measurement technique discussed in last chapter is evaluated with the established accelerometer based force measurement technique and also the stress wave force balance technique using transient strain measurement.

3.2 Experimental Setup and Instrumentation

3.2.1 Model Details

Experiments are conducted on a conical aluminum model attached with the brass stress bar at its base. The reason behind the hemispherical and blunt cone shapes is its usage for hypersonic flights. The test model considered for the experiment is shown in Fig.3.1.

Figure 3.1: Photograph of the strain gage conical model with brass stress bar.

Similar to the model discussed in chapter 2, here also an aluminum cone having 20^0 semi cone angle, 70 mm base diameter, 90 mm long and 6mm nose radius is attached to a brass bar of length 150 mm, outer diameter 22 mm and wall thickness of 1.5 mm with the help of screw thread mechanism. The size of the model compared to the previous one is large because, for the free flying model obtaining the strain is difficult but the heavier model can undergo higher magnitude of strain compared to the small model. High sensitive miniature accelerometer [PCB Piezotronics Inc., Model No: 352C67] is mounted inside the

aluminum model parallel to the axis of the model which is in the direction of the applied load. Strain gauge is mounted on the stress bar for transient strain measurement during the experiment. Here accelerometer, laser vibrometer and strain gauges are used to measure the acceleration, velocity and strain in the system. The arrangements for acceleration and velocity measurement are same as discussed in chapter 2. The arrangement for strain measurement is discussed in the following section.

3.2.2 Strain Measurement

Various components used for the strain measurement during the experiments are discussed in detail the present section.

(A) Semiconductor strain gages

Strain gages are sensors that are used to measure strain or deformation. Strain gages work by the principle that a strain in a metal or semi-conductor causes change in resistance under the application of load, which when measured can be related to the strain. There are different types of strain gages, namely, metallic, foil gages and semiconductor strain gages, which can be either piezo-resistive or piezoelectric.

Semiconductor based strain gauges are most suitable for present studies due to their fast response time. Kulite encapsulated gages are used in the present experiments and the details are as mentioned in Kulite semiconductor strain gauge Manual (2001). Encapsulation embeds the gage in a protective epoxy/glass matrix. When compared to conventional metallic wire and foil gages, Kulite semiconductor gages offer some significant advantages as:

Higher sensitivity, smaller sizes, higher resistance, higher fatigue life, low hysteresis.

Gage factor is the term used to define the fractional change in resistance of a gage with applied strain. Metal wire and foil gages have gage factors between 2 and 4. The semiconductor gages have gage factors between 45 and 200. Presently used encapsulated semiconductor strain gage is shown in Fig. 3.2 and its specifications are given in Table 3.1.

Figure 3.2: Photograph of the semiconductor strain gauge with two leads for connections.

Table 3.1: Specification of the Kulite encapsulated semiconductor strain gages

Model	S/UEP-350-090
Manufacturer	Kulite Semiconductors, Inc.,USA
Resistance	350 Ohms
Gage Factor	130
Sensitivity relation	Gage output = (volts in)*(GF)*(Total Strain) / 4

(B) Instrumentation amplifier

The resistance change in these test models is expected to be very small in spite of use brass stress bar. Therefore an instrumentation amplifier has been used to amplify the strain gauge output. The INA 128 (Texas Instruments, USA) is a low power, general purpose instrumentation amplifiers offering excellent accuracy for the amplification of the voltage signal. Their versatile 3-op amp design and small size make them ideal for a wide range of applications. Therefore this amplifier has been used in present explorations. A single external resistor sets any gain from 1 to 10,000. Thus made INA128, shown in Fig. 3.3, provides an industry standard gain. The offset voltage of the amplifier is also very small. The gain relation for the INA 128 amplifier is given by

$$G = 1 + \frac{50K\Omega}{R_G} \tag{3.1}$$

Here G is the gain of the amplifier, R_G is the gain resistance

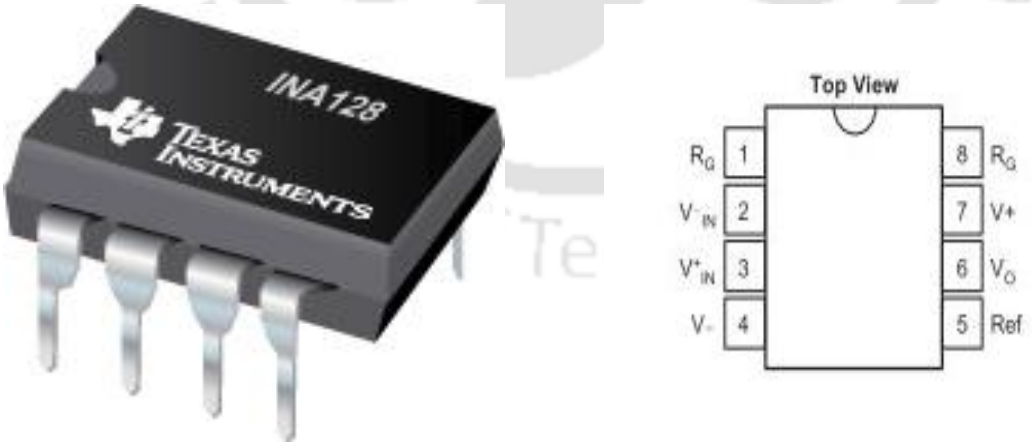

Figure 3.3: Photograph of instrumentation amplifier INA128.

(C) Voltage Regulator

Voltage regulator is essential for present experiments to provide required voltage. LM78L05 is a 5 volt positive voltage regulator and LM79L05 is 5 volt negative voltage

regulator. This voltage regulator is used in the circuit to provide the constant input voltage to the amplifier IC as well as to the transducer (strain gage). This regulator is as shown in Fig. 3.4.

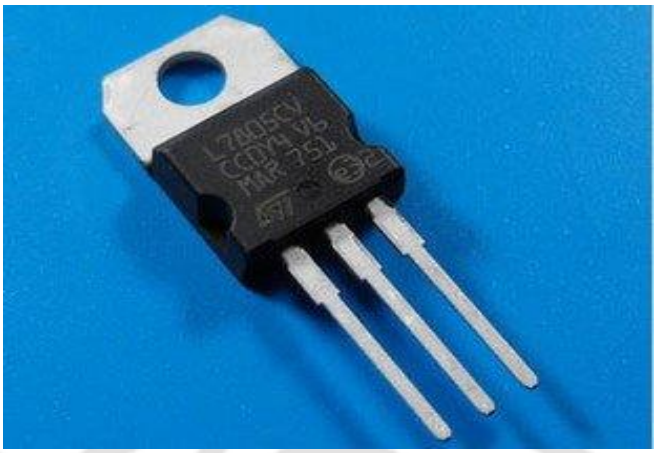

Figure 3.4: A Constant 5V regulator 7805.

(D) Strain Gage and Amplifier Circuit

Semiconductor strain gage output signal from the Wheatstone bridge is of very low strength hence for improving the strength of the signal the instrumentation amplifiers is used. Circuit diagram of strain gage assembly for the strain measurement and also the amplifier circuit has been designed and fabricated in house as shown in Fig. 3.5. The amplifier circuit works on a ±5V dual power supply.

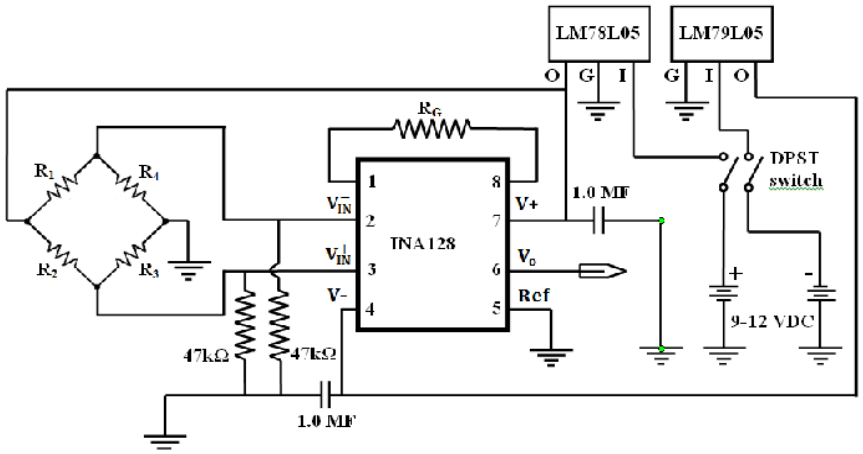

Figure 3.5: Schematic diagram of Wheat stone bridge.

A capacitor of 1.0 MF is connected between the +5 *V* input of the amplifier and ground, to handle any frequency response from the circuit. It will cut out the any oscillating feedback and pass it to the ground before it gets going to the amplifier IC. A resister with

higher resistance is connected at the signal input end of an amplifier IC to bypass the input bias current build-up in the circuit to the ground. The circuit designed and fabricated for strain measurement using the strain gauge through Wheat stone bridge circuit and corresponding amplifier circuit is shown in Fig. 3.6.

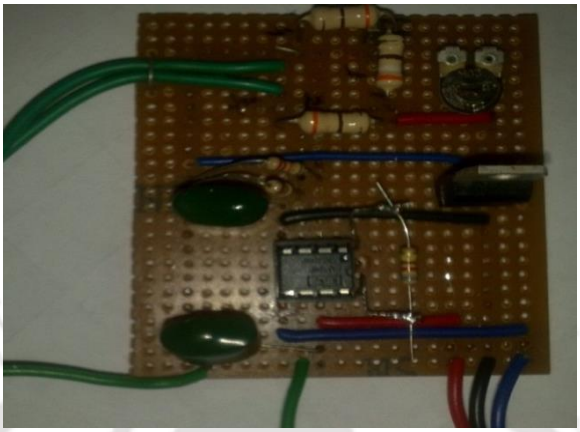

Figure 3.6: Photograph of the circuit diagram of wheat stone bridge and the amplifier.

The details of the experimental setup, the procedure for the experiments along with the test conditions are discussed in the following section.

3.2.3 Experimental Setup

Schematic of the experimental setup used for conducting the present step load tests is shown in Fig. 3.7. It consists of the rigid frame same as that of (Fig.2.3) model suspended freely by the help of two flexible wires which allows it to move in the horizontal direction. Also a horizontal cable attached at the end of the stress bar for keeping the model in the stable position. The flat surface of the cone base has been made as the choice to focus the laser beam of rotational vibrometer.

Wire cut technique discussed by Mee (2003) has been adopted to apply the step load for calibrating the force balances. A galvanized iron wire of 0.38 mm diameter, attached to the aluminum model through screw is allowed to hold the weighing pan at other end. A stand with the pulley arrangement is also fabricated to guide the wire and to maintain the zero angle of incidence between the applied force and test model. The aluminum model with the brass stress bar is provided with the fixing arrangement at the end of the stress bar to the frame for placing the model in the correct position during the experiment. Different weights are considered such as 2kg and 2.5 kg in this test for step load application.

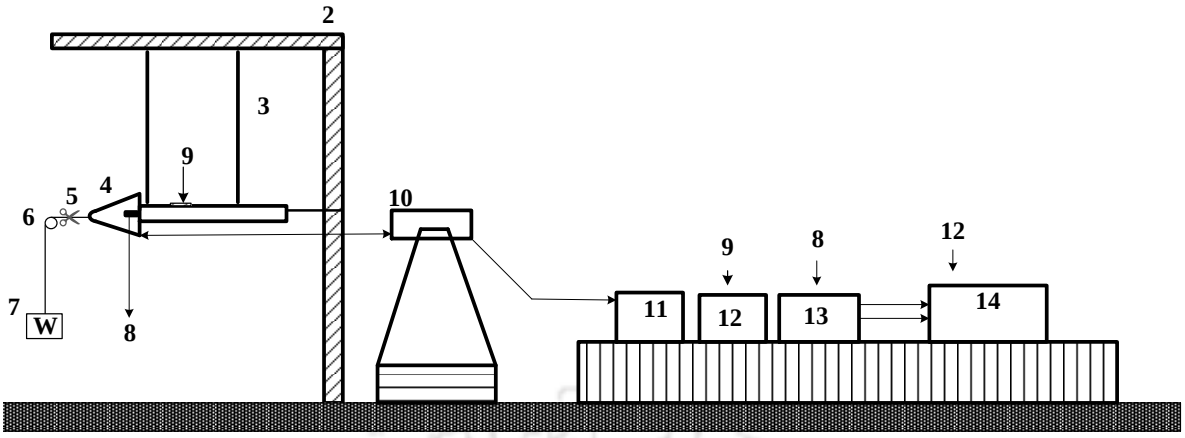

1

1. Concrete Bed
2. Inverted L- shaped frame
3. Flexible wires
4. Aluminum model with stress bar
5. Wire cutter
6. Pully, 7. Weighing pan
8. PCB piezo-electric accelerometer
9. Strain gage
10 .Laser vibrometer sensor head
11. Contorller of laser vibrometer
12. Strain gauge circuit with amplifier
13. PCB signal conditioner
14. Digital oscilloscope

Figure 3.7: Schematic diagram of experimental setup for step load test.

3.3 Results and Discussion

3.3.1. Experimental Measurements

Two different step forces of 22 N and 27 N are applied on the conical model by suspending the weights of 2 kg and 2.5 kg respectively and the weight of the pan is 200 gm. The horizontal calibration setup has been used for these experiments. The time history of the two forces applied on the model can be represented as shown in Fig. 3.8. Terminologies used in the figures are given in Table 3.2.

Table 3.2: Nomenclature used in the figures of chapter -3.

F-1 and F-2	Force histories for Case-1 and Case-2
A-1 and A-2	Acceleration histories for Case-1 and Case-2
V-1 and V-2	Velocity histories for Case-1 and Case-2
S-1 and S-2	Strain histories for Case-1 and Case-2
M, R	Measured, Recovered signals
e. g: R-F1-A : Recovered force history for case-1 from measured acceleration for case-1	

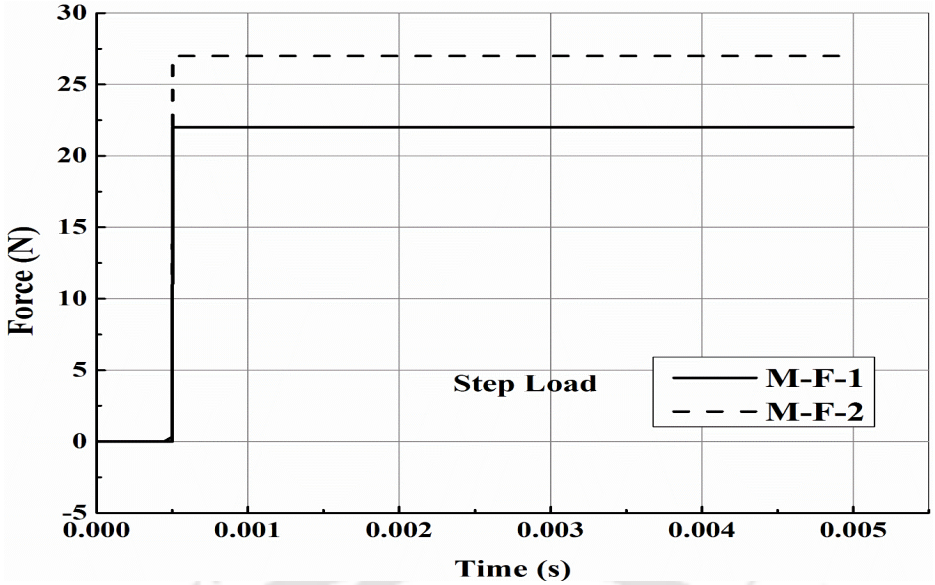

Figure 3.8: Step load history of 22 N and 25 N during the calibration tests.

Acceleration, velocity and strain histories are recorded during the step force application on the conical model. All these measurements are recorded for the period of 5 milliseconds duration. The results obtained from the experiment are used for the analysis of the system and thus to obtain the system characteristic function or the transfer function of the system under two different loadings.

The acceleration history for the applied step load is shown in the Fig. 3.9. It clearly resembles the typical trend of the step load applied on the body. This signal has been filtered with a low pass filter for filtering the low magnitude and low frequency disturbance data from the experiment. Since the wire cut process is a sensitive process at most care has to be taken during the test to avoid the low magnitude and low frequency disturbance in the signals. The undulations observed in the acceleration signal are due to the disturbance in signal during the load application. Also it is seen from the figure that the acceleration is drooping after a certain time of 2 ms.

The velocity history for the two different step loads applied on the model during calibration tests are shown in Fig 3.10. The velocity history is also plotted for a time of 5ms and it has been observed that the velocity gradually increases with time of the 5 ms. However, slope of the line decreases with increase in time which depicts the decrease in acceleration magnitude after certain time.

It can also be seen that there is no undulations in the velocity measurement since it is a non-contact type and the model motion is smooth over the measured time. This is the

advantage in the non-contact type such that the signal can be neat and clean with less low magnitude and low frequency disturbance and accurate.

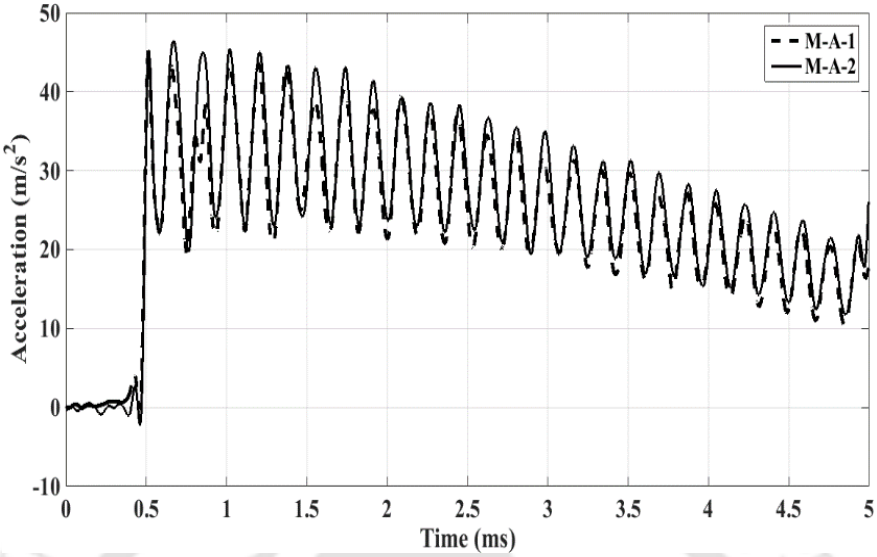

Figure 3.9: Comparison of measured acceleration history for two different step loads.

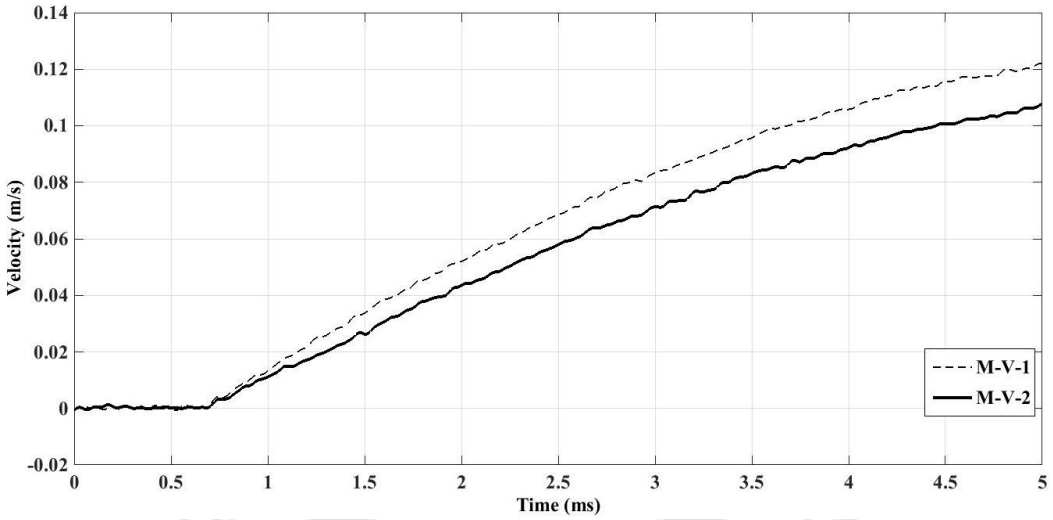

Figure 3.10: Comparison of measured velocity history for two different step loads.

The time history of the transient strain from the step load calibration experiments is shown inFig. 3.11. It can be observed that the signal has low magnitude and low frequency disturbance. Since the load applied on the model is of lower magnitude and there is no fixed support for the model that constrained to give a decent amount of strain and also the amplifier circuit and the connections are also responsible to add the low magnitude and low frequency disturbance to the strain signal. The magnitude of the strain obtained during these kinds of tests is very small compared to the other parameters due to the lower magnitude of force. The strain has increase in trend up to 0.5 ms. The higher magnitude of the strain can be observed using high step load calibration.

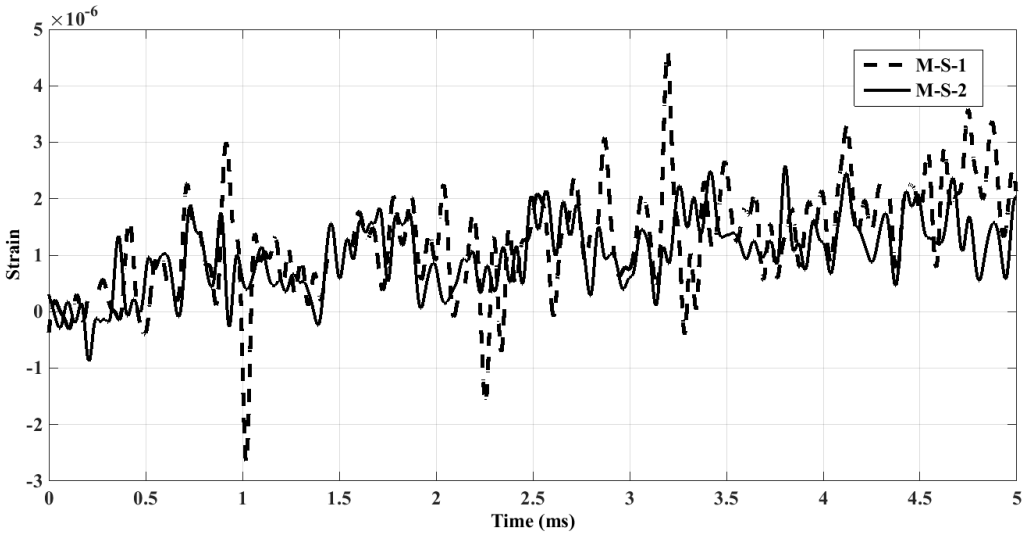

Figure 3.11: Strain history for two trials of the conical model for step loading condition.

3.3.2 Recovery of Step Load from the Calibration Tests

Fast Fourier Transform (FFT) based MATLAB program, discussed in chapter 2, has been used initially to obtain the transfer function and then to recover the force.

Here the response for the step load of 27 N is first used to obtain the system response or the transfer function which is then used to recover the step load of magnitude of 22 N using the response of the same. The same procedure is then executed for recovering the step load of 27 N using the transfer function obtained from the 22 N step load response. Figure 3.12 shows such recovered forces using measured acceleration from the cut weight test.

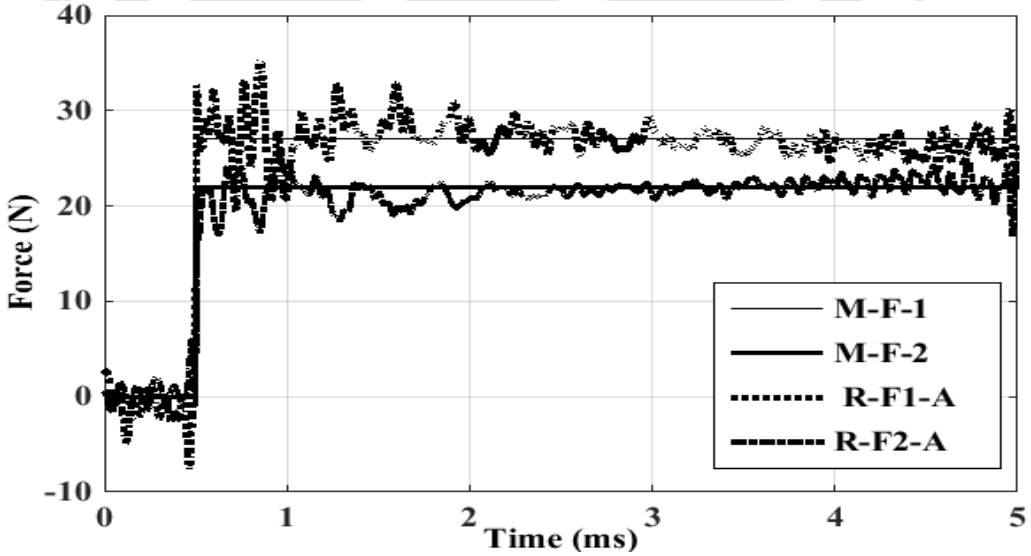

Figure 3.12: Comparison of measured and recovered force histories from acceleration history during step load calibration.

In the acceleration based recovery, it can be seen that the starting of the signal gives the over prediction of the force but during the time of 2 to 4 ms the forces are able to recover well by the transfer function with the time averaged error in the range of 2 %. But during the time of 4 to 5 ms, the acccuracy of the force is also reduced. The overall accuracy of the force predicted using the measured acceleration found to be reliable for the prediction of step load. The force recovery for the two step forces from the measured velocity is shown in the Fig. 3.13.

Recovery using velocity based measuremets confirm the applicability of non-intrusive force measurement using laser based velocity measurements.

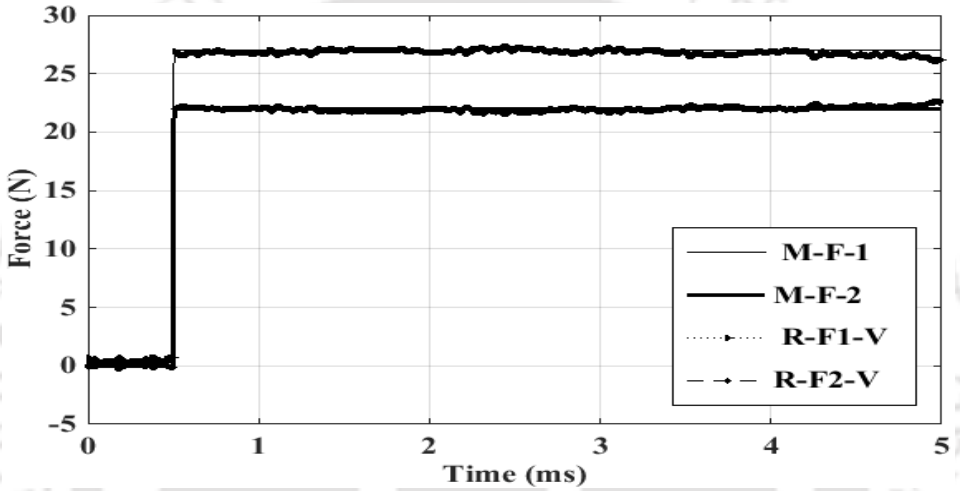

Figure 3.13: Comparison of measured and recovered force from velocity history during step load.

This non-contact type force measurement exhibits similarity with the contact type acceleration measurement in terms of the simplicity of measurement and onwards data processing. Increase in acquisition rate during step loading experiments can lead to improve the force recovery from the velocity signal as compared to the same discussed in last chapter for impulse loading. Similar recovery for the two step forces from the measured strain is shown in the Fig. 3.14.

Use of semiconductor high sensitivity strain gauges is seen to be helpful for force recovery force from small magnitude stain history. This force recovery is found to be oscillatory. Thus, all the three figures show excellent recovery of the forces however the deviations of the predicted value from the actual is observed due to the low magnitude and low frequency disturbance in the measured data from the experiment.

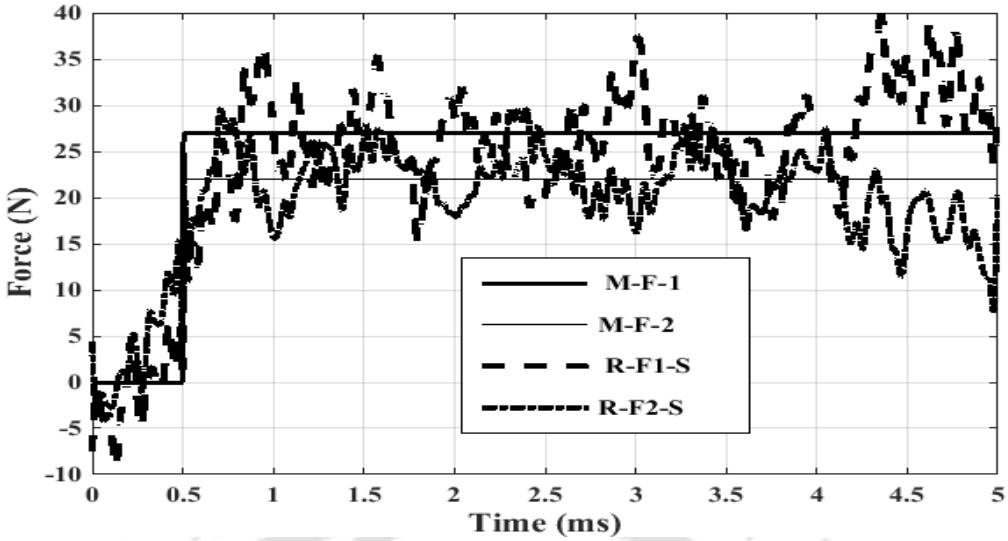

Figure 3.14: Comparison of measured and recovered force from strain history during step load.

3.4 Conclusions

Calibration test rig has been successfully developed for application of step load on a test model. Intrusive strain and acceleration measurements along with the non-intrusive velocity measurement are carried out during these calibration tests. The Fourier transform based convolution and de-convolution techniques are then implemented for establishing the transfer function and onwards force recovery. It is observed that the accuracy of the de-convolution technique during the transfer function calculation is sensitive to the low magnitude and low frequency disturbance in the signal measured during the experiment. Since the low magnitude and low frequency disturbance in the strain and the acceleration signals are observed to be more compared to the velocity history of the experiment, the prediction accuracy is also more for the velocity based recovery. In overall, excellent agreement has been noticed for recovery of force in the accelerometer based techniques and with high sampling rate in case of laser based velocity measurement technique. However in case of the strain gauge based force prediction the magnitude of the strain is very small and also the signal was very low magnitude and low frequency disturbance which affected the recovery of the force which results in reduction in the accuracy of prediction.

CHAPTER 4

COMPUTATIONAL METHODOLOGY FOR DESIGN OF ACCELEROMETER BASED MUTICOMPONENT FORCE BALANCES

Overview

Force measurement is one of the potential research topics in the field of hypersonic aerodynamics. Accelerometer force balance has been an appreciated choice for prediction of aerodynamic coefficients such as drag (C_d), lift (C_l) and moment (C_m) coefficients. In the present work the widely used AGARD (Advisory Group for Aerodynamic Research and Development) model has been considered to study the one way fluid structure interaction (FSI) at a flow condition of Mach 8 computationally. Unlike in the previous two chapters where single component force balances have been used in the present case three component force balance has been considered. Simulations have been carried out to obtain the optimum location and sensitivity of the accelerometers. Parametric study has been carried out by changing the property of the rubber material used in the AGARD model. This work will find application for conducting ground based short duration experiments using three components force balance.

Hence one way FSI analysis has been performed on the AGARD model of blunt nosed configuration with aft cylindrical body with L/D ratio of 4.44 equipped with internal rubber based accelerometer force balance system. This analysis has been carried out successfully for the simulation time of 2 milliseconds which corresponds to shock tunnel test duration to quantify drag (C_d), lift (C_l) and moment (C_m) coefficients and the performance of a three component accelerometer force balance. It is also seen that the flexibility of rubber material provides negligible resistance which enables free-flying condition to the test model under application of aerodynamic force. The intensity of the reaction force and moment and rubber deformation are checked by present simulations. Critical comments have also been made about the location of accelerometer mounting station for a three component force balance system. Present studies have successfully demonstrated that the one way FSI is an effective tool for designing force measurement experiments.

4.1 Introduction

Design of a flight vehicle is strongly dependent on its flow regime. Lower drag force and in turn lesser fuel consumption comprise the objective for flight vehicle design in subsonic or supersonic speed limits. Moreover, minimal surface heating for safety of the flight has been the foremost concern at hypersonic speeds. In view of this, generic hypersonic configurations are blunt nosed shape as explained by Sahoo (2003). Increase in wave drag experienced by the hypersonic vehicles and enhanced fuel requirement of the mission are the obvious consequences of highly blunted configurations. Hence, precise prediction of the force has always been the task ahead of the researchers working in the field of hypersonic aerodynamics. High enthalpy or hypervelocity impulse facilities like shock tunnels have been the apparent choice for force measurement and onwards prediction of aerodynamic coefficients. The computational fluid dynamics (CFD) analysis is one of the key tools to analyze the interaction of fluid and spacecraft. Actual flight test is also an alternative for prediction of the forces on the hypersonic configuration during its flight. Among the three conventional means of force predictions, testing in impulse facilities, the method proposed by Reddy (1978) has been the choice of many researchers due to moderate costs as compared to the flight tests and evolved instrumentation and sophistication. Moreover, computational tools have been considered for design of experiments so as to further reduce the experimental cost and acquire the test results more effectively.

Daniel and Mee (1995) carried out finite element (FE) analysis of the stress wave balance for design of a compact internal stress wave balance and selection of locations for strain gauge mounting on a conical model. Sahoo et al. (2007) carried out the FE simulations using NISA software package on a blunt cone model for the design of the accelerometer balances to use in the shock tunnel facilities and also studied the effect of flexibility of rubber material on the performance of accelerometer force balance so as to achieve free-flying condition. Smith et al. (2001) also performed FE analysis for the stress wave force balances for finding the force and moments. The FSI analysis is used in many areas to find out the interaction between the solid and fluid such as aero elastic effect on the turbine blade by Lee et al. (2012), wind shear effect on blade with non-linear geometry by Zhang et al. (2014). The literature based findings encourage the use of commercial computational tools in the design of experiments phase.

In view of the above, in the present work, detailed computational analysis of the accelerometer force balance is planned using fluid structure interaction via a commercial software ANSYS. Here the AGARD model used by Saravanan et al. (2009) during their shock tunnel tests (Fig. 4.1) has been considered. It is basically a blunt nosed cylinder of 51 mm outer diameter, 3 mm wall thickness and of length to diameter (*L*/*D)* ratio 4.44. The model is supported on a fixed support (marked 4), the rubber rings (marked 3) and the steel rings (marked 2). The dimension of all the parts of the model are shown in Fig. 4.1. In actual experimental setup the model is mounted on a solid rod to which the rubber ring is glued and the steel ring is screwed. One way fluid structure interaction (FSI) is used to achieve the set goals.

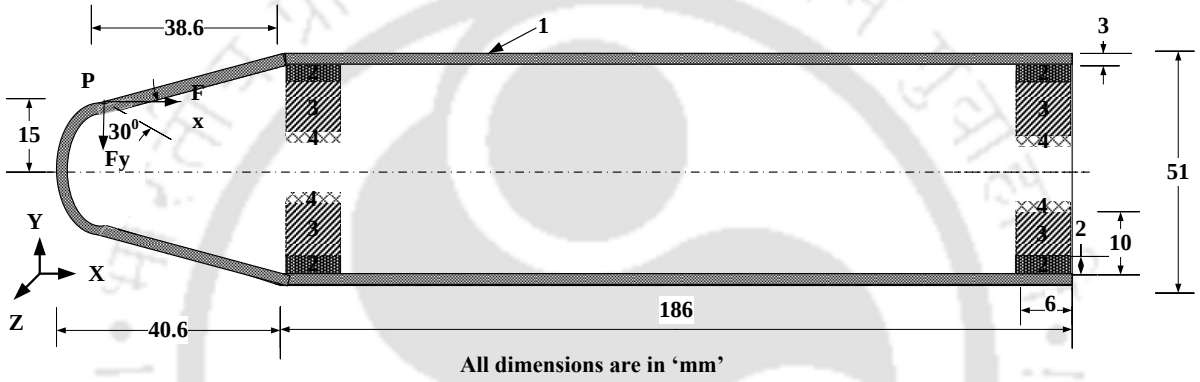

Figure 4.1: Schematic of the AGARD model considered for the computational analysis. (1 = Aluminum AGARD model, 2 = Steel rings, 3 = Rubber rings, 4 = Fixed support, P = Load application location, Saravanan et al. (2009)).

In one way FSI, CFD simulations are initially carried out to evolve the pressure field on the object of interest using known free stream conditions. This surface pressure is then transferred to the structural module to get the acceleration at various locations and reactions at the support.

The proposed one way FSI based studies are essential since FE analysis has been reported only for the choice of rubber material. Apart from this, there are certain assumptions in the accelerometer force balance based measurements. One such major assumption is the negligible magnitude of reaction forces and moments offered by rubber material in the experimental test duration. Therefore such possibility of 'free flying condition' in case of rubber based force balance needs to be examined. In view of this combined CFD and finite element (FE) simulation of AGARD model integrated with the

accelerometer balance is carried out to evaluate drag(C_d), lift $(C_l)$and moment (C_m)coefficients.

The reaction force, moment at the rubber support and the deformation of the rubber due to the applied pressure is also estimated from the FEM simulation. Such analysis is also useful for optimum selection of the test time and to select the location of accelerometer to maximize the strength of the signal. This modeling is found essential for design of experiment to predict the location of the sensor, magnitude of the signal for a given model material, data acquisition setting etc. The vital details regarding modelling and critical analysis of rubber based accelerometer force balance is given in following sections.

4.2 One way-FSI analysis using ANSYS

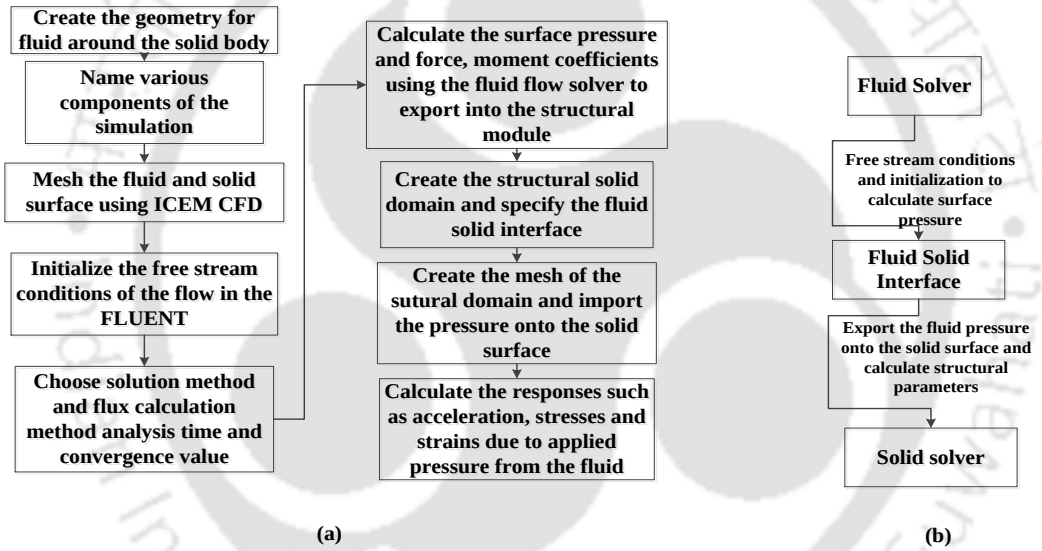

Figure 4.2: Flow chart of the ANSYS based one way FSI. (b) Schematic of one way FSI.

One-way coupling or the one way FSI methodology is also named as the un-coupled approach. In this methodology fluid flow based governing equations are solved initially to obtain the forces or force field on the desired configuration. Thus obtained forces and moments are then provided as input to the finite element solver to get the structural changes like deformation, strain, acceleration. Moreover, in this monologue, no data transfer takes place to the fluid flow solver from the structural solver. This is the major reason for the name of this method as one-way coupling or one way FSI. The schematic of the one way FSI methodology is shown in Fig. 4.2. In the present studies, all the simulations are performed in ANSYS workbench 14.5 which is equipped with Fluent for CFD and the Transient structural solver for the structural analysis.

4.2.1 Geometry Modeling and Meshing

Fluid and solid domains are created in the design modeler for the proposed conical AGARD model. Since the solid model is axisymmetric, cylindrical outer domain is created as the fluid domain. The outer surface of the solid model subtracted from the fluid domain and the structured meshing has been generated around the solid body for performing the fluid flow simulations. Apart from the mesh independence studies, care has been taken to capture all the flow features.

The accelerometer balance is also modeled inside the hollow axisymmetric solid domain with the detailed solid geometry containing the steel rings inside the model, inside the steel rings the rubber bushes and the rubber bushes are mounted on the sting. Figure. 4.1 shows the schematic of the solid model and the internal configurations. While the integrated fluid and solid domains are shown in Fig. 4.3. In line with the reality, the inner surfaces of the rubbers are fixed by imposing the displacement boundary conditions at those locations. The properties of the steel, rubber and aluminum used in present computations are shown in the Table 4.1. After the geometric modeling, ICEM module of the ANSYS is used for meshing. The structural model with hexahedral meshing is shown in Fig. 4.4 while Fig. 4.5 shows the locations where acceleration has been monitored. Details of the solid model are given in Table 4.2. Details of mesh considered for FE analysis is given in Table 4.3. The test model has been simulated using the one way FSI for four angles of attack namely 0, 4, 8, and 12.

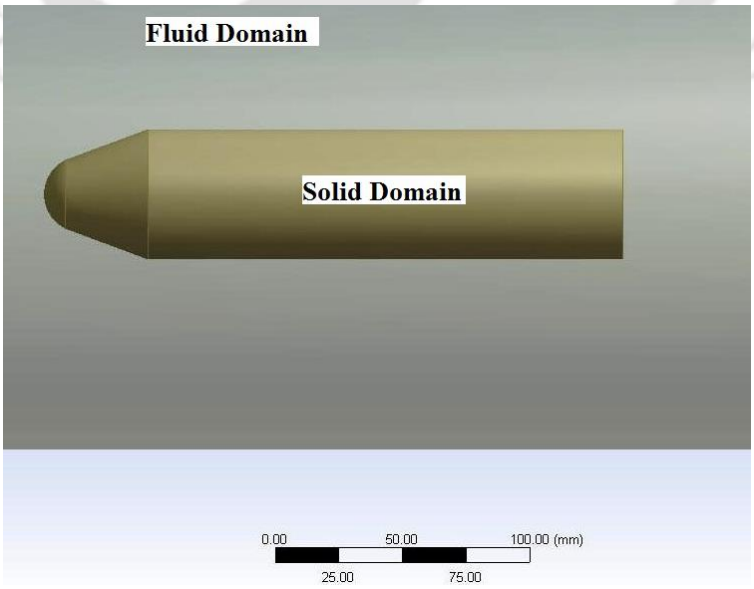

Figure 4.3: Integrated fluid and solid domains used in the present computation.

Table 4.1: Material properties of the solid model

Material	Density(kg/m^3)	Young's Modulus	Poisson's Ratio
Aluminum	2770	71 GPa	0.32
Stainless Steel	7750	193 GPa	0.31
Neoprene Rubber	960	0.3 MPa	0.49

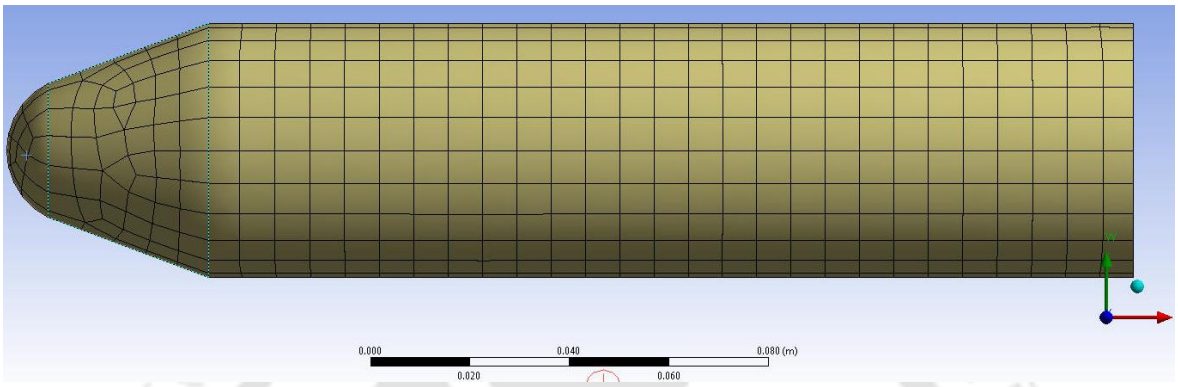

Figure 4.4: Structural model and its typical meshing considered for present simulations.

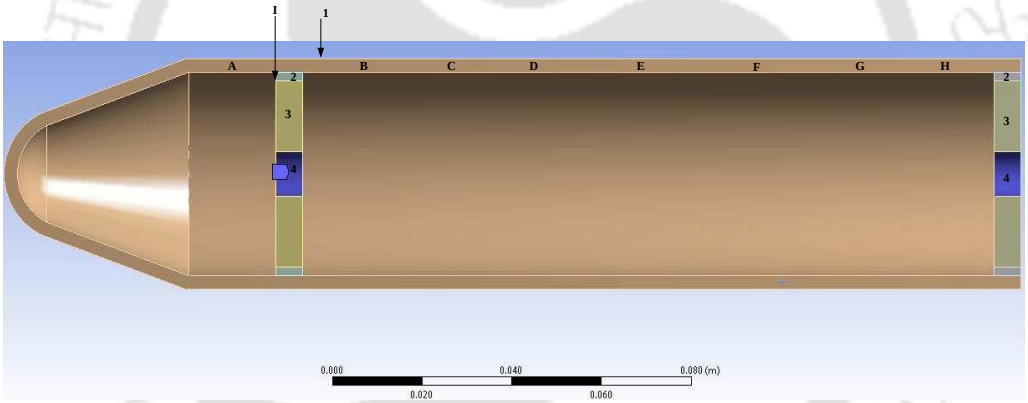

Figure 4.5: AGARD model displayed with response measured locations.

Table 4.2: Details of Solid model

Mass in kg	Centre of Gravity location from nose in mm
0.365	81.11

Table 4.3: Details of meshed solid and fluid domain

Angle of Attack	CFD mesh nodes	FEM mesh nodes
0	245392	8831
4	226218	11331
8	486840	32119
12	518762	14395

4.2.2 Fluid flow analysis or CFD analysis

This section deals with the CFD simulations which are carried out using FLUENT for the proposed test model. In the present studies, Euler or inviscid flow simulations are considered to obtain the pressure distribution on the model surface. The free stream conditions used by Saravanan et al. (2009) form the input for CFD simulations. Here, free stream pressure (p_∞) is 212 Pa, free-stream temperature (T_∞) is 149 K and the Mach number is 8.0. Density based methodology has been opted for computations along with the Implicit AUSM scheme for inviscid flux computations. Here Air is considered as the working fluid with the assumption of ideal gas having specific heat at constant pressure (C_p) as 1.005 KJ/kg. K and molecular weight as 28.996 g/mol. Pressure and Mach number contours obtained from the present simulations are as shown in Fig. 4.6 and Fig. 4.7 respectively for zero degree angle of incidence.

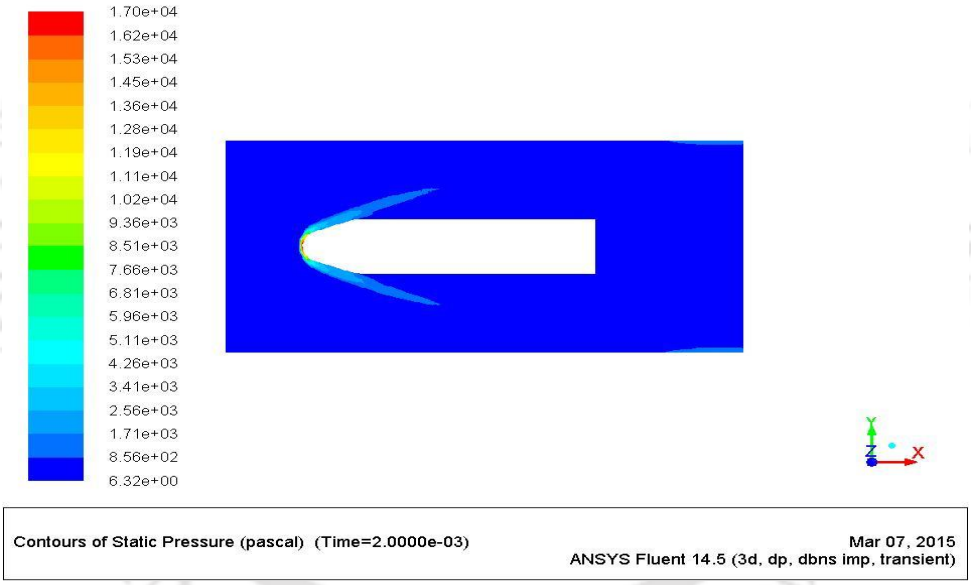

Figure 4.6: Static pressure contours of AGARD model for given free stream conditions from CFD using FLUENT.

Figure 4.6 shows that the static pressure is very high at the leading edge of the model but the intensity of the pressure is very minute in the other regions.

The Mach number clearly portrays (Fig. 4.7) the ability of present simulations to capture the shock profiles well. Comparison of various aerodynamic coefficients obtained from present simulations with the literature reported findings is as shown in Fig. 4.8. Thus Drag coefficient (C_d) (Figure 4.8(a)), lift coefficient (C_l) (Figure 4.8(b)) and moment coefficient (C_m) (Figure 4.8(c)), are the main outputs from these CFD simulations. Magnitude of all these aerodynamic coefficients at different angle of attacks is in well

agreement with the literature reported results of Saravanan et al. (2009). As seen in the figure, drag force component gradually increases with increase in the angle of attack due increment in high pressure region. Due to the same reason, lift force obtained from the CFD simulations shows increment with angle of attack.

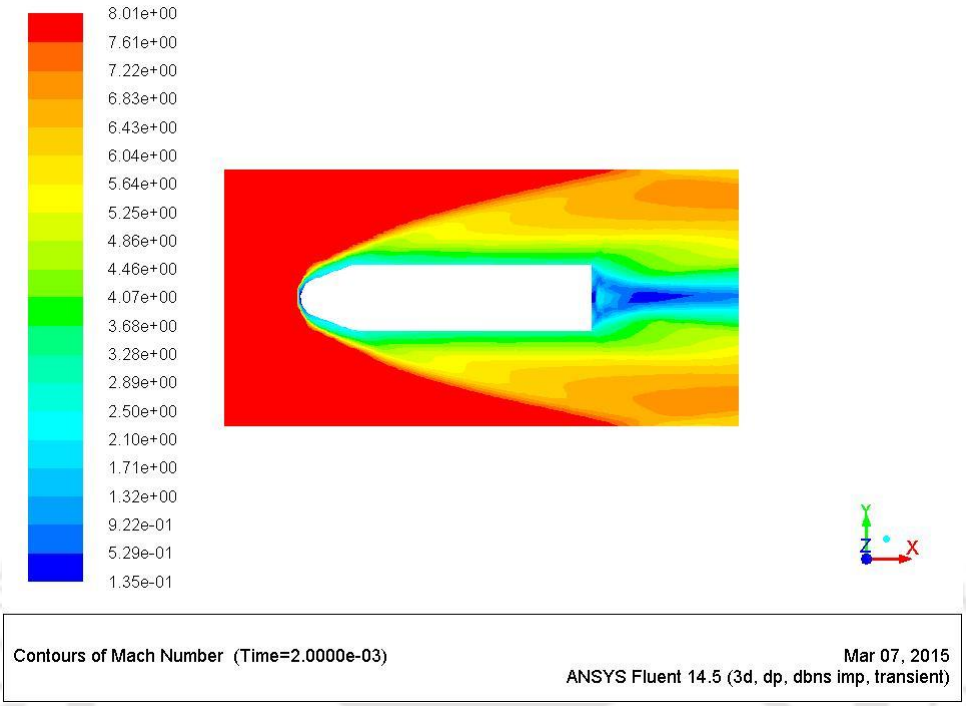

Figure 4.7: Mach number contours of AGARD model for given free stream conditions from CFD using Fluent.

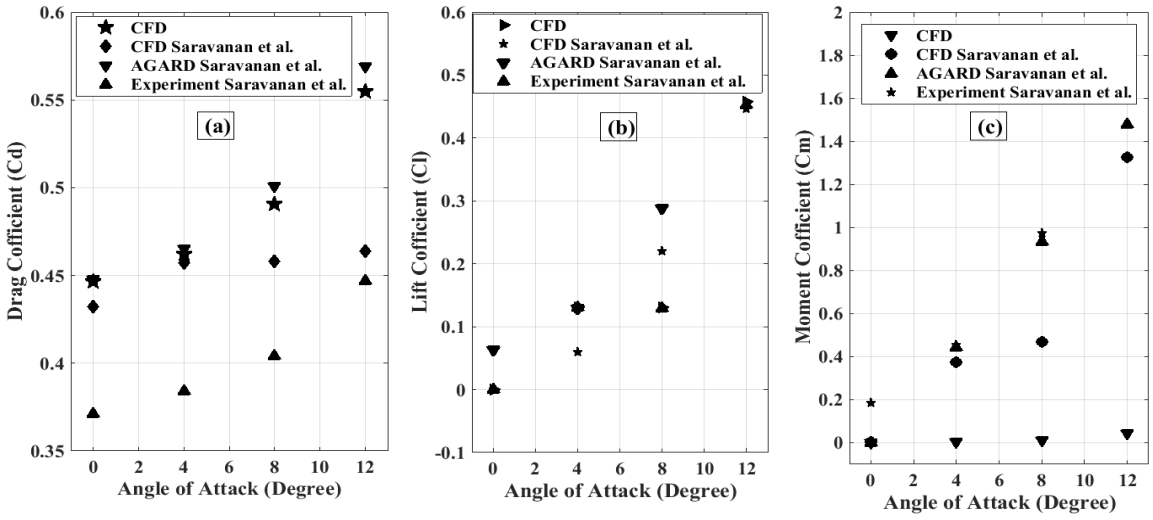

Figure 4.8: Comparison of (a) drag coefficient (C_d), (b) lift coefficient (C_l), (c) moment coefficient (C_m).

4.2.3 Transient structural analysis of the AGARD model

The time integration in the case of one way FSI and FE analysis is implicit type Standard Newmark time integration method. Transient structural module of the commercial solver ANSYS is used for analyzing the performance of three component accelerometer balance. The output from the Fluent, mainly pressure on the solid-fluid interface, is passed as the input to the structural solid domain. The inner surface of the rubber bushes is constrained from its motion for simulation of rubber based accelerometer force balance for simulating the free-flying condition. The structural domain is also solved using the same time settings as that of Fluent to obtain the acceleration of the model at specified locations. Both free flying and fixed-fixed conditions of the rubber in the force balance are used for verification of free flying nature obtained from the force applied on the surface of structural solid surface.

4.3 Analysis of Accelerometer Force Balance

Transient structural simulations are carried out for the duration of 2 milliseconds which is in the range of typical test duration of a hypersonic shock tunnel (0.7 to 2 ms). In this phase, magnitudes of accelerations are monitored at different locations on the surface of the body. The deformation of the interface point of the rubber and steel ring (marked I, J in Fig. 4.3) is traced in the axial, normal and azimuthal direction for the applied force which gives the deformation of the model in short test duration. It is observed that the deformation at both locations I and J are same. So for only one position at 'I' the results have been shown in Fig.4.9. It shows the deformation of the rubber for the applied force and also gives the idea of how much the rubber deforms in this short test time and it is in the allowable range of its yield point so that it can come back to its original state after the removal of the force.

Figure 4.10 shows the variation of acceleration with time in axial and normal direction for the free flying, and fixed boundary condition. The free-flying boundary condition is referred here as free while fixed boundary condition pertaining to accelerometer force balance is referred here as fixed. Excellent agreement between the acceleration signals for location 'I' is evident from Fig. 4.10.

Hence the assumption of free flying condition in the presence of flexible rubber material is seen to be valid for the typical shock tunnel experimental duration. The major reason for this validity is the lower values of reaction forces and moments offered from the support. Time trace of these support force reactions for different angles of attack are shown

in Fig. 4.11 and Fig. 4.12 which shows the axial and normal reaction force respectively. The nomenclature used in the succeeding figures of this chapter is mentioned in Table 4.4.

Table 4.4: Nomenclature used in the figures of chapter-4.

D-X, Y, Z	Deformation in X, Y and Z direction
A-X, Y	Acceleration component along X and Y axis
R-X,Y	Reaction force along X and Y direction
R-M-X, Y, Z	Reaction moment in X, Y and Z direction

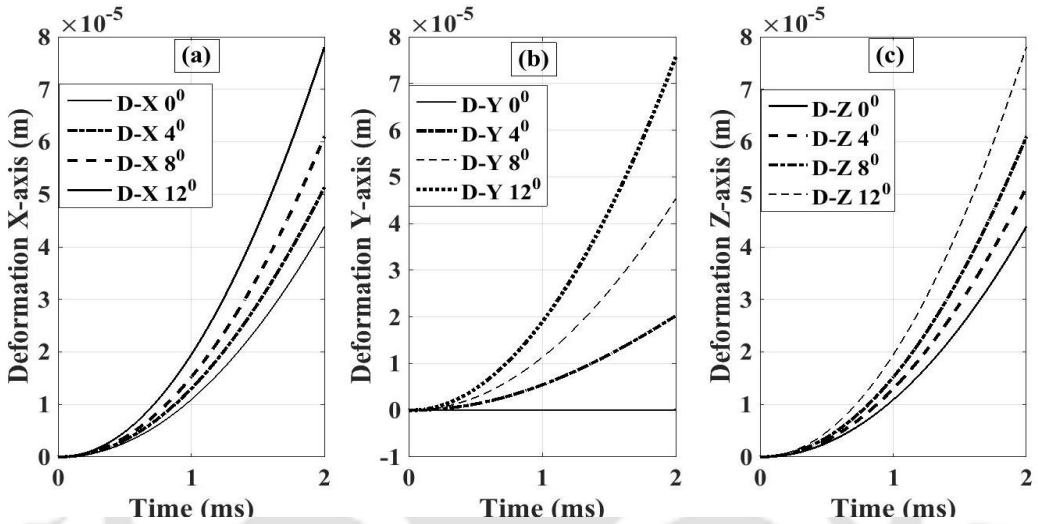

Figure 4.9: Deformation history at the interface of the rubber and the steel ring of AGARD model for different angle of attacks, (a) axial deformation, (b) normal deformation, (c) azimuthal deformation.

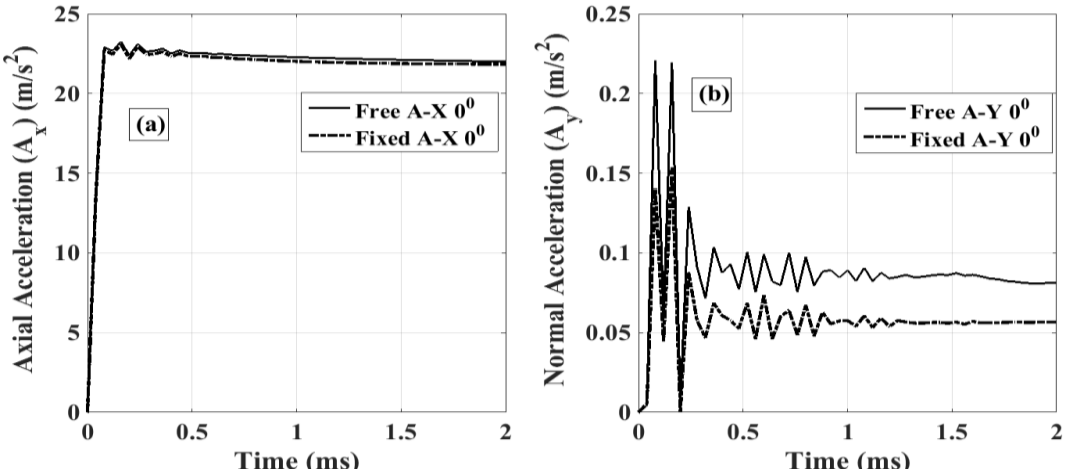

Figure 4.10: Acceleration history of free-free and fixed configuration in (a) axial and (b) normal direction at location B.

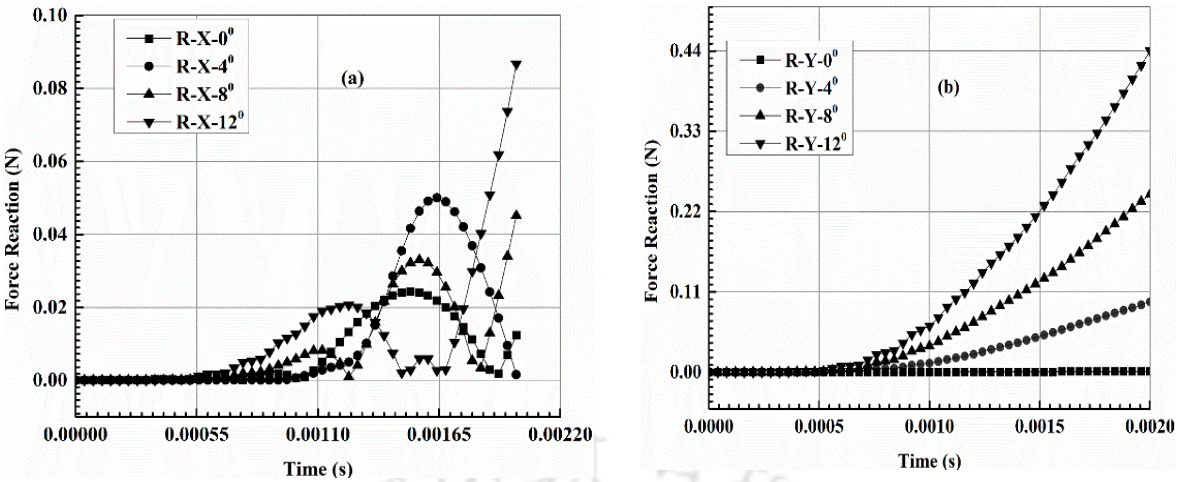

Figure 4.11: (a) Axial, (b) Normal reaction force histories for AGARD model for different angle of attacks from one way FSI simulation.

Reaction moment magnitude and its variation with angle of attack is as shown in Fig.4.12. (a) axial moment reaction and (b) normal moment reactions and (c) azimuthal moment reaction. Axial and normal moment reactions do not exist because the moment is applied only due to pitching which suffers a reaction moment in Z-direction which is more as compared to the moment in other two directions at the end of simulation time. However the maximum values of azimuthal moment depends on the test duration and angles of attack. The moment is very less till 1ms 1% but a sudden rise of the moment is observed after 1ms which is 10% of the applied moment. On the similar line, support reaction moment is also of negligible magnitude. Therefore, it is evident that the free-flying condition is possible for the accelerometer force balance with rubber based flexible mounting system due to low magnitude reaction forces and moments. This is the major reason for fabrication of the test models using aluminum materials which helps to use low sensitivity accelerometers for force measurement. These simulations are thus useful which predict the strength of acceleration signal for a given model material which can be used to make a proper choice of accelerometer and also to set the data acquisition system.

Present studies are also extended to investigate the optimum location of accelerometer mounting station for front and aft-lift accelerometers. The acceleration variation with angle of attack in axial and normal direction at location 'B' is shown in Fig. 4.13. The front and aft lift accelerations at different angle of attacks along the length is shown in Fig. 4.14.

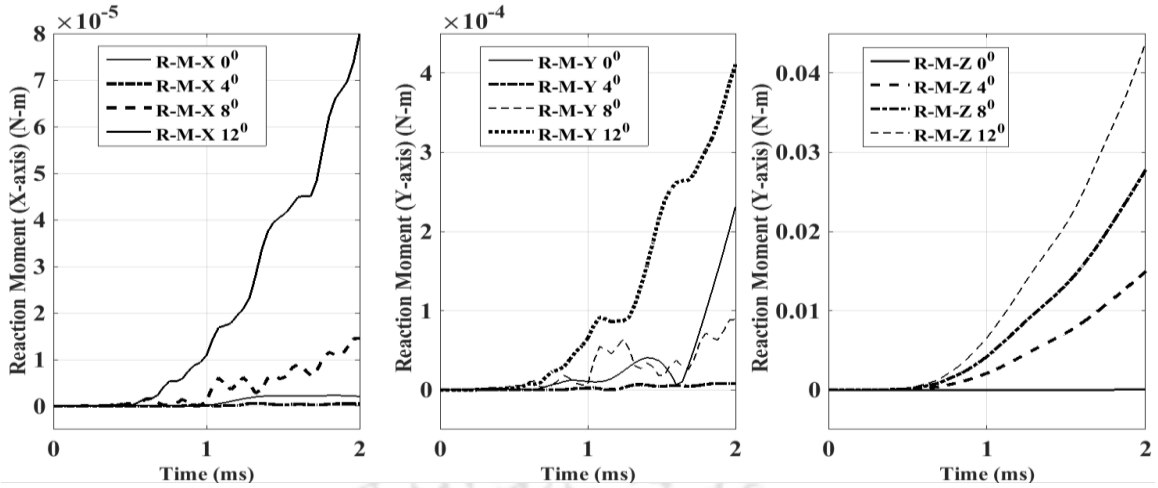

Figure 4.12: Reaction moment history obtained for AGARD model for different angle of attacks. (a) Axial moment, (b) normal moment, (c) azimuthal moment.

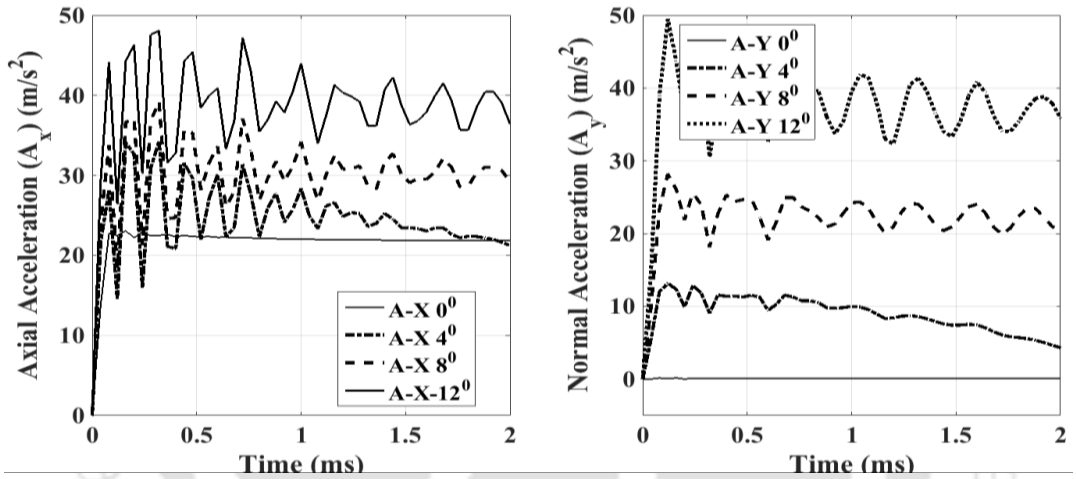

Figure 4.13: Acceleration history of the model at location 'B' subjected to force with various angle of attacks. (a) Axial, (b) Normal acceleration.

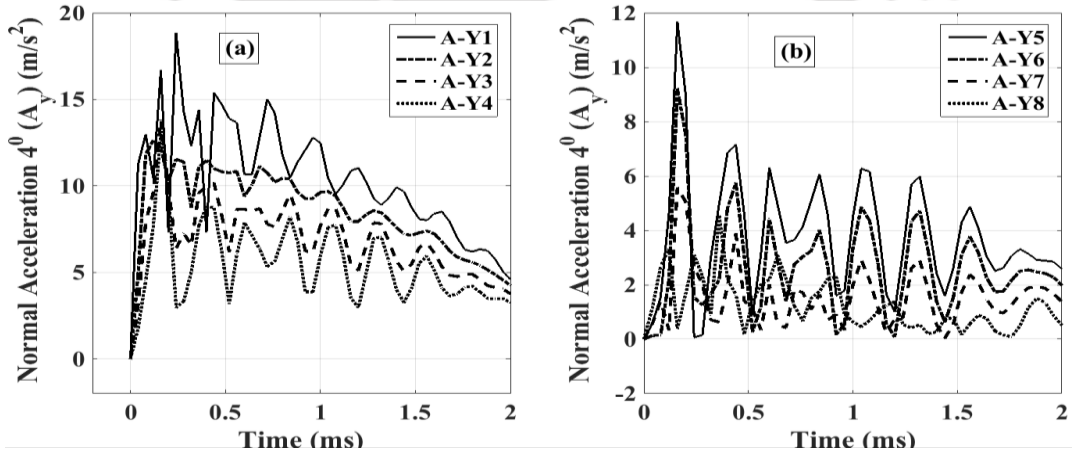

Figure 4.14: Acceleration history for the 4^0 angle of attack along the length of the model. (a) Before the center of gravity, (b) After the center of gravity.

In Figure. 4.14 location 1 to 8 corresponds to that of the 'A' to 'H' as mentioned earlier in Fig. 4.5.

It is clear from this fig. 4.13 that the strength of acceleration signal is high at the leading edge and also smooth but with increase in the distance from the leading edge the magnitude of the acceleration decreases and the fluctuations of acceleration also increases. The length of the model is one of the factors which affects the magnitude of acceleration for the applied force on the body. Hence for the longer and slender bodies to be used in the shock tunnel test the accelerometers should be kept near to the leading edge to avoid the low magnitude and low frequency disturbance and the reflections of the acceleration signals. Such enhanced acceleration signal would increase the signal to low magnitude and low frequency disturbance ratio or permit to use the low sensitivity accelerometers. The normal accelerations are also plotted for the 4^0 angle of attack (Fig. 4.14).

4.4 Conclusions

Simulations for fluid flow and structural solver are carried out successfully to access the performance of accelerometer based force balance. These simulations are carried out for both free-flying condition and constrained motion of rubber bush for time duration corresponding to typical shock tunnel test time (2 milliseconds). Drag (Cd), lift (Cl) and moment (Cm) coefficients are obtained from the CFD analysis and are in good agreement with the literature reported values. The magnitude of the reaction force in the axial and normal direction are within the range 1 % of the applied force, however for 12^0 angle of attack the magnitude of normal reaction force increases abruptly up to 5 % once the test time crosses 1 ms. But the other angle of attack gives low value of reaction force even in case of 2 ms. Hence the test time and angle of attack are the influential parameters for the reaction force. Same thing is observed with reaction moment also. Sufficient flexible rubber bush material is seen to provide the free-flying condition to the test model under application of aerodynamic force. It has also been noticed that the aluminum models provides higher strength of acceleration signal or supports the applicability of low sensitivity accelerometer. From present one way FSI analysis, it has been suggested that the accelerometers used for the lift measurement are recommended to put near to the leading edge of the model. Also the normal acceleration signal droops beyond the 1ms test time and the drooping increases beyond that point. Thus the current FE simulations for accelerometer force balance are found suitable as a tool for design of force measurement experiments.

CHAPTER 5

DESIGN OF A NEW ARTIFICIAL NEURO-FUZZY INFRERENCE SYSTEM FOR PREDICTION OF SHORT DURATION FORCES

Overview

Present chapter deals with the application of Finite Element Method (FEM) and intelligent soft computing techniques viz. Neural Network (NN), Artificial Neuro-Fuzzy Inference System (ANFIS) for the prediction of short duration impulse, ramp and hat forces. Two configurations have been considered in these investigations and FE analysis has been carried out on the two models viz. hemispherical model (Model A shown in Fig. 5.1) and Advisory Group for Aerospace Research and Development (AGARD) model (Model B in Fig. 5.2). The axial and normal accelerations for various applied forces is obtained at various locations. These known applied input force and output acceleration of the system are used for the training of the NN and ANFIS. After the training is completed, the optimum parameters are obtained and they are used for the prediction of the unknown forces and the moments. It is observed that the neural network is unable to recover the unknown forces and moments. However ANFIS based better strategy is evolved for prediction of the same forces and moments. Thus novelty of these studies lies in assessment and successful implementation of the soft computing techniques like neural network and ANFIS for prediction of the unknown short duration force and moment time histories.

5.1 Introduction

Blunt cones are generally designed for hypersonic missions to reduce the surface heating loads. However, such configurations amplify the forces and moments acting on the spacecraft. Therefore prediction of forces and moments is essential for high speed applications in order to predict the range of the vehicle and to arrive at the deflection of the control surfaces for necessary action. High enthalpy test facilities like shock tunnels are the ground based experimental set-ups generally considered to simulate the inflight loading on the proposed spacecraft configuration. Prediction of the forces and moments from such experiments using acceleration or stain signals has been the topic of investigation for various research groups such as Robison (2006), Smith (2001) and Daniel and Mee (1995).

The accelerometer based force measurement technique is largely based on requirement of free flying or un-restrained condition of the test model during the experiments. One such concept of a free flying test model was employed by Naumann et al. (1991) during their experiments in the shock tunnel. Similar concept of accelerometer force balance was designed by Vidal (1956). It was then extended by Joshi and Reddy (1986) for the measurement of force on the typical hypersonic configuration by using rubber based support system. Sahoo et al. (2007) demonstrated practical use of the rubber springs and it was proved that the effect is insignificant and consequently the model can be assumed to move as a free-body during the tunnel run time. In these measurements, it had been assumed that the resistance offered by the rubber for the movement of the test model is negligible and the model mounting system along with the test model attains the steady state within the test duration which is of the order of 1 millisecond. These assumptions reduce the complications in prediction of the force by evading the calibration of the measurement system. Although most of the literature reported investigations neglect the reaction offered by the rubber, Menezes et al. (2011), considered the same by accepting the assumption of steady state in acceleration measurement. However, Kulkarni and Reddy (2008), during their shock tunnel testing using accelerometer force balance, employed de-convolution technique to recover the force on a blunt cone model and thus extended the application of this technique excluding the assumptions made earlier.

Simmons and Sanderson (1991) developed a stress wave force balance technique which directly predicts the applied drag force on a non-lifting model from the stress wave data measured in the structure under consideration. Here the test model and support system

are assumed to constitute a linear dynamic system under sudden application of aerodynamic load. Such stress wave force balance needs to undergo an extensive calibration before conducting the experiments in the test facility. These calibration experiments are essential to obtain the system response function matrix. Mee (2003) (Shock waves) described numerous experimental calibration methods to find the system response function. Among some miscellaneous force measurement techniques, force measurement using a non-contact type laser balance for applied load of impulsive nature has been carried out which was discussed in chapter 2. Here as well, calibration and de-convolution have been considered for force recovery.

In all the above mentioned literature, prediction of forces is either carried out using a simplified methodology based on some assumptions or by using de-convolution technique. But some of these predictions are limited to very simple models and single degree of freedom system. Rest of the studies for the prediction of the short duration force are based on rigorous calibration and extensive mathematical formulation. These limitations in turn limit the extension of these techniques for complex configurations and higher degree of freedom systems. Hence it is felt to consider the soft computing techniques which are successful and widely used for force prediction in various mechanical processes. Rath et al. (2010) used neural network (NN) model for the prediction of rolling force. Nayak et al. (2014) predicted cutting force during milling using the ANFIS model. Panda et al. (2008) predicted flank wear using back propagation neural network during drilling, Rizal et al. (2013) obtained online tool wear during turning process. Azari et al. (2014) used neural networks, multi regression and ANFIS for prediction of forging force during radial forging process. Rapid damage detection in the automobile structures has been performed by Zhu and Wu (2014) using ANFIS and interval modelling techniques.

In view of the wide acceptance of soft computing techniques in various fields of science and engineering, implementation of the same for force recovery in high speed flows is the major objective of present study. This study is essential since it evades the use of complex convolution and de-convolution algorithms. Soft computing techniques are thought as an alternative to these conventional methodologies since such techniques are considered for many complex processes or for higher degree of freedom mechanical systems. Besides, these techniques have never been considered for recovery of short duration forces generally encountered during the experiments in hypersonic flow regime which is the prime motive of present investigations. However, successful implementation demands for proper evaluation of soft computing techniques for their consideration in this field. Apart from this,

development of methodology for proper execution of the concerned technique for accurate prediction and associated error analysis needs to be evolved. Thus, major attention of the present study is centered on the implementation and possible consideration of the standard soft computing techniques viz. NN and ANFIS for recovery of transient force. In view of this, all the possible parametric variations are considered while implementing these techniques for recovering the three dimensional forces and moment system using the three component accelerometer force balance.

Initially finite element (FE) simulations are carried out to acquire the accelerations at three pre-set locations for time varying applied force. These accelerations are then considered for recovery of the forces and moments using the soft computing techniques under consideration. Details of the test model, FE analysis and parametric variation in the implementation of force recovery are discussed in the following sections.

5.2 Numerical Modelling

5.2.1 Finite Element (FE) Modeling

Two models are considered for the present analysis on which the impulse loads are applied and the accelerations are obtained using FEM. Two models which are, model-A and model-B. Model-A shown in Fig. 5.1. It resembles with the test model of the hemispherical shape with supporting structure as considered by Sahoo et al. (2003). It essentially is a generic hemispherical model of aluminum material attached to a 150 mm long brass bar. The model is free to move in axial (X) and normal (Y) direction but is constrained in the azimuthal (Z) direction. The second configuration considered is a standard model used for aerodynamic force measurement in hypersonic environment by AGARD. This Model-B of length to diameter (L/D) ratio of 4.44 is shown in Fig. 5.2. Such AGARD model has also been tested in hypersonic shock tunnel by Saravanan et al. (2009). Therefore the analysis for the test Model-B is carried out with the part of model mounting system such as steel rings and rubber bushes which are fixed inside the aluminum body so as to obtain the free flying condition. The displacement boundary conditions are imposed on inner area of the rubber by constraining it such that there is no motion conditions are also as given in Fig 5.2 where inner surface of the rubber is fixed hence there is no permissible displacement of the corresponding nodes in any direction. The same model has been used in the analysis carried out in chapter 4 but the difference is that the

forces that causes the acceleration are also obtained from the CFD simulation and are exported to the structural analysis. In the present case the forces data is given directly on to the structural model and the corresponding acceleration is obtained from the simulations.

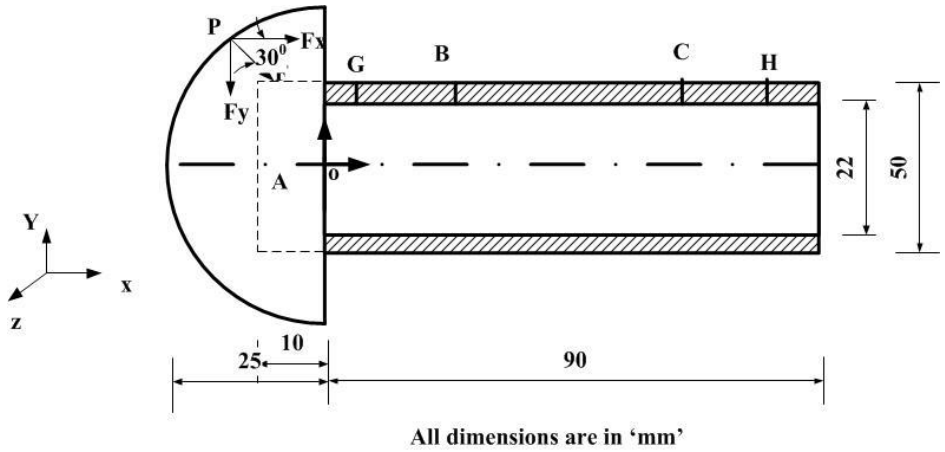

Figure 5.1: Schematic diagram of hemispherical model with stress bar (Model-A).

Transient finite element analysis has been carried out for both the models using ANSYS (Version. 14.5) for the simulation time of 5 milliseconds which corresponds to the range of shock tunnel experimental test time. During meshing for these test models, 10-noded tetrahedral (Solid 187) elements are used. After the detailed mesh independence studies, the number of elements obtained in case of hemisphere (model-A) is 29040 and the number of elements used for the analysis of the AGARD model (Model -B) is 13808.

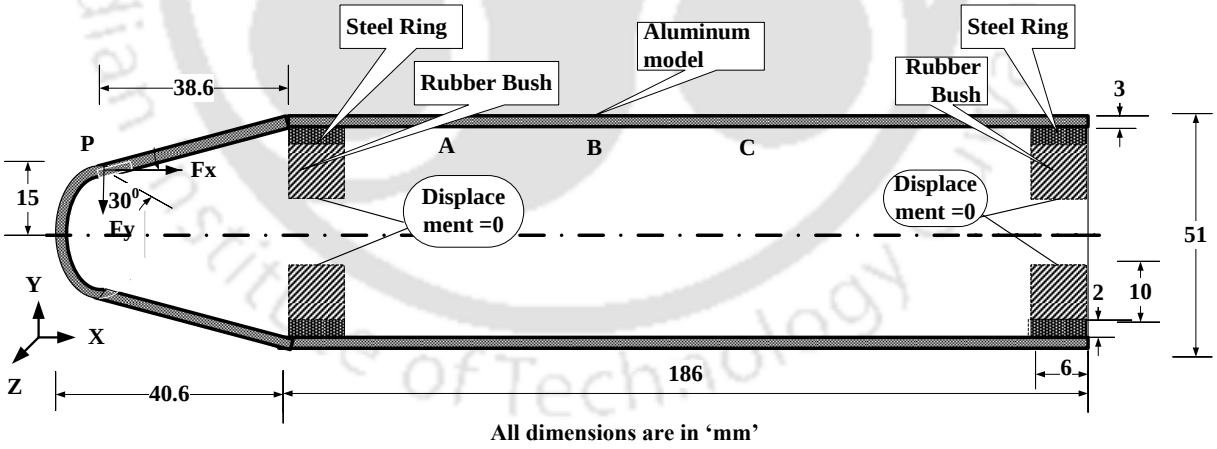

Figure 5.2: Schematic diagram of AGARD model with rubber based three component force balance. (Model-B).

During the FE simulations, zero displacement in Z-direction has been imposed at nodes G, H (Model-A) which allows the body to move only in the X- and Y- directions. For model-B the inner area of the rubber bushes has been imposed with zero displacement in all the directions as shown in Fig. 5.2. Force of different temporal variations and magnitude

has been applied at point P in both the cases. The acceleration signals for each of these applied forces have been recorded at points A, B and C locations as shown in Fig.5.1 and Fig. 5.2. Acceleration signals obtained in some cases are then used for training the neural network and the ANFIS models along with the respective forces; while acceleration signals from rest of the cases are used to recover the corresponding applied forces.

5.2.2 Introduction to Neural Network and its Applications

In the present era, sophisticated artificial intelligence methods or soft computing techniques are widely used in all most all the fields of engineering such as optimization, design, control systems, data classification and optimum parameter estimation during the mechanical processes such as drilling, milling and rolling. The main principle of one such soft computing technique, neural network (NN), is to predict the unknown data from training of the various input variable. It is a statistical non-linear data modeling tool. Neural network in general is a set of various interconnected elements called neurons in a structured manner which are useful for solving the relationship between input and output for any complex process. Structure of such neural network is as shown in Fig. 5.3. The artificial neurons are similar to the human neurons. These are designed based on the inspiration of the biological neuron system and their structure. Unsorted data can also be handled during the training of the neural network model. These neurons form the system between the input and the output. There are two different stages while working with the neural networks which are training and testing. Multi- layer neural networks are generally used for the training and testing, where there are input layers, output layers and several hidden layers. The input layer consists of the factors that influence the output parameters such as response from the system. Hidden layers are present in between input and output layers. The hidden layers use these inputs of the system and assign the model weights and send it to the output layers. The size of the input layer depends on the number of input parameters.

While finding the system characteristics or training the network it takes the data from the input and output given by the user and then assigns the weights. This intern acts as an adaptive capability which is learning of the system from the given data. Here, the transfer functions determine the model weights between any two layers. There are several types of transfer functions such as Tan sigmoid, Log sigmoid and pure linear (MATLAB, 2014). During training with one such transfer function, weights will be used to predict the data given to the NN. The output ‘U’ of each neuron is then calculated from Eqn. 5.1.

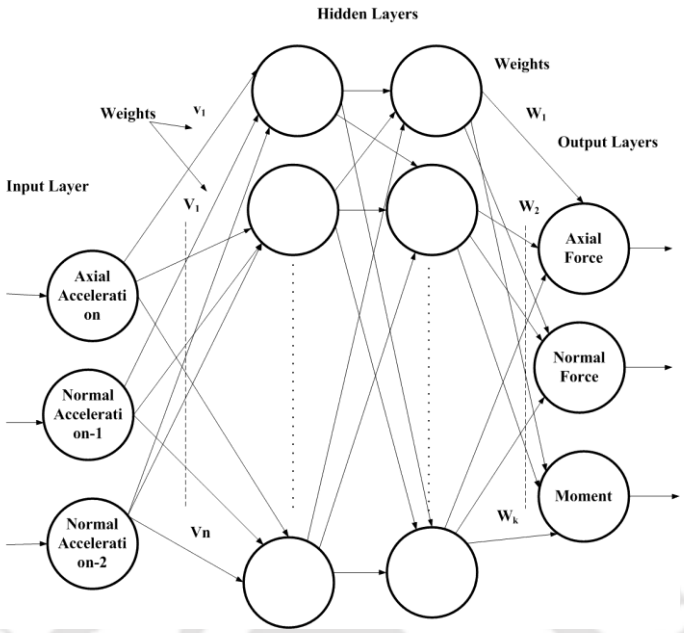

Figure 5.3: The NN structure for prediction of the axial force, normal force and the moment from the two hidden layered network. Pratihar (2009).

$$U = \mathrm{f}\left(\sum_{i=0}^{n}(w_i \times x_i) + b_i\right) \tag{5.1}$$

Here U is the output from the neural network, n is the number of inputs of the input layer. w_i is the weights related to the connection of the input and the hidden layer as well as the hidden layer to output layers, x_i Represents input values from the preceding layer, b_i is the biased value of the network, f is the activation function used for the analysis.

Feed forward back propagation technique is preferably used for training of the network, the training method depends upon the nature of the training data. During feed forward back propagation, the difference between the actual output value and the determined value using the model weights is calculated in terms of mean square error (MSE) which was explained by Panda (2008). During back propagation training of the network, if P sets of values with 'n' number of inputs are considered for the analysis then the MSE can be calculated using the following formula

$$\mathrm{MSE} = \frac{1}{P \times K} \times \sum_{p=1}^{P} \sum_{k=1}^{n} K[(d_k)p - O_k \times p)]^2 \tag{5.2}$$

The deviation in the k^{th} layer and the O^k is the output of the k^{th} layer, K is the total number of outputs. Such methodology of neural network used in the commercial software MATLAB is considered for implementation in present work. There are various network

types available in neural networks which are feed forward back propagation (FFBP), cascade forward back propagation (CFBP) and layer recurrent (LR).

5.2.3 Introduction to ANFIS based modelling

ANFIS is a combination of the neural network and the fuzzy logic. Thus it has the adaptive capability from the neural network and the approximation capability from the fuzzy logic. This method was designed by Jang (1993). It is very much useful for prediction in various fields of engineering. Use of ANFIS can be explained through first order Sugeno type fuzzy inference system. This is useful for the mapping of an input crisp set of data with the output using the fuzzy set theory. In ANFIS there are six layers including one input layer, one output layer and four hidden layers. Each layer sends the signals to the next connected layer for further processing. The input layer transmits the input crisp set to the next layer called as first hidden layer and then the fuzzification occurs which compares the input data and assigns the membership weights based on the nearness of the input to the output of the fuzzy set. In the next layer the fuzzy rules are formed and during this process the activation function or the membership function is assigned to the each input. Each of the neuron gets the input from the antecedent neuron having a rule. The neurons in this layer receive data from all the rules where normalization of the values is performed. Such normalized layer is useful for obtaining firing strength. The fifth layer is the de-fuzzification layer which receives the normalized values from the rules and also receives inputs from the first layer based on which it computes the weighted consequent value for each rule of a neuron. The sixth layer is also called as summation layer and it gives the output by combining the results from all the rules and the neurons. It consists of only one neuron. Soft computing technique, ANFIS, is very much useful for solving the analytically complex and mathematically difficult problems with good accuracy. These are discussed in detail by Loganathan and Girija (2013). Through these techniques the natural laws can be applied to a process or a system. The structure and the working of an ANFIS model is shown in Fig. 5.4.

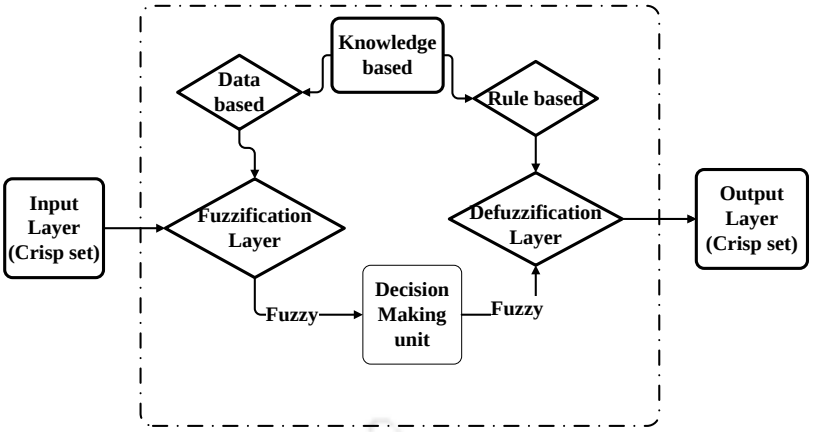

Figure 5.4: ANFIS flow diagram for prediction of un-known data.

In the present work, MATLAB based ANFIS code is developed to suit for our results and the basic model was taken from the MATLAB help. Different types of membership functions are available in this ANFIS. A Membership Function (MF) is a curve that defines how each point in the input space is mapped to a membership value (or degree of membership) between 0 and 1. Thus MF allows us to graphically represent a fuzzy set. One of the key issues in all fuzzy sets is how to determine fuzzy MFs. Actually MF can take any form, but there are some common examples that appear in real applications. In such cases, MF can be chosen by the user arbitrarily, based on the user's experience and or can be designed using machine learning methods (e.g., artificial neural networks, genetic algorithms, etc.). These MFs are broadly classified into 5 categories: Piecewise Linear Functions, Gaussian Functions, Bell-Shaped Function, Sigmoidal Function, and Polynomial Based Functions.

In the present work all the membership functions are checked for finding the optimum and suitable function for the obtained results. It has been observed that the Gauss MF has given the highly accurate results during the prediction.

5.2.4 Gaussian Function

There are two kinds of Gaussian functions viz. Gauss MF and two sided Gauss MF (Gauss2 MF). The symmetric Gaussian membership function is represented by equation 5.4 which mainly depends upon two parameters namely 'σ' which is a measure of the width of the curve and 'c' which denotes center or peak value. For larger value of σ, the curve is flatter and vice versa. This MF is shaped like Gaussian (normal) distribution, but scaled to have a maximum value of 1 as shown by Fig. 5.5. Area under the Gaussian distribution curve is 1. Two sided Gaussian MF (gauss2mf) consists of two halves. Left half consists of one value of σ and c while the right half has different values for the same parameter.

$$f(x;\ \sigma,c) = e^{\frac{-(x-c)^2}{2\sigma^2}} \tag{5.4}$$

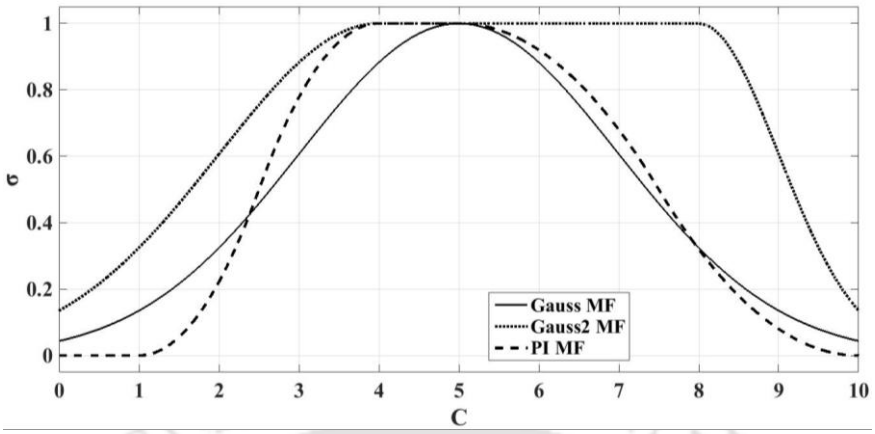

Figure 5.5: Gaussian MF, Gauss 2 MF, Pi MF.

Gauss MF facilitate obtaining smooth, continuously differentiable surface and theoretical analysis of a fuzzy system. As Gauss2 MF is not symmetrical about the center, the unity condition is not satisfied hence it can be advantageous solution over Gauss for specific problems.

5.2.5 Pi Shaped Function

This MF is product of S MF and Z MF represented by equation 5.5. It can be seen from equation that it depends on 4 parameters from which a, and d locate at the "feet" of the curve, (in the 'C' axis) while b and c at its shoulders (along the sigma axis). This function is continuously differentiable in the whole range thus smoother than a triangular function. The shape resembles Pi hence called as Pi MF as shown in Fig. 5.5.

$$f(x;a,b,c,d) = \begin{cases} 0, x \le a \\ 2\left(\frac{x-a}{b-a}\right)^2, a \le x \le \frac{a+b}{2} \\ 1-2\left(\frac{x-b}{b-a}\right)^2, \frac{a+b}{2} \le x \le b \\ 1, b \le x \le c \\ 1-2\left(\frac{x-c}{d-c}\right)^2, c \le x \le \frac{c+d}{2} \\ 2\left(\frac{x-d}{d-c}\right)^2, \frac{c+d}{2} \le x \le d \\ 0, x \ge d \end{cases} \tag{5.5}$$

5.2.5 Implementation of NN and ANFIS for Force Prediction

ANFIS has been used for the prediction of the force and the moments obtained from the simulation by training using the known input force and the known output acceleration. In the phase of training, ANFIS module of MATLAB uses different membership function

(MF's) for normalizing the input data. Similar MFs are also available to normalize the output data. There are two types of output membership functions such as linear and constant. The MF to be used depends on the type of data to be trained and it can be chosen based on the user's experience. Using either of these MFs, one can opt for training strategy out of available ones which are back propagation and hybrid methods. Back propagation method uses least square method whereas hybrid method follows least square method to find initial structure of ANFIS model and gradient descent method to determine the model weights. Implemented such methodologies in both the soft computing techniques and associated errors are discussed here onwards.

5.3 Results and discussion

5.3.1 Results from finite element analysis

In the present investigation, recovery of impulse, ramp and hat forces of 20 N and 30 N magnitudes have been analyzed using NN and ANFIS. For such predictions, impulse forces of 10 N and 50 N are used for the training of NN and ANFIS model. Training with the ramp and hat forces are also performed but the ramp and hat force training data is unable to recover the impulse and ramp and hat due to its limitation of having the limited number of frequencies. Figure 5.6 shows typical time history of X, Y-components of impulse, ramp and hat forces which comprise the resultant force of 20 N magnitude. These forces are considered in FE analysis for application at location P (Fig. 5.1 and Fig. 5.2) at an angle of attack of 30^0 with the X-axis. Ramp force and hat force are also applied at the same location with same angle of attack in the FE analysis in either case.

In the prediction of the impulse force, the averaged % of error is calculated as the ratio of the deviation between the upper and the lower limit of the predicted peak force to the applied peak force. However in case of step, ramp and hat force the time averaged % of error has been calculated in the constant slope line with corresponding time. It is calculated as the ratio between the average predicted forces to the average applied forces.

The acceleration signals are obtained as the outcome of FE simulations for applied impulse, ramp and hat forces. Here X-component signal is acquired at location A while the Y-component of acceleration time history is acquired at locations B and C shown in Fig. 5.1 and Fig. 5.2. Typical X- component of acceleration signal, for test Model-A, seems to be very smooth for all three kinds of forces as shown in Fig. 5.7 (a). However for Y-component of acceleration signals, for the same test model, as shown in Fig. 5.7 (b), there

exists much undulation due to the fact that the normal acceleration is obtained at a location away from the point of application of force. The induced moment due to angle of the force also affect the trend of X and Y-components of acceleration.

The appropriate prediction of forces and moment acting on the test Model from the FE based acceleration signals involves basic task of finding Neural Network (NN) and ANFIS architecture with optimum network parameters. The influencing parameters for NN includes network type, training function type, type and number of hidden layers with associated number of neurons. The parameters considered for ANFIS are, type of input MF, output MF and training method. The X-component of 20 N impulse force applied at angle of 30^0 to X-axis has been considered for the testing of both the models.

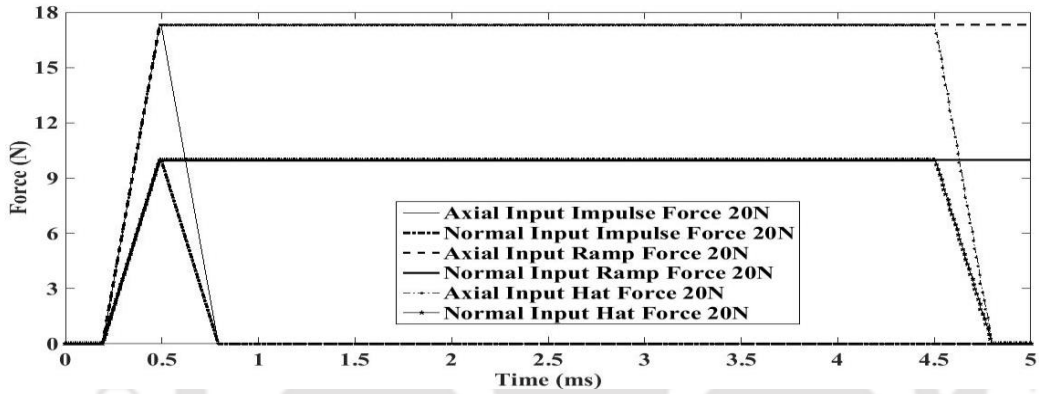

Figure 5.6: Time history of impulse, ramp and hat forces of resultant 20 N and 30 N.

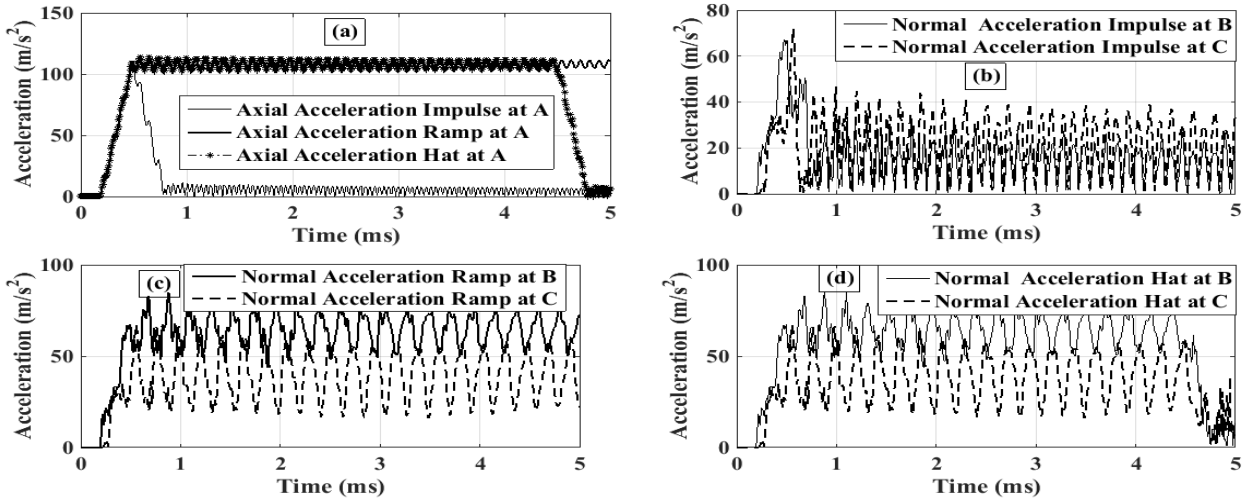

Figure 5.7: Time history of (a) axial acceleration for impulse, ramp and hat force (b) normal accelerations for impulse, (c) ramp and (d) hat forces obtained from model A by applying 20 N forces at 30^0.

The training and the testing of the ANFIS used for the prediction is discussed in the next section.

5.4 Force Recovery Using Neural Network

In this process variation of type of network, training function and number of hidden layers along with the number of neurons associated and their types have been considered. Recovery of an applied impulse force of peak value 20 N is considered for this comparison in case of Model- A. The network type variation basically relies on the data to be used. In such case the requirement of training, input and output data collectively restrict the choice of the network type to some extent. There are three different kinds of training function viz. Trainlm, Traingdm, Trainr, are available which can be used for the training of the data for the prediction. In the present case of MATLAB based force recovery studies, the training function "Trainlm" is used while varying the network type. Along with this some considerations include single output layer, two hidden layers with 25 and 15 numbers of neurons. Figure 5.8 (a) shows the comparison of the applied force with the recovered force using FFBP, CFBP and LR networks when 20 N force is applied at point P on Model-A at an angle of 30^0 to X-axis. Here, the recovered force is in good agreement with the applied force in terms of magnitude with an error for peak to be ± 4.6 %. However, in terms of trend, every network type gives little deviation. But the accuracy of the back propagation network is found to be more promising and hence it is only considered for further study in the present work. In this case the input force data and the output acceleration data are used for the training of the neural network model and during this process, the input data file containing the time series in the first column, the one axial acceleration followed by two normal accelerations along with the force data given in the last column of the file is given as input to the program. During testing the training accelerations are replaced by the testing accelerations and the force is given as zeros. During the training the NN model assigns the weights and forms the optimum structure. During the testing the same optimized structure is used for the prediction of the unknown force.

In Figure 5.8 (b) the recovered forces are compared with the applied impulse force by taking three training functions viz. Trainlm, Traingdm and Trainr with feed forward back propagation keeping rest all other parameters (No. of hidden layers 2 with 25 and 15 neurons respectively) same as in earlier case. It is observed that except the Trainlm, none of

the training type is seen to be an appropriate choice as a large variation in magnitude and trend is seen with other two training type, while recovering impulse force having magnitude 20 N. The Trainlm is found to have better recovery in terms of nature of the signal as the error in recovering the peak is limited to 2.77%.

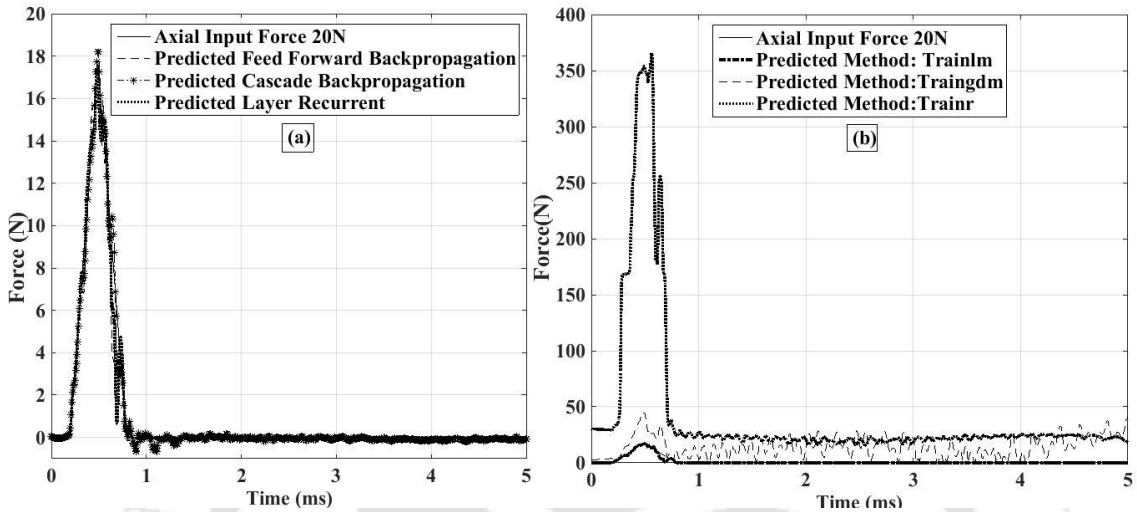

Figure 5.8: Comparison of force prediction with various (a) neural network structures, (b) training methods.

After studying the effect of type of network and number of training functions on the recovered results, now number of hidden layers and associated number of neurons are considered as the varying parameter. The effect of number of hidden layers and neurons on the recovery of the force signal is plotted in Fig. 5.9 (a). The recovered forces are obtained using single, two and three hidden layers. While 25 neurons are considered for the single hidden layer, 25, 15 and 30, 20 neurons are considered for the two hidden layer network. Similarly for three hidden layers, 25, 15, 10 neurons are considered. Though more parametric studies have been carried out, it is observed that two hidden layers with 25, 15 neurons accurately recover the applied force. This force prediction not only satisfies the temporal nature of the signal but also bears the peak error of 2.3%.

Finally the type of hidden and output layer has been varied among the existing combinations of Tan Sigmoid, Log Sigmoid, and Pure Linear. The recovery of the same impulse force is shown in Fig. 5.9 (b). During the training process, two hidden layers are used and the output layer is considered as one, however the number of neurons associated with the hidden layer during the recovery is 25 and 15. The combination of same layer type i.e. Tan Sigmoid for all the hidden layers and output layer predicts forces as zero magnitude. Similarly the Log Sigmoid for hidden layer and output layer gives a constant

value of 21.24 N. By combining the available choices it is evident from the figure that consideration of hidden layers as Tan Sigmoid and output layer as Pure Linear shows least error of 2.3% . Consideration of all layers as Pure Linear does not improve the prediction but under predicts the peak by 4.16% .

Collectively, implementation of NN for force recovery points that the network type should be Feed forward back propagation, training type should be Trainlm, number of hidden layer must be 2 having transfer function type Tan-Sigmoid with associated number of neurons 25 and 15 and single output layer of type Pure Linear. This combination is expected to give better recovery of the short duration transient force signal. However, it has been noticed that the best composition of the inputs for NN is able to recover impulse force well (Fig.5.8) with an accuracy of 2.3% but it is not able to recover the ramp and hat forces accurately which can be observed in Fig.5.10.

Neural network with optimized parameter over predicts the magnitude by 44.34% during recovery of 20 N hat force whereas under prediction of magnitude by 36.49% is observed while recovering 20 N ramp force. It is because the neural network training method was not able to represent the system characteristic very well during the testing in case of the ramp and hat type of forces because the NN is based on the learning capability of the input data and output data during the training.

Neural network with optimized parameter over predicts the magnitude by 44.34% during recovery of 20 N hat force whereas under prediction of magnitude by 36.49% is observed while recovering 20 N ramp force.

It is because the neural network training method was not able to represent the system characteristic very well during the testing in case of the ramp and hat type of forces because the NN is based on the learning capability of the input data and output data during the training.

Therefore force recovery has been investigated in detail using ANFIS due to such inconsistent recovery of force using NN.

5.4.1 Force Recovery for Model-A using ANFIS

The input membership function, output membership function (MF) and training type are varied in ANFIS based prediction methodology to find the optimum combination for accurate prediction of the transient force. Thus obtained results are discussed in this section.

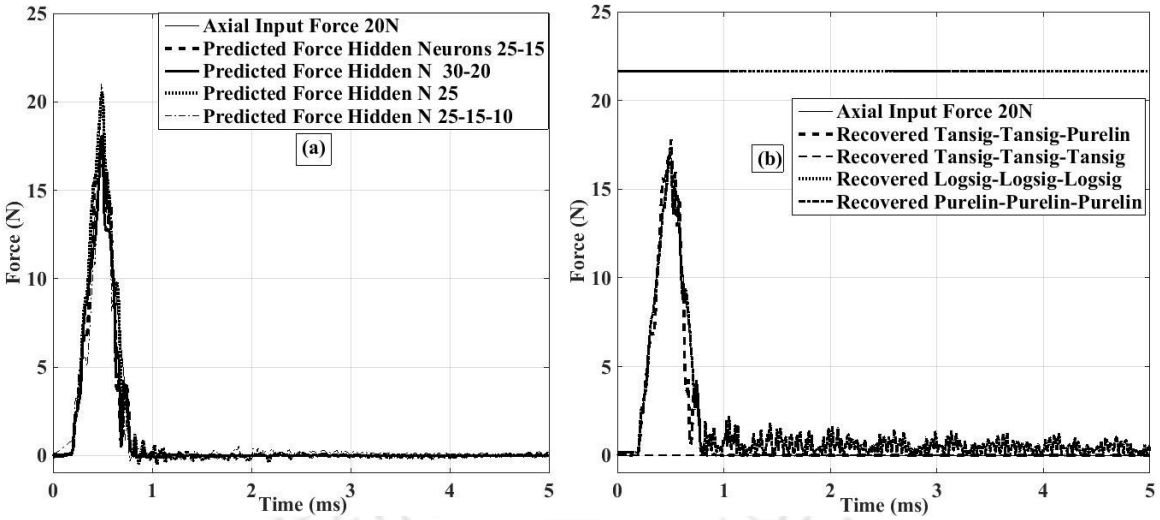

Figure 5.9: Comparison of accuracy in force prediction with (a) number of hidden layers with neurons (b) combination of hidden, output layers.

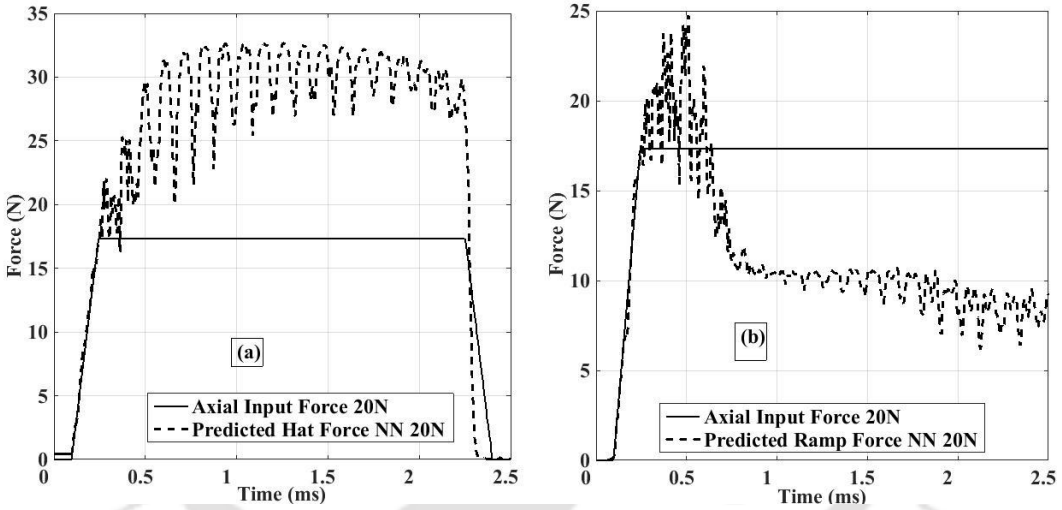

Figure 5.10: Comparison of recovery of (a) hat force and (b) ramp force of 20 N using neural network.

5.4.2 Comparison of Type of Input and Output Membership Functions

MATLAB (2014) based ANFIS module is equipped with various input memberships functions such as Gauss MF, Gauss2 MF and Pi MF. Figure 5.11 (a) shows the comparison of predicted force for these membership functions from acceleration signals for impulse force of peak value 20 N in case of Model-A. The force predicted from the Gauss MF and Gauss 2 MF gives the same trend as the applied force. However the predicted peak value has an error of $\pm 3.81\%$ using Gauss MF. But in case of Gauss2 MF the error is $\pm 13.41\%$. While considering Pi MF, the peak value of the force and the temporal variation are different due to which it shows two peaks instead of one. Here, Gauss MF is

able to represent the impulse force well since it is continuously differentiable and symmetric about center as like impulse force. However, Gauss2 MF is unable to represent the impulse force correctly as it is un-symmetric even though it is continuously differentiable. Moreover, Pi MF is the smother version of the triangular MF and it is un-symmetric in nature, so it is not able to predict the impulse force correctly.

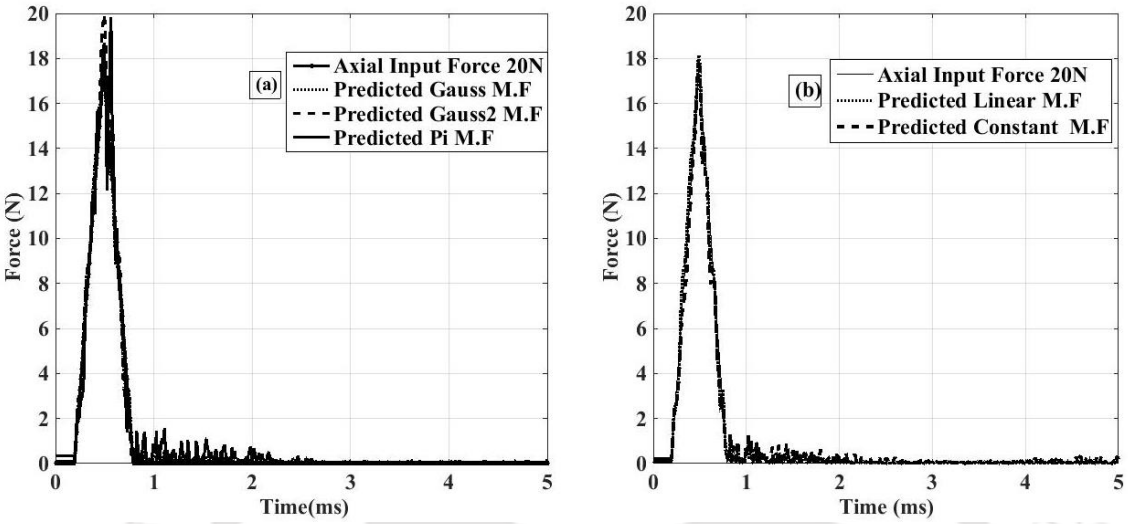

Figure 5.11: Comparison of axial component of 20N impulse force with various (a) input membership, (b) output membership functions.

Unlike input membership functions, the choices of output membership functions are Linear MF and Constant MF. Figure 5.11 (b) shows the comparison of output membership functions for the prediction of impulse force where Gaussian MF is used as the input membership function. Here, Linear MF recovered the applied force with an error of $\pm 4.62\%$. However the constant MF is able to predict the peak value with error of $\pm 3.81\%$. Even though there is slight shrinkage in the time history of the recovered force but the magnitude is well recovered with greater accuracy.

5.4.3 Comparison of Back Propagation and Hybrid Mode of Training Methods

Training of the input data in ANFIS methodology can be done either by back propagation method or by hybrid method. Apart from choice among these methods, expertise of the user is important in choosing the epochs for these training methods. Figure 5.12 (a) shows the prediction of 20 N impulse applied on Model-A using these training methods. Here, training is performed using hybrid method with 20 epochs as well as the back propagation with 100 epochs (which can be chosen based on the user experience). In the case of impulse force the peak value is considered as the reference value and the difference between the input and the predicted peak value is calculated and the ratio of the

difference to the input value is treated as the error. But while calculating the error for the forces like ramp and the hat, ratio of difference between the time average of steady portion from the predicted and the steady portion from the input force is considered as error. Impulse force is predicted with $\pm 3.81\%$ error for the data obtained using hybrid training. But in case of the back propagation the error is very high is $\pm$ 93.4%. Apart from this it is observed that the hybrid type of training is able to recover the force accurately irrespective of the number of epochs with threshold value of 3. Since the back propagation is sensitive to the initial condition and also it calculates the local minima so it has limitations in predicting the force accurately.

Figure 5.12 (b) shows the comparison of performance of back propagation training method with variation in number of epochs. Different numbers of epochs are considered for testing the back propagation training, such as 100, 200, 300 and 600 respectively. The error in predicted force from 100 epochs is $\pm 93.4\%$, for 200 epochs is $\pm 38.6\%$, for 300 epochs is $\pm 9.63\%$ and for 400 epochs it is $\pm 5.6\%$. From all these results it is evident that the performance of the back propagation increases with increase in number of epochs. It is mainly due to increase in the learning rate of the back propagation with number of epochs which in turn reduces the error in prediction. After analyzing these results it is observed that the hybrid type of training can be used for accurate prediction with minute threshold number of epochs. The back propagation training requires more number of epochs i.e. it requires more computational time for higher number of inputs and linguistic rules, for accurate prediction.

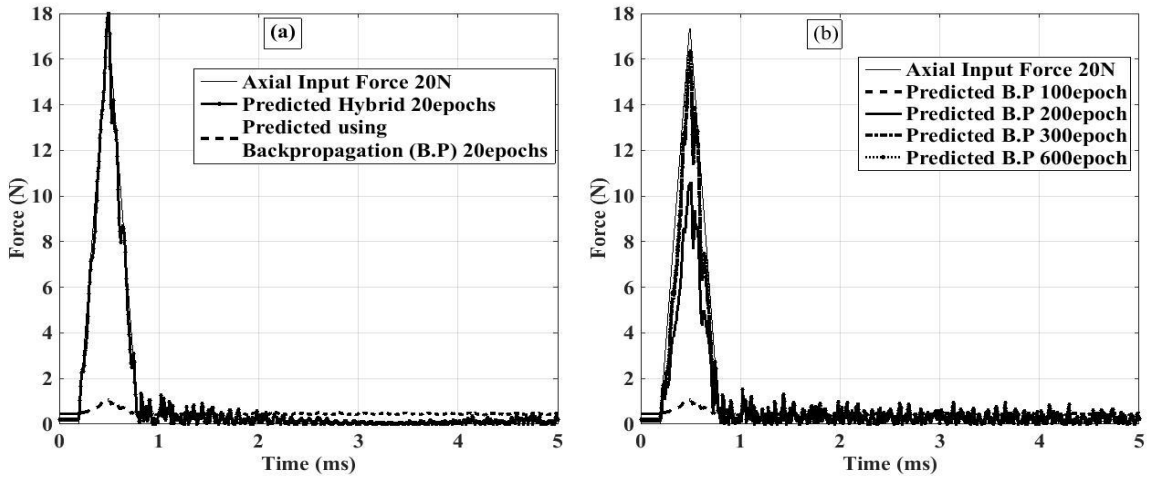

Figure 5.12: Comparison of (a) hybrid and back propagation training methods (b) Epoch dependence of back propagation method for prediction of X-component of 20 N impulse force.

In view of these parametric variations for ANFIS, it can be understood that the accurate prediction of force can be obtained by considering the input membership function as "Gauss", output membership function as "Constant type" and training type as "Hybrid". Now this combination of input and output membership functions and training type are used to recover the X, Y-components of forces, and moment for impulse, ramp, and hat force of 20 N and 30 N applied at an angle of 30^0 about X-axis.

5.4.4 Prediction of Short Duration Forces on Model-A Using Optimum ANFIS Structure

Figure 5.13 presents the comparison between recovered and applied X, Y-component of force and resulting moment for 20 N and 30 N peak value impulses. The recovered X-component of force has an error of ±3.81% for 20 N force and error of ±8.16% is observed for applied force of 30 N as shown in Fig. 5.13 (a). It can be observed from Fig. 5.13 (b) that recovered Y-component 20 N force has an error of ±3.9% and 30 N force has ±8.2%. The predicted moment induced in Z-direction for 20 N force has an error of ±4.58% and the 30 N force has an error of ±8.26% which can be clearly observed from Fig. 5.13 (c). It can be clearly summarized from the above results that the error in prediction increases with increase in magnitude of the force in case of ANFIS.

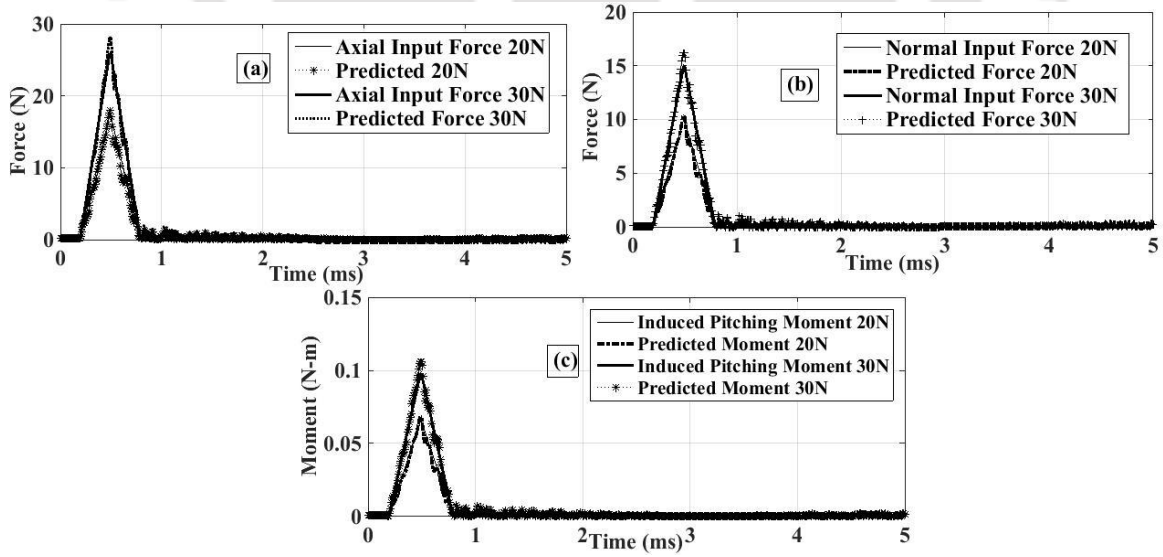

Figure 5.13: Comparison of input and predicted (a) axial component (b) normal component (c) moment of impulse forces of 20 N and 30 N.

The consolidated ANFIS methodology when applied for recovery of ramp force applied on Model-A is compared in Fig. 5.14. This figure represents the comparison of applied and predicted time history of X, Y-component of ramp force of 20 N, 30 N and corresponding moment. The X-component of applied and recovered forces are shown in Fig. 5.14 (a). The observed time averaged error is ±3.69% for 20 N and ±0.91% for 30 N. From Fig. 5.14 (b), it can be observed that the time averaged error for Y-component force of 20 N is ±3.59% and for 30 N it is to be ±1.89%.

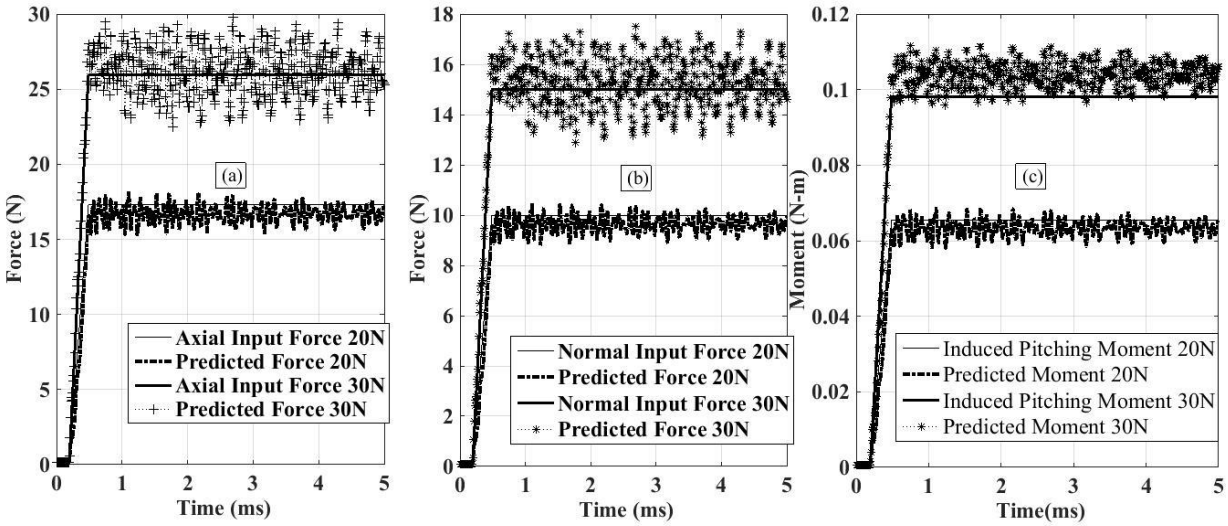

Figure 5.14: Comparison of input and predicted (a) axial component (b) normal component (c) moment of ramp forces of 20 N and 30 N.

While recovering the resulting moment about Z-axis, the time averaged error is found to be ±3.18% for 20 N and ±6.03% for 30 N as shown in Fig. 5.14 (c). Reduction in time averaged error in predicting the plateau of the ramp force can be noticed with increase in magnitude of the ramp force.

Similarly, Fig. 5.15 shows the time history of applied and recovered X, Y-components and corresponding moment for hat force of 20 N, 30 N. The X-component of applied and recovered forces are as shown in Fig. 5.15 (a). The recovered force matches well with the applied force with time averaged error of ±3.71% for 20 N and time averaged error of ±5.87% for 30 N. In case of Y-component of force the time averaged error is found to be ±3.6% for 20 N and a time averaged error of ±5.9% for 30 N as shown in Fig. 5.15(b). A time averaged error of ±3.1% for 20 N and ±6.0% for 30 N has been observed in predicting the resulting moment about Z-axis as shown in Fig. 5.15(c). These figures force to retain the conclusion for the errors drawn from the impulse force case.

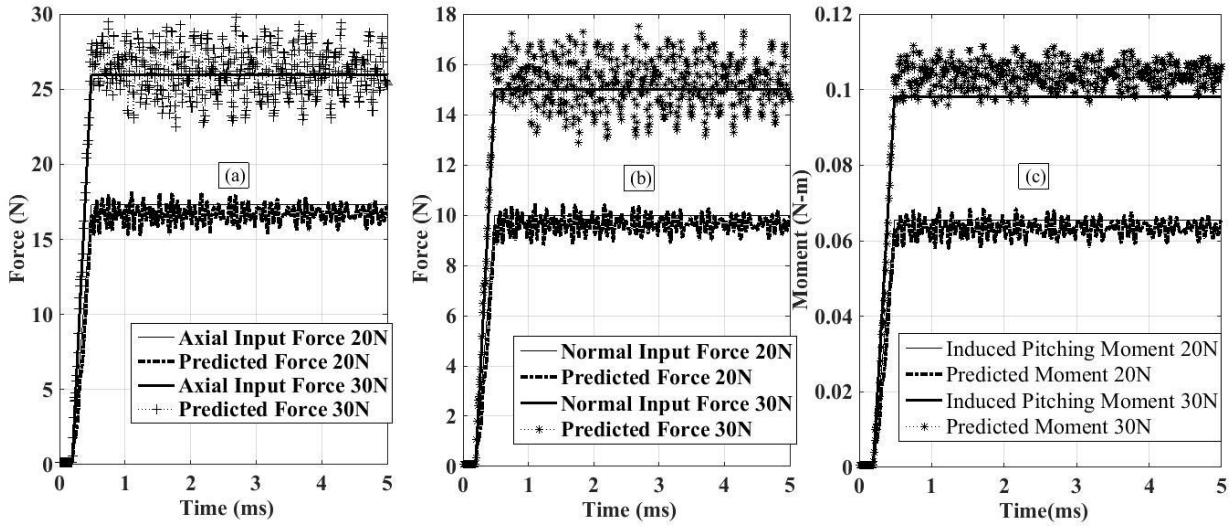

Figure 5.15: Comparison of input and predicted (a) axial component (b) normal component (c) moment of hat forces of 20 N and 30 N.

5.4.5 Prediction of short duration forces on model-b using optimum ANFIS structure

Three input impulse, ramp and hat type of forces of magnitudes 20 N and 30 N are applied on AGARD model at "P" (Fig. 5.2) at the same angle of 30^0 with X-axis. The corresponding FEM results and consolidated ANFIS methodology are used to predict the forces and moment for this test model. Figure 5.16 (a) shows the time history of X-component of force and the comparison with the recovered force using ANFIS. It is observed that all the force and moment components are recovered well, as the recovered force has an error of ±1.02% for 20 N and an error of ±2.82% for 30 N. Errors of the same order of magnitude and trend are found while recovering the Y-component forces as shown in Fig. 5.16 (b) and the moment about Z- axis as shown in Fig. 5.16 (c). After observation of all the recovered impulse force components using ANFIS, it is concluded that for impulse force the accuracy of recovery decreases with increase in the magnitude of force, and accuracy solely depends on the trend of the training acceleration data. Recovery of components of ramp forces and associated moment (Fig. 5.17) and component of hat forces and associated moment (Fig. 5.18) also re-assert this observation. Thus although ANFIS has been observed have an edge over the NN for predicting the small duration transient forces, error in the associated prediction is found to be dependent on the magnitude of forces used in training the data. Thus it is advisable to follow the consolidated ANFIS methodology with lesser spread in the input force magnitudes used for training in order to reduce the prediction error.

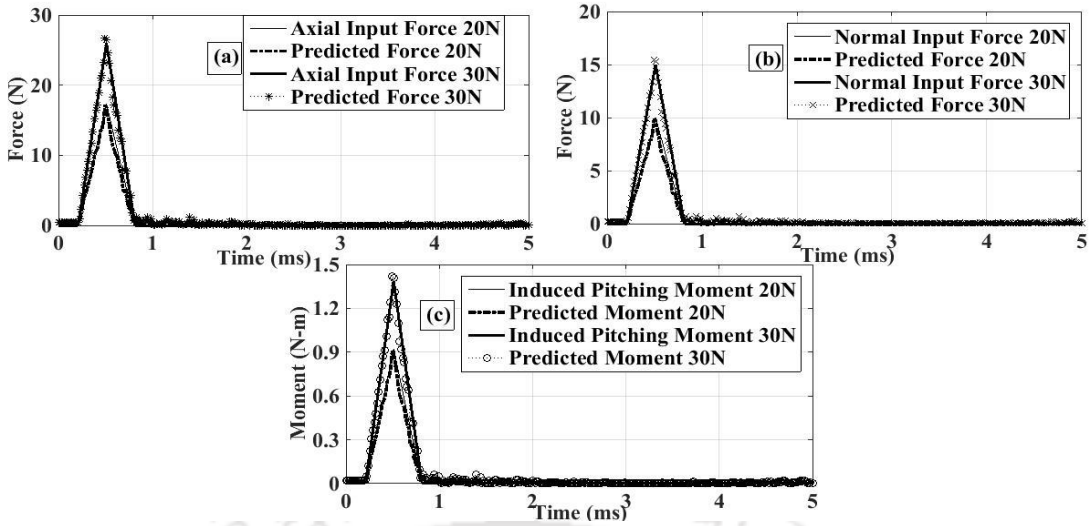

Figure 5.16: Comparison of input and predicted (a) axial component (b) normal component (c) moment of impulse, forces of 20 N and 30 N on AGARD model.

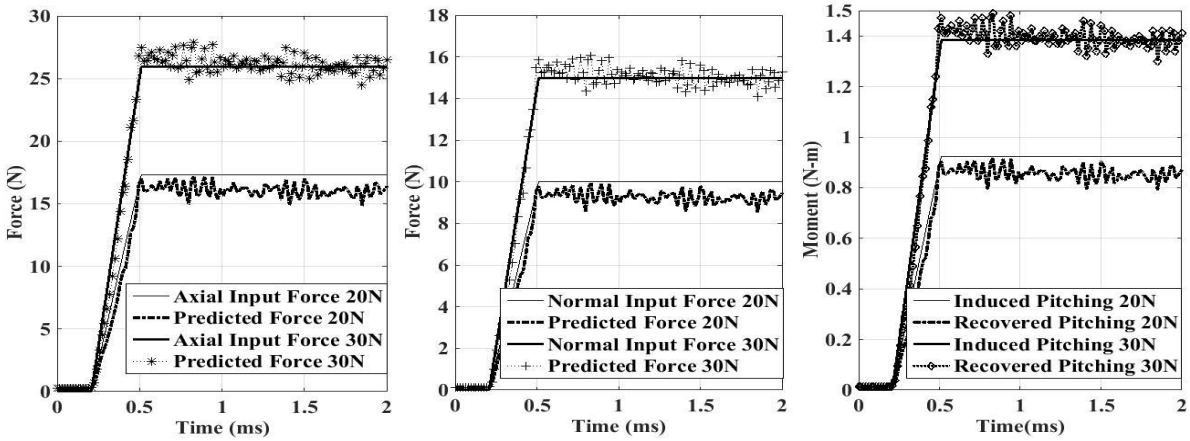

Figure 5.17: Comparison of input and predicted (a) axial component (b) normal component (c) moment, of ramp forces of 20 N and 30 N on AGARD model.

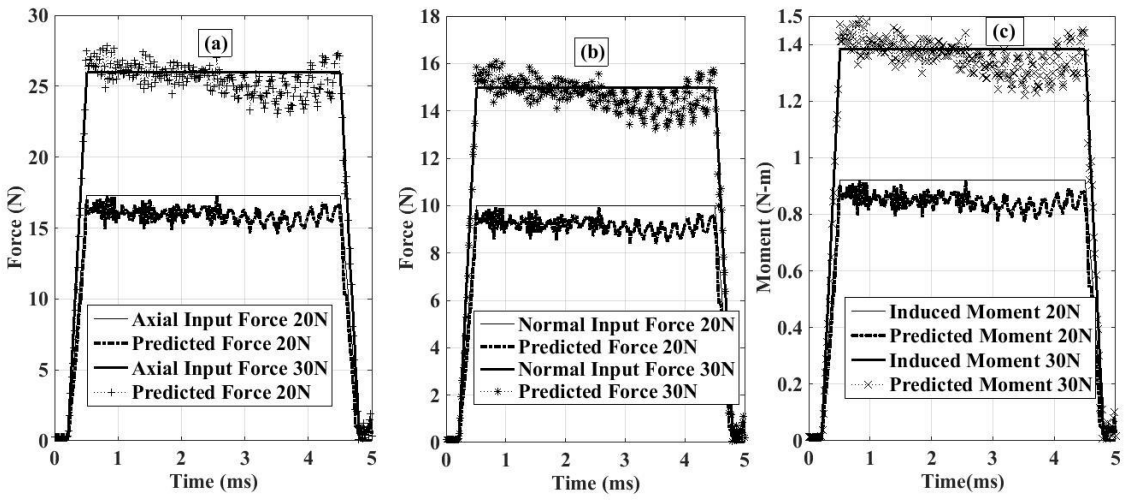

Figure 5.18: Comparison of input and predicted (a) axial component (b) normal component (c) moment, of hat forces of 20 N and 30 N on AGARD model.

5.5 Conclusions

Current investigations demonstrate the methodology of transient force prediction using standard soft computing techniques. These studies are found very useful for the applications of impulsive testing of aerospace configurations for force measurement. Impulse, ramp and hat forces are initially applied on the test models during FE studies and thus obtained results are analyzed using neural network (NN) and artificial neuro fuzzy inference system (ANFIS). It has been observed that while the NN has successfully recovered the impulse force, it has failed to recover the ramp and hat type of forces. But the combination method of neural network and fuzzy logic i.e. ANFIS model is able to predict well all the three types of forces with more than 90% accuracy. Hence this method is recommended to be used for the prediction of transient dynamic forces. Thus present studies support the use of soft computing techniques for transient force prediction after proper assessment since such implementations are neither based on simplified assumption nor are based on rigorous mathematical input for calibration. These predictions are also accessed for the error during the prediction as mentioned and it has been observed that the ANFIS can be used for short duration force prediction generally encountered in high speed aerospace applications.

CHAPTER 6

EXPERIMENTAL INVESTIGATION OF HEMISPHERICAL MODEL USING THREE COMPNENT ACCELEROMETER BALANCE IN SHOCK TUNNEL`

Overview

This chapter describes the tests conducted in the shock tunnel along with the computational simulations for the comparison. Hemispherical model is considered for the experimental testing corresponding to free stream conditions of Mach 8. During the experiments three component accelerometer balance is housed inside the model. The calibration tests are also conducted on the same model where the loads are applied at location 3 (Fig. 6.10) for the acceleration response measurement. Details of design, calibration, analysis of the three component accelerometer force balance along with the force prediction using soft computing techniques and conventional technique are also part of the present chapter. During these studies it has been observed that the soft computing techniques can be easily implemented for the force prediction in actual shock tunnel tests.

6.1 Introduction to Force Measurement in Impulse Hypersonic Test Facilities

Estimation of aerodynamic coefficients for any hypersonic vehicle is highly desirable to derive the range of the vehicle or to predict the fuel requirement. Therefore research in this field is centered about the prediction of forces and moments. Such estimates can be made using powerful techniques such as CFD, analytical techniques or empirical relations, ground testing and flight calibration techniques. Ground based testing is a golden mean in terms of cost and prediction capability. Various facilities are established throughout the world for the analysis of the hypersonic aerodynamics of the vehicles. Among them impulse facilities are most commonly used for generation of high enthalpy flow. These facilities are useful for generating the free stream conditions in the order of Mach 5 to 25 based on the requirements. The specialty of these facilities is its short testing duration. In case of shock tunnels high speed steady flow remains for the test time of 0.5 to 2 ms.

Various researches have performed the ground based tests for the performance analysis of the aerodynamic models. Blow down tunnels are generally used for generating the flow or vehicle velocity up to 2.5 km/s but the real gas effects starts (Variable density, Vibrational modes, Dissociation, Plasma Ionization) only after the vehicle or flow speed of 5 Km/s. The higher speeds can be achieved by heating the test gas in the test section using an electric arc discharge techniques which are discussed by Lukasiewicz et al. (1967) and Rapuc (1993). or else the high speed piston can be used with high velocity discussed by Stalker (1967) but the test times are of the order 10- 100 ms. But the shock tunnels facilities with reflected shock mode are most preferable for the hypersonic testing as explained by Stalker (1989) due to their high enthalpy conditions and its high speed flow generation capability. These types of shock tunnels are used extensively for the purpose of generating the high velocity flows of about 4 Km/s. The free piston shock tunnel was developed in the University of Queensland, Australia by Stalker (1988) which leads to the construction of the many such facilities at such as GALCIT at Cal. Tech by Hornung et al. (1991) and Gottingen (HEG facility) at Germany as mentioned by Beck et al. (1991).

Force measurements are carried out by numerous researchers in the impulse hypersonic facilities. Jesson and Gronig (1989) devolved the strain gauge based force balance. The stress wave force balance technique was then developed (Simmons and Sanderson (1991)) which can be very much useful for the short duration facilities. Nauman

et al. (1991) proposed an accelerometer based force measurement technique to be used in the shock tunnel during the test time of 1 millisecond and the main attraction of the technique was the mounting system that releases the model and holds after 10 ms. Later Joshi and Reddy (1986) have used the accelerometer balance for the force measurement in shock tunnel to test over the slender cone bodies and later this work has been extended by Menezes et al. (2011) and Sahoo et al. (2003) on the blunt cone bodies to test for the force measurement using accelerometer force balance. The step load and impulse load tests are conducted on a conical model with static and the dynamic calibration methods to find out the system response function of the system by Praveen et al. (2013). These models are again tested in the shock tunnel for the stress wave force balance validation. The accelerometer balance is also designed for the measurement of roll, drag and lift on a blunt nosed triangular body by Menezes et al. (2011) and comparison shows good accuracy with the Newtonian theory. Also Trivedi and Menezes (2012) measured yaw, pitch and side force on the triangular body using the accelerometer force balance in the shock tunnel.

Considering all these methods for the force measurement in the high speed test facilities, shock tunnel tests are considered herein for force measurement. Calibration of force balances has been prominently considered for stress wave based forces balances while accelerometer force balances have been generally used with certain simplified assumptions. Apart from this, the calibration techniques related to stress wave force balance are based on rigorous mathematics. Hence, present chapter deals with earlier established soft computing techniques of ANFIS based methodology for force prediction in shock tunnel based force measurement experiments using accelerometer force balance. Such shock tunnel testing and associated design of the hemispherical body along with analysis of three component accelerometer force balance are discussed. The pitot tests are also conducted for predicting the free stream pressure and the Mach number. Comparison of results obtained from soft computing techniques, CFD methods with the conventional methods for different angle of attack conditions is considered to evaluate the prediction capability of presently proposed methodology. Thus following sections elaborately deal with the test facility, model design, calibration, force balance, shock tunnel testing and force prediction using different methods.

6.2 Description of Shock Tunnel for hypersonic testing

A shock tunnel is said as the integrated experimental facility of the two major portions viz. shock tube and wind tunnel. Shock tube is comprised of the driver section and

the driven section separated by metallic diaphragm. Tunnel portion consists of nozzle, test section and dump tank. The schematic diagram of the shock tunnel at Indian Institute of Technology, Bombay, India (IITB-ST) is shown in Fig. 6.1 and the photographic view of the tunnel is as shown in Fig. 6.2. Various components involved in the shock tunnel assembly with their application are discussed in the present section.

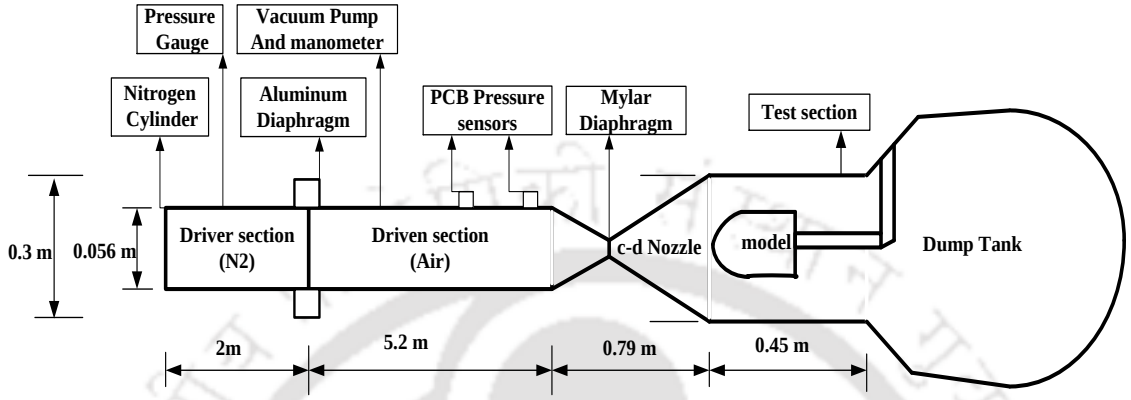

Figure 6.1: Schematic diagram of reflected mode shock tunnel with various sections and instruments.

Figure 6.2: Photograph of the IITB shock tunnel with all components.

6.2.1 Shock tube

It is the primary section that initiates the shock by using the pressure difference between the two sections to generate high speed flow. It is made of stainless steel tube of 76 mm outer diameter and inner diameter of 51.5 mm. The driver section is 2 m long and the

driven section has length of 5.185 m. The inner walls of the shock tube are machined with the accuracy of 10 microns to reduce the layer formation inside the tube. The two sections are separated by diaphragm. Shock tube is permanently equipped with two PCB pressure sensors having Model no: 102A04 and 102A, with sensitivities of 5 mV/Psi and 1 mV/Psi, respectively. These two pressure sensors mounted in the driven section are separated by 50.5 mm. Here onwards the pressure sensor mounted towards the driven section end (Model no: 102A) will be referred as pressure sensor 'B' and the other pressure sensor (Model no: 102A04) will be referred as pressure sensor 'A'.

6.2.2 Nozzle

The shock tube ends before the nozzle in the shock tunnel arrangement and both are separated by a mylar paper diaphragm. This is an important section in the whole shock tunnel arrangement which causes the flow to expand and hence to attain the required free stream conditions. It is therefore the convergent divergent (c-d) nozzle which expands the air behind the reflected shock to the desired Mach number. The entrance and the exit of the nozzle are connected to the shock tube and test section respectively with help of flanges and care has been taken so that there is no gap during the assembly**.** The divergent portion of the nozzle is conical type with semi cone angle of 20^0 which is made of a mild steel sheet of 5 mm thickness. The exit diameter of the nozzle is 300 mm and the throat diameter of the nozzle is 23 mm. It has a length of 800 mm and the fine polished sheets are chosen for the fabrication of the nozzle such that the smooth laminar flow can be created during the test.

6.2.3 Test section

The model is kept inside the test section where the mounting can be done at different angles of attacks. The arrangement is made such that the model can be supported horizontally and also in an inclined direction. This test section has square cross section of size 300 mm x 300 mm with 450 mm length. There is a provision of glass on one side of the test section to observe the model during the test flow.

6.2.4 Dump tank

The last part of the shock tunnel is called as the dump tank. This is a horizontally mountable tank supported on the wheels. It is connected with the nozzle section through the test section. It has the wiring mechanism of the sensors. Model supporting mechanism is

also integral part of the dump tank. It has connection with the vacuum pumps such as roots and rotor pumps for vacuum creation during the experiment so as to attain required low pressure in the tunnel portion during the experiments.

6.3 Shock Tunnel Calibration Experiments

Initial experiments in Hypersonic Shock Tunnel (IITB-ST) of Aerospace engineering department at IIT Bombay, India are specially conducted for calibration of test section freestream conditions. During these experiments, two sections of shock tube are separated by an aluminum diaphragm of 1.2 mm thickness.

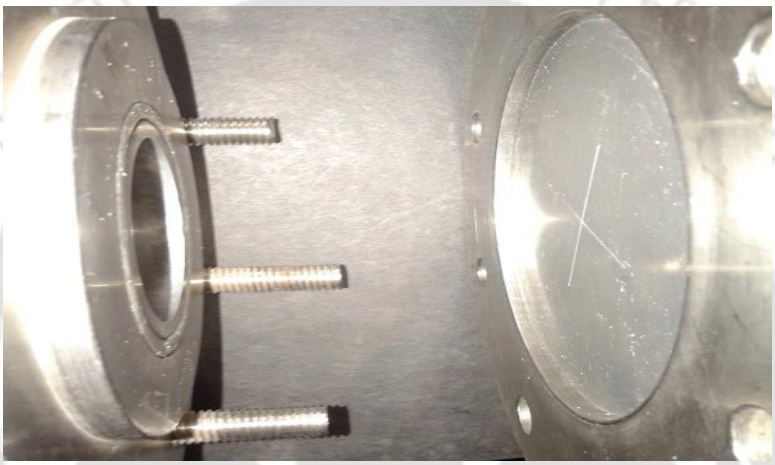

Figure 6.3: Photograph of diaphragm between the driver and driven sections of shock tunnel.

The diaphragm is machined with two grooves in perpendicular directions from the center and the depth of the grove is 1/3rd of the thickness which takes care for the uniform bursting of the diaphragm. Such diaphragm mounting is shown in Fig. 6.3. A mylar paper diaphragm is kept in between the exit of the driven section and entrance of the convergent divergent nozzle.

A pitot sensor is mounted in the test section to measure the stagnation pressure behind the normal shock. It is a PCB sensor (Model No: 102A08) of sensitivity 100 mV/psi. Air pressure maintained in the driven section of the tube is 33.86 kPa and the dump tank pressure is of the order 10^{-3}mbar. Nitrogen gas is used as the driver gas and diaphragm rapture pressure is noticed as 2.6 MPa. All the experiments are found almost repeatable. Typical signals of pressure sensors A and B mounted in shock tube are shown in Fig. 6.4 and Fig. 6.5 respectively.

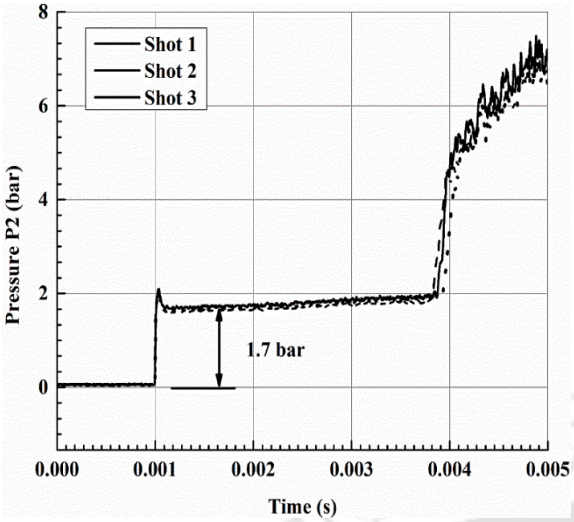

Figure 6.4: Time history of driver section pressure recorded by sensor A

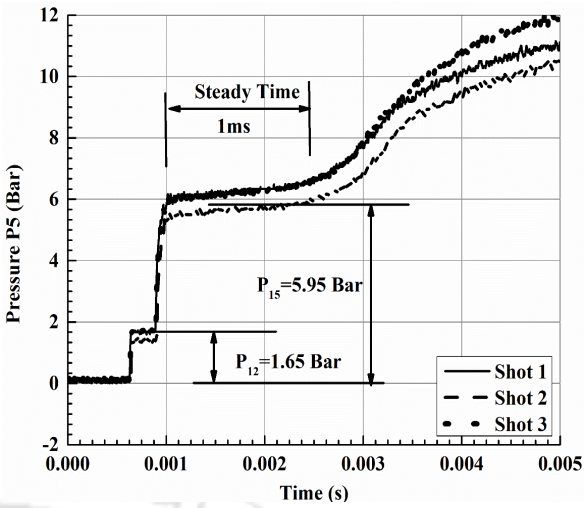

Figure 6.5: Time history of driven section pressure recorded by sensor B

Signals from sensor A and Sensor B are plotted together for the same experiment are shown in Fig. 6.6. This signal is then used for estimating the shock speed and stagnation conditions at the entry of the nozzle. Pitot probe mounted in the test section gives the stagnation properties behind the normal shock which is shown in Fig. 6.7. This signal shows the rise time or the nozzle starting time and the test time for the given experiment. Repeatability of the present experiments is clear from this figure as well. It is evident from this figure that the nozzle starting time is around 0.8 milliseconds and the steady test time is around 1.4 milliseconds. Test conditions can be evaluated using these signals. Thus obtained test conditions are given in Table 6.1.

6.4 Model Description

For the present shock tunnel tests a hemispherical test model has been used. This model is fabricated from aluminum and it is 101 mm long. Its base diameter is 56 mm and the wall thickness is 3.5 mm. Schematic of the test model integrated with the force balance is shown in Fig. 6.8. This model is housed inside with three uniaxial accelerometers of PCB Piezotronics Inc., USA make. Details of these accelerometers are given in Table 6.2. One accelerometer is used for the measurement of the axial acceleration while the other two accelerometers measures normal acceleration referred here as front normal and aft normal. The accelerometer mounted ahead of the center of gravity (C.G) or towards nose portion of

the model and mounted normal to the model axis measures front normal and the other one mounted behind the CG measures aft normal.

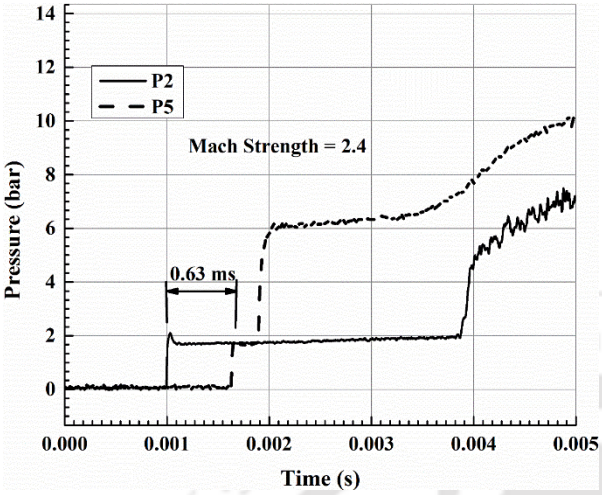

Figure 6.6: Time history of pressure traces obtained from sensors A and B

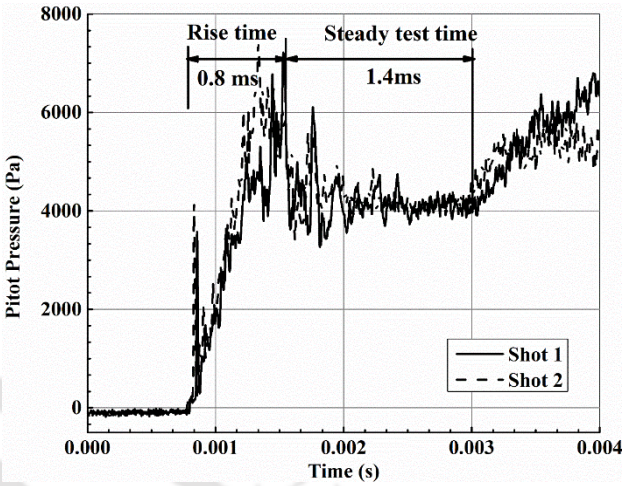

Figure 6.7: Time history of Pitot pressure recorded in test section

Table 6.1: Free stream conditions used for the shock tunnel tests for Mach 8 flow.

Driver Gas	Nitrogen (N_2)
Test Gas	Air (γ=1.4)
Reservoir / Driver Gas Pressure (P_4)	(2.6 M Pa)
Driven section pressure (P_1)	(33.86 k Pa)
Free stream pressure (P_∞)	(65 bar)
Primary Diaphragm thickness (t_d)	$(1.2$ mm$)$
The Mach Strength (MS)	2.14
Tunnel Vacuum level	1×10^{-3} m.bar
Stagnation pressure (P_0)	629 k Pa
Stagnation temperature (T_0)	938 K
Stagnation Enthalpy (H_0)	0.95 M.J/ kg
Free stream Reynolds No (Re_∞)	$9.524\text{x}10^6$ m^{-1}

This accelerometer balance uses rubber bushes to provide free floating condition

during the experiments. Steel rings are used to fix the balance inside the test model. Both the steel rings have outer diameter (O.D) 50 mm with 12 mm width and 7 mm thickness. The rubber bushed mounted inside the steel ring have O.D 36 mm, thickness 11.75 mm and width 6 mm. Such model is fixed in the test section with the help of a sting arrangement to keep it stable. The accelerometers cables are sent through the sting so that it should not be affected by the flow. Nomenclature used in this chapter is given in Table 6.2.

Table 6. 2: Nomenclature used in figures of chapter-6

F.N A	Front normal accelerometer
A.N A	Aft normal accelerometer
R.A.F	Recovered axial force
R.N.F	Recovered normal force
F.N A-M	Front normal acceleration measured
A.N A-M	Aft normal acceleration measured

Table 6.3: Details of accelerometer used in the force balance.

S. No	Location	Serial No	Model No	Sensitivity ($mv/m/s^2$)
1	Axial accelerometer	122127	352C67	10.29
2	Front normal accelerometer	93832	352C67/010AC	10.05
3	Aft normal accelerometer	122128	352C67	10.21

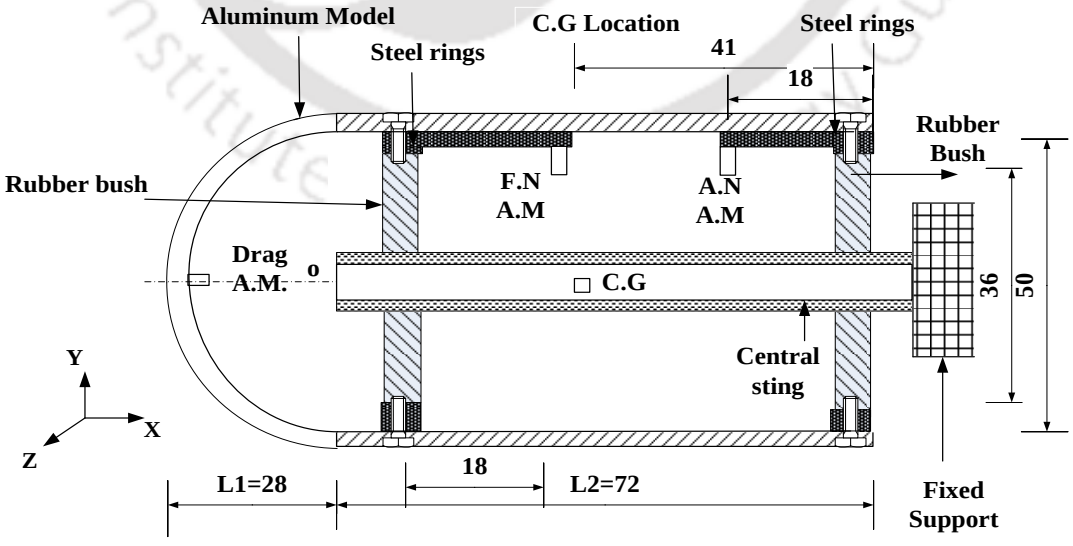

Figure 6.8: Schematic diagram of the test model integrated with the force balance.

6.5 Force Prediction Using Conventional Technique or Accelerometer Force Balance Theory

This section describes prediction of the forces based on the accelerometer force balance theory for the model tested for Mach 8 conditions in the shock tunnel. This method was earlier proposed by Vidal (1956) and then was used by Reddy et al (1986). This technique is useful for the calculation of the axial force and the normal force using the measured acceleration of the hemispherical body which are evaluated as given below.

$$F_{Axial} = A(X) \times m \tag{6.1}$$

$$F_{Normal} = L_2 \times A_{y1} + L_1 \times A_{y2} \tag{6.2}$$

$$e = \frac{I \times (A_{y1} - A_{y2})}{m \times (L_2 \times A_{y1} + L_1 \times A_{y2})} \tag{6.3}$$

Here F_{Axial} symbolizes the axial force along the length of the body.

F_{Normal} Symbolizes the normal force perpendicular to the body.

m is the mass of the model and accelerometer balance assembly.

$A\,(X)$ is the steady state acceleration measured along the longitudinal axis of the body.

A_{y1} is the acceleration from the front normal accelerometer.

A_{y2} is the acceleration from the aft normal accelerometer.

L_1 is the distance from the C.G. location to the front normal accelerometer location.

L_2 is the distance from the C.G. location to the aft normal accelerometer location.

e is the center of pressure location of the model.

This method is also used for calculation of the forces and pitching moment coefficient for a three component accelerometer balance on a hemispherical body.

$$\text{Coefficient of Drag } C_d = \left(\frac{F_{Axial} \times \cos(\alpha) + F_{Normal} \times \sin(\alpha)}{q_\infty \times S} \right) \tag{6.4}$$

$$\text{Coefficient of Lift } C_l = \left(\frac{F_{Normal} \times \cos(\alpha) - F_{Axial} \times \sin(\alpha)}{q_\infty \times S} \right) \tag{6.5}$$

$$\text{Coefficient of Moment } C_m = \left(\frac{F_{Normal} \times (C.G + e)}{D_b \times q_\infty \times S} \right) \tag{6.6}$$

The Axial force and the normal force are measured from the measured accelerations; these are used for the calculation of the force and the moment coefficients.

α is the angle of attack of the body with the flow direction.

S is the surface area of the body exposed to the flow.

D_b is the base diameter of the hemisphere.

q_∞ is the free stream dynamic pressure calculated using the Eqn.6.7

$$q_\infty = \frac{\gamma}{2} \times p_\infty \times M_\infty^{\,2} \tag{6.7}$$

Here p_∞ is the free stream pressure, M_∞ is the free stream Mach number, γ represents specific heat ratio.

6.6 Force Balance Calibration Experiments

In the initial calibration procedure, center of gravity (C.G) of the model is determined which would be required to evaluate the forces and moment using conventional theory of multi component accelerometer force balance. The center of gravity of the model is measured using the nylon wire suspension method and is estimated to be at a distance of 60 mm from the tip. The model is suspended horizontally from a rigid stand with the help of a wire and the model is adjusted such that its axis is parallel to the ground. It has also been cross verified using the spirit level. The setup for the measurement of the C.G of the model is shown in Fig.6.9.

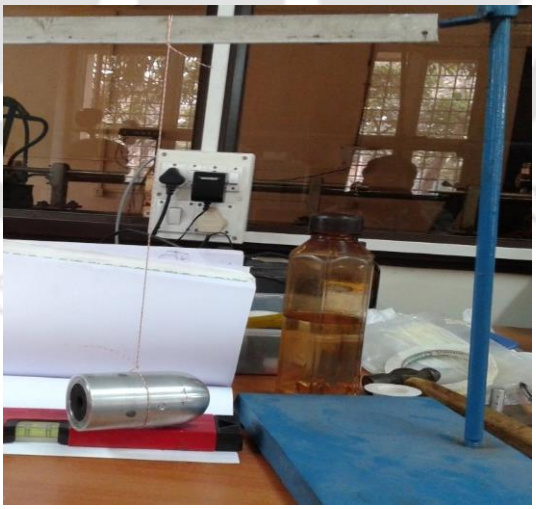

Figure 6.9: Setup for determination of center of gravity location of the model.

Force measurements using three component accelerometer force balance are reported in the literature. Since all those findings are based on the conventional theory of the accelerometer force balance. Hence initiatives are taken herein for calibration of the three component force balance using soft computing technique. These calibration

tests on the aluminum model are carried out using the impact hammer (PCB: Model no: 306C01). Three component accelerometer balance is fixed inside the model for measurement of accelerations during the calibration tests. The model has been applied with impulses at location 'P' on the spherical portion in a plane passing through its axis. The force applied location makes an inclination of 22^0 to the vertical axis. Schematic of the test model along with the specific force application locations are shown in Fig. 6.10. The loads are applied using the impact hammer at all the locations and care has been taken to apply the force along the local normal of the surface. This was ensured by putting the screw in the each of the hole during the application of the impulse force on the model. This model was fixed in a bench vice in the complete force balance calibration procedure. Force and acceleration signals are obtained in each experiment. Signals of one such experiment are used for training the soft computing algorithm as explained in earlier chapter. Thus trained methodology is initially used to recover the forces applied during the calibration experiments.

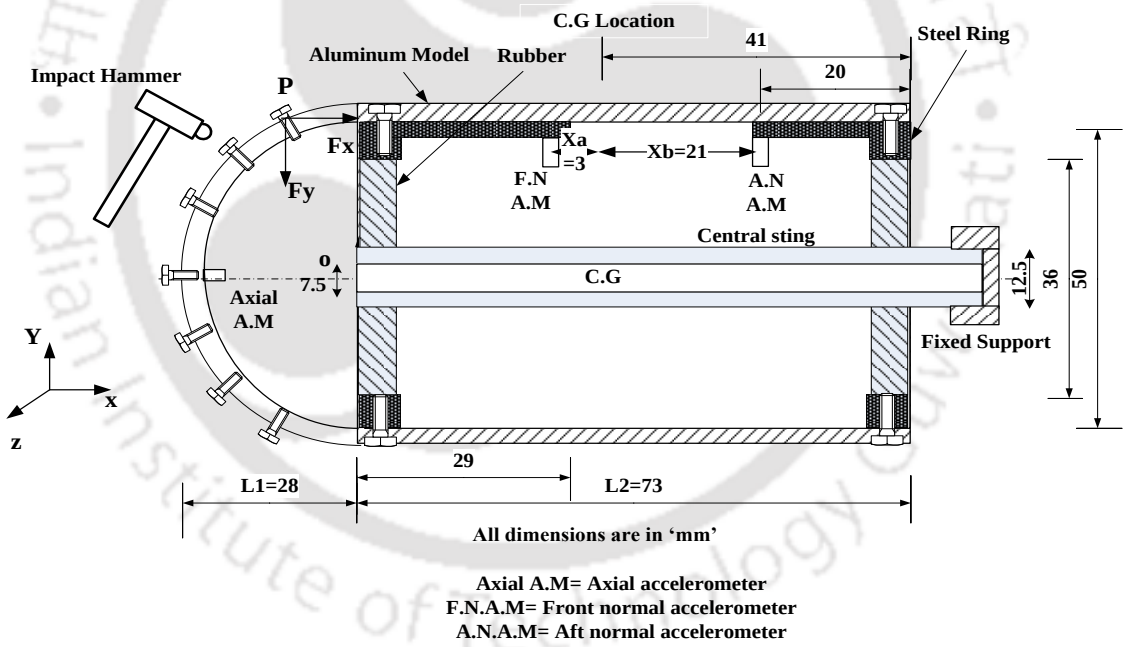

Figure 6.10: Schematic of the model for the experiment with the calibration load locations.

During the calibration the force is applied along the local normal of the body surface and the forces are resolved along and normal to the axis of the model which are termed as X and Y axes respectively. The pitching moment is also resolved according to the location of the C.G. The force histories along with the accelerometer responses are considered for the training of the ANFIS algorithm. This technique has also been found suitable for the accurate prediction of the three component simulated forces as discussed in Chapter 5 where the details of ANFIS parameters used for the analysis are also discussed. The same

optimized ANFIS network has been incorporated for force recovery in the present investigation. During the training of the ANFIS, the parameters used are axial acceleration, front normal acceleration and aft normal acceleration for input, forces and moments are considered as output. In this case hybrid type of training with 500 epochs is used for the training of the ANFIS structure. Gaussian type of input membership function and constant type of output membership function has been selected for the present analysis. Further unknown forces and moment are predicted from the acceleration responses using the trained structure of ANFIS. Force applied at an angle 22^0 from the axis of the model is used here for discussion of recovery of forces and moments. Figure 6.11 shows the applied axial component of an impulse force on the model and the recovered force using ANFIS which shows good accuracy of 91.35 % for prediction of the peak.

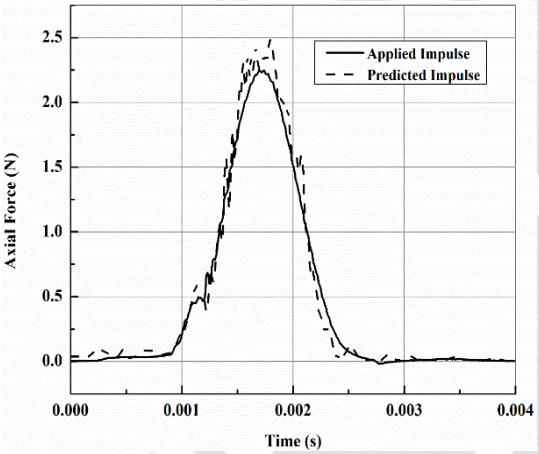

Figure 6.11: Comparison of the applied and recovered axial force applied during calibration experiments.

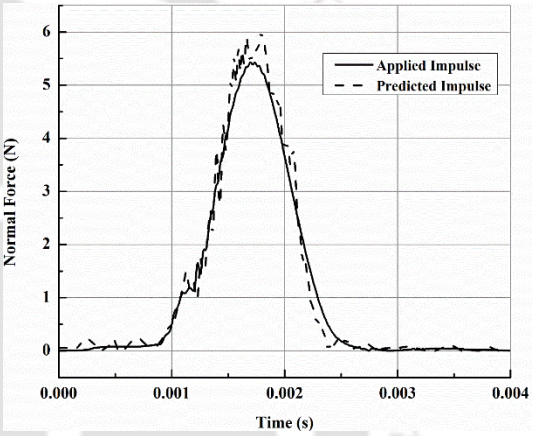

Figure 6.12: Comparison of the applied and recovered normal force applied during calibration experiments

However the trend or the history is seen to be correctly captured. The major error is due to the low magnitude and low frequency disturbance in the acceleration data used for the training and also for the testing. This shows the good agreement between the applied and the recovered force. The applied and recovered normal force during the calibration test at the same location on the hemispherical model is shown in Fig. 6.12.

It has also same accuracy as the axial force. The induced moment in the body due to the angle of incidence of the force was calculated from the components of forces along the X- and Y- directions about the center of gravity of the model. The moment obtained about Z-axis is plotted along with the predicted values from the ANFIS method of force prediction. The magnitude of the moment is very low value with a magnitude 0.1679 N-m shown in Fig. 6.13. The accuracy of the prediction in case of the

moment induced in the body is high compared to the axial and the normal force prediction on the same model.

6.7 Shock Tunnel Tests for Force Measurement

Shock tunnel tests are conducted for the same conditions which were considered for calibration of the tunnel and shown in Table 6.1. Test model equipped with the accelerometer force balance mounted in the test section is shown in Fig. 6.14. The model was tested using the two different angles of attack (AOA) viz. 0^0 and 15^0. The data acquisition system (DAQ) used is a high speed NI PCI-6115 S Series DAQ from National Instruments Inc.

It has interface with the computer and has the capability to acquire the data from the sensors with a sampling rate of 10 MS/s per single channel and 64 MB worth on board memory. The data acquired is converted from the analogue to the digital form through the ADC installed in the computer. Lab view-software is used for the data acquisition which is linked to the DAQ cards. Triggering is given from one of the sensors mounted in the shock tube (sensor A) which activates the DAQ for the response measurement. The accelerometers are connected to this DAQ through the signal conditioner for measurement of the acceleration obtained during the test. The acceleration history of the hemispherical model with 0^0 AOA is shown in Fig. 6.15.

The steady state acceleration magnitude over a time of 1.015 ms is considered for the drag acceleration which is observed as 12.14 m/s^2.The transient and steady state time span is close to that of pitot signal. The tests are also conducted for the 15^0AOA in the shock tunnel with the same free stream conditions as that of the 0^0 (Table: 6.1). In this case the model is fixed at 15^0 angle of attack to the flow. Therefore the model is subjected to the lift force and pitching moment along with the drag. These components are calculated using the responses obtained from three different accelerometers. Here the front normal accelerometer is located at distance of 3 mm from the C.G and the aft normal accelerometer is located at a distance of the 21 mm from the C.G. Figure 6.16 shows the drag acceleration of the model with 15^0 AOA.

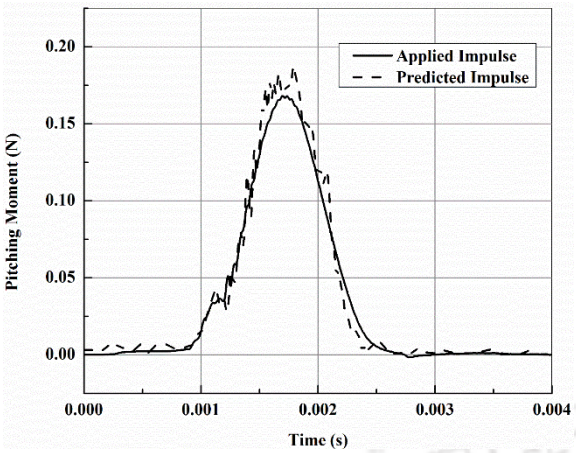

Figure 6.13: Comparison of the applied and recovered moment applied during calibration experiments.

Figure 6.14: Photograph of the model mounted in the test section of the shock tunnel for force measurement.

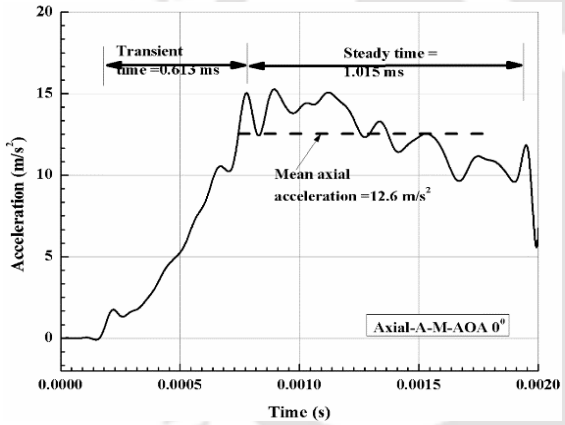

Figure 6.15: Axial Acceleration history for 0^0 AOA.

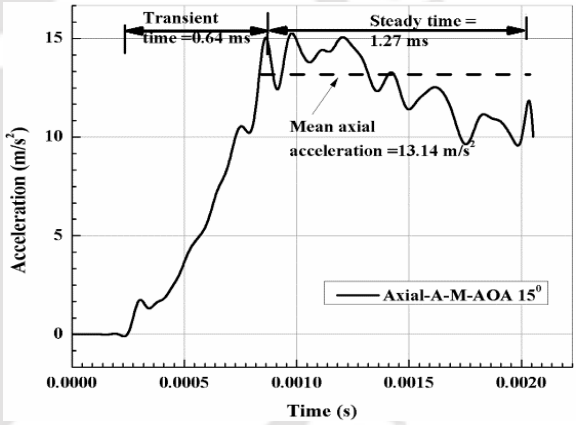

Figure 6.16: Axial Acceleration history for 15^0 AOA.

The steady state drag acceleration magnitude increased with the increase in the AOA which can be clearly seen from the figure. The front lift acceleration for 15^0 AOA is shown in Fig.6.17 which indicates transient time of 0.772 ms followed by steady state time of 1.44 ms. The average acceleration of the steady test time is found to be 11.32 m/s^2.The average magnitude of the aft accelerometer along the normal direction of the body is measured as 10.2 m/s^2 shown in Fig.6.17. The consistency in the measurement of the accelerometer history was observed in the both front and aft normal accelerations during the repeatability test at same AOA.

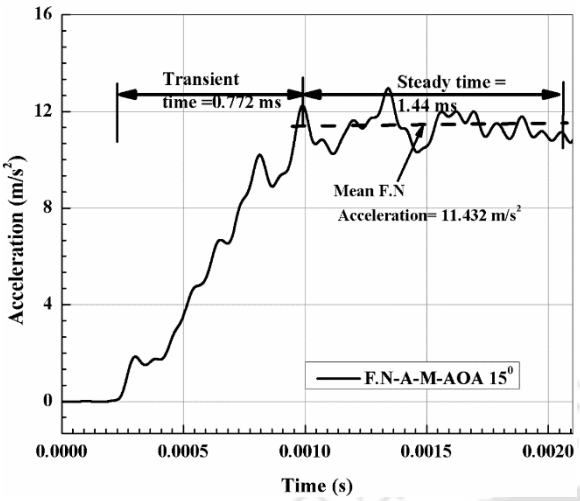

Figure 6.17: Normal acceleration from front normal accelerometer for 15^0 AOA.

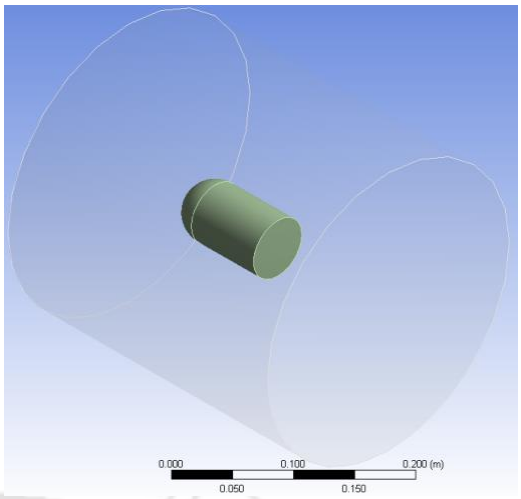

Figure 6.18: Fluid and solid domain of the CFD analysis.

6.8 Force Prediction Using CFD Analysis

CFD analysis has been performed on the hemispherical body using ANSYS Workbench and Fluent solver module. The surface pressure generated along with the force and moment by the fluid flow over the solid body coefficients is calculated. The hemispherical model dimensions are considered to be same as the experiment. The model is enclosed by a cylindrical shape fluid domain of 0.3m long and 0.28 m diameter. The hemispherical body with cylindrical portion of 0.056 m has been created and subtracted from the fluid domain to create the wall surface in the fluid domain for further analysis. Both the fluid and the solid domains are shown in the Fig 6.18. This whole domain is exported into the ICEM module for creating the structured meshing. Structured mashing has been created over the domain with elements size 0.005 mm using the blocking method. Fine meshing has been created around the wall for the clear visibility of shock, pressure and Mach contours during the simulation. The mesh created in the ICEM is saved as unstructured type and is exported into Fluent for the further analysis. The meshed model is shown in Fig. 6.19. The mesh specification considered for present CFD analysis after detailed mesh independence studies are given in Table 6.3. Experimental freestream conditions are specified at the inlet of the computational domain. Pressure outlet boundary condition has been considered for the outlet. Density based solver with AUSM (Advection Upstream

Splitting Method) is considered as the flux splitting scheme with first order accuracy for present Euler simulations.

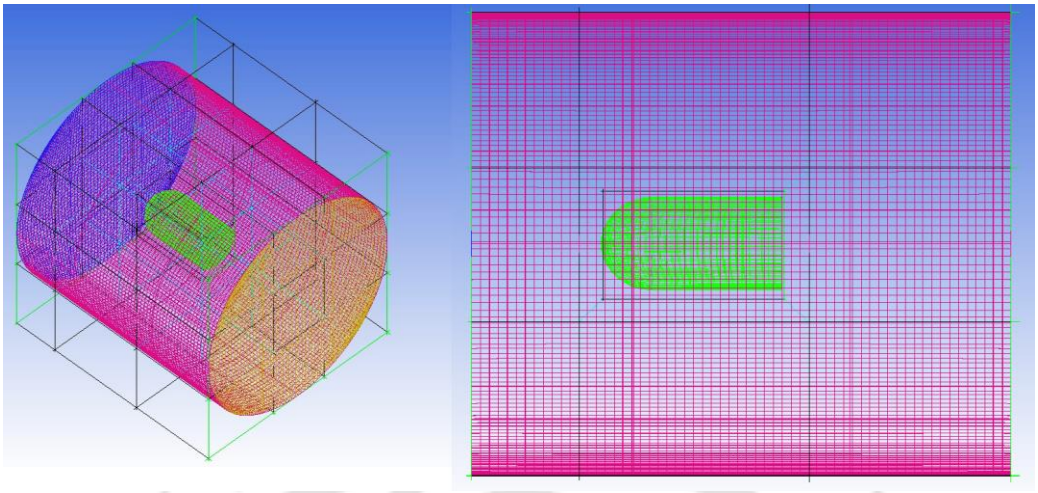

Figure 6.19: Meshed model of hemispherical body using ICEM.

6.9 Results and Discussion

6.9.1 Force prediction using the CFD

From the simulation static pressure, Mach number, drag coefficient, lift coefficient and moment coefficient are obtained. Typical pressure and Mach number contours are shown in Fig. 6.20 and Fig. 6.21 respectively. Forces and moments obtained from CFD analysis for 0^0 and 15^0 AOA conditions are given in Table 6.3 and Table 6.4 respectively.

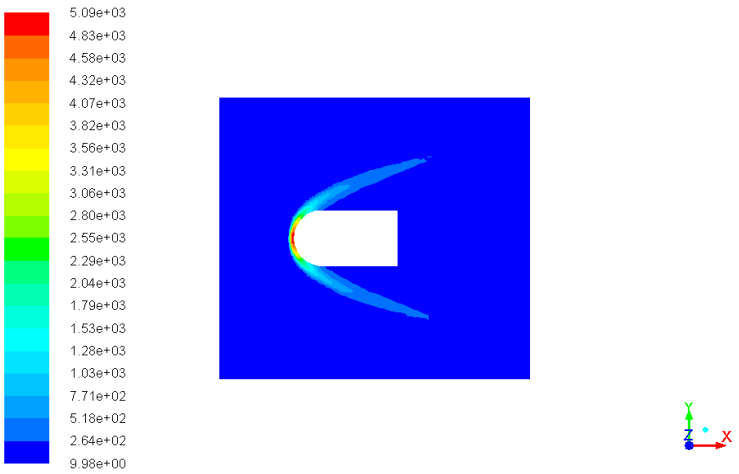

Figure 6.20: Pressure contour from CFD analysis for shock tunnel conditions for 0^0 AOA.

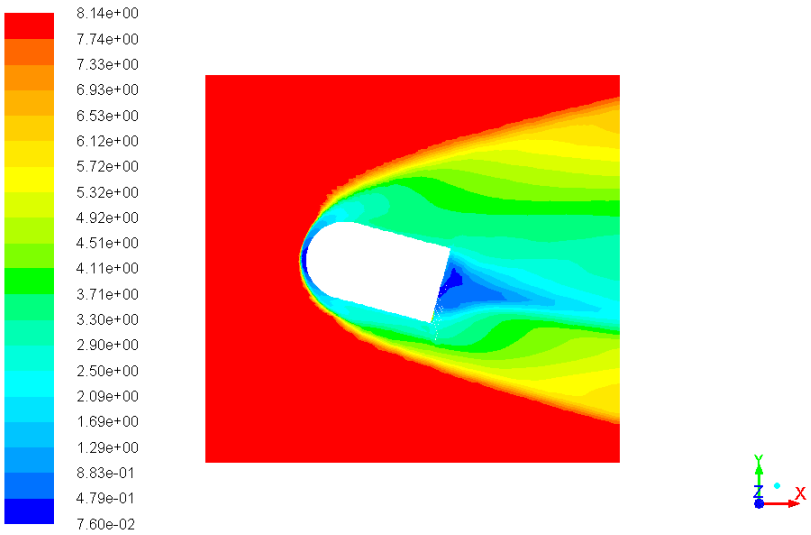

Figure 6.21: Mach number contour from CFD analysis for shock tunnel conditions for 15^0 AOA.

6.9.2 ANFIS based prediction

The soft computing technique, ANFIS, has also been used for prediction of the unknown force history. Figure 6.22 shows the axial force predicted for 0^0 AOA using ANFIS. It is clear from the figure that the force in the axial direction is having the magnitude of 3.446 which is nearly equal to the force predicted from the conventional method with the deviation of 12% (Table 6.4). Thus this method is able to recover the steady state experimental force with good accuracy from the measured acceleration during the experiment. On the other hand the conventional methods are useful only to predict the peak values of the forces and moments but not the time history of the force distribution over the body. At the same time, CFD predictions are very much high comparable to the conventional and soft computing techniques.

The predicted axial force for 15^0 AOA using ANFIS is shown in Fig.6.23. The increase in axial force with AOA is observed in the present figure. However the predicted axial force by this technique has deviation of 85% with respect to the conventional method. It is due to the higher angle of attack at which the conventional accelerometer force balance theory exhibits deviation as observed in the literature (Menezes et al. (2011)). The axial force predicted from the CFD shows the same trend as that of 0^0 and over predicts the axial force.

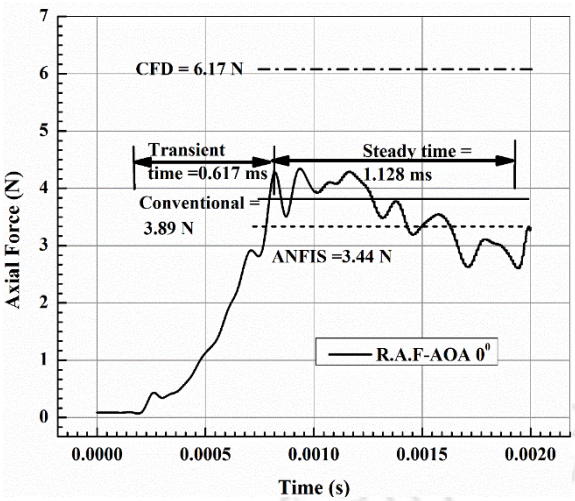

Figure 6.22: Axial force prediction for 0^0 AOA using ANFIS.

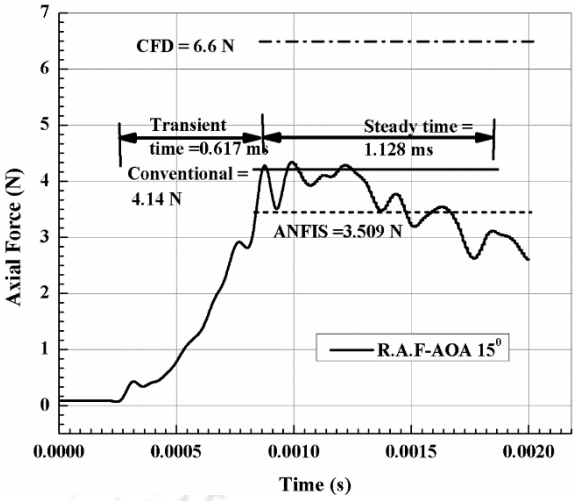

Figure 6.23: Axial force predicted for 15^0 AOA using ANFIS.

Figure 6.24 shows the predicted normal component of the experimental force for 15^0 AOA. The average experimental force predicted from the ANFIS technique is observed as 4.5N and the force predicted using the conventional techniques has a peak magnitude of 4.15 N. The prediction of the force shows the good agreement between the conventional and the ANFIS with the deviation of 16%. The aerodynamic coefficients obtained from various methods for this AOA case are compared in Table 6.5. Computational prediction using CFD always over predicts the experimental force and moment coefficients and it is consistent with the results obtained by Saravanan et al. (2009). Finally the predicted magnitudes of the force, moments, and also coefficients of drag, lift and the moment obtained from the three different methods are illustrated in the flowing table which gives the clear quantification of the parameters. These results showed the good performance of the ANFIS for better performance to predict the unknown force induced on the model during the shock tunnel tests.

Table 6.4: Table containing the axial and normal predicted forces using various techniques.

Angle of attack	Axial Force (A.F)			Normal Force (N.F)		
	Conventional	ANFIS	CFD	Conventional	ANFIS	CFD
0^0	3.93	3.44	6.13	0	0	0
15^0	4.134	4.683	6.625	3.456	4.683	1.03

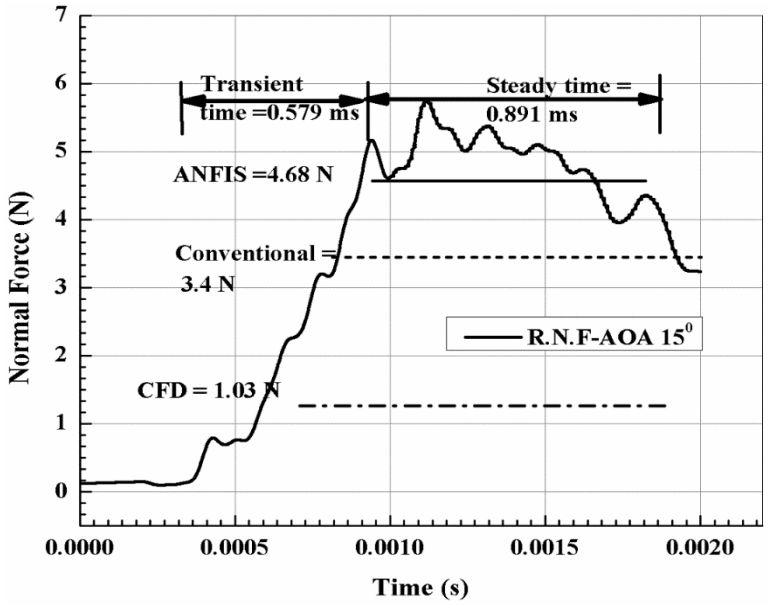

Figure 6.24: Normal predicted force for 15^0 AOA using ANFIS.

Table 6.5: Predicted force magnitude along with the force coefficient.

Method of prediction	Angle of attack (AOA)	Drag coefficient (C_d)	Lift coefficient (C_l)	Moment coefficient (C_m)
Conventional (Newtonian method)	0^0	0.5524	0	0
	15^0	0.6682	0.31	0.389
ANFIS	0^0	0.4550	0	0
	15^0	0.629	0.43	0.45
CFD	0^0	0.85	0	0
	15^0	0.91	0.138	0

6.10 Conclusions

The shock tunnel tests are successfully conducted on a hemispherical test model for force measurement using the three component accelerometer balance. Initial experiments in the tunnel are carried out for calibration of the tunnel which depicted the freestream conditions corresponding to Mach 8. The inbuilt force balance based model is calibrated for force measurement using impulse hammer. These calibration tests are found self-consistent. The soft computing technique ANFIS is used for the first time to recover the experimental force applied on the model during the shock tunnel test. These predictions are compared with the conventional or accelerometer force balance theory along with the CFD based predictions. Encouraging agreement has been observed for these predictions.

CHAPTER 7

CONCLUSIONS AND FUTURE RECOMMENDATIONS

7.1 Conclusions

The experiments for hypersonic flow regimes are of minute duration with complex nature therefore their analysis is a challenging task. The improvement of technologies and the efforts of various researchers have made it possible to achieve the hypersonic vehicle modeling and design with appropriate methods for the analysis. Measurement techniques for forces and moments in such facilities have also gained from this advancement. However, present investigations are centered on the need for development of non-intrusive technique for force measurement, use of computational tools for force balance design and development of soft computing based strategy and its implementation for force recovery. Therefore this chapter deals with the associated outcomes of the present findings.

7.1.1 General conclusions

1. Calibration test rig has been successfully developed for application of step load and impulse loads on a test model for implementation of single component accelerometer balance and stress wave force balance tests for small scaled blunt cone and hemispherical models.
2. One dimensional non-intrusive laser based calibration tests are conducted and it is found that velocity based force prediction is not able to exactly recover the applied impulse force well. However the indirect measurement of acceleration using laser vibrometer is able to correctly recover the applied impulse. Finite element analysis is also performed on the model for the evaluation of experiments.
3. Wheatstone bridge and amplifier circuit have been designed using semiconductor strain gauge and instrumentation amplifier. The fast Fourier transform (FFT) based convolution and de-convolution techniques are then implemented for establishing the transfer function and onwards force recovery. Excellent agreement has been noticed for recovery of single component force using accelerometer and stress wave force balance techniques.
4. Fluid structure interaction (FSI) analysis has been carried out on the advisory group for

aeronautical research and development (AGARD) model for finding the force coefficients and quantification of the accuracy of the computational techniques in comparison to the experimental techniques. The results showed that tests can be conducted within the test time of 1 ms, at higher angles of attacks also. However after the test time of 1.5 ms, the reaction of the rubber increase causing the decrease in the acceleration of the model due to non-validity of the free-flying condition.

5. The three dimensional finite element analysis has been carried out by using the hemispherical model (model -A) and AGARD model (model -B) at angle of attack 30^0 and the magnitudes of the force components are predicted using the soft computing techniques. Two different soft computing techniques such as neural networks (NN) and artificial neuro fuzzy inference system (ANFIS) are used for the recovery of the forces and moments of the model under the Mach 8 flow condition.

6. Finally all the efforts are taken to use the hemispherical model with three component accelerometer force balance for the force measurement in the shock tunnel facility at Indian Institute of Technology Bombay, India. Nitrogen is used as driver gas and air is used as the test gas with test condition of Mach 8. The force induced during the test are analysed from the accelerometer balance. Calibration tests are also conducted for finding the system response for various magnitudes of impulse forces.

7. These calibration data along with the response from the accelerometers are used for the prediction of the experimental forces using ANFIS and it is observed that these techniques are well suited and very much useful for the prediction of the experimental forces and moments with high accuracy.

The specific conclusions drawn from this work that are mentioned below.

7.1.2 Specific conclusions

(a) One dimensional calibration tests

- From single component non-intrusive force measurement method, it is concluded that the laser vibrometer can be used for conducting the short duration force measurement. As this is non-intrusive or non-contact type it can be used in remote location and hazardous environment not-suitable for human beings.
- It has also been observed that the laser based force measurement technique is almost accurate in comparison with the established accelerometer force balance technique for

the impulse loading condition. It is also observed that the experimental and finite element simulations are in well agreement with each other.

- The stress wave force balance technique has been used for establishing the step load calibration technique and the standardization of the method has been performed using the accelerometer force balance technique.
- The laser based force measurement technique using step load was established for short duration. It is found that the accuracy of the force prediction using the laser based method is having the higher accuracy in case of impulse load compared to the step load.

(b) Three dimensional FSI analysis

- One way fluid structure interaction has been performed on AGARD model with three component accelerometer balance and it has been concluded that with increase in angle of attack of the model the properties of the rubber are affected and loses linearity property. Which finally leads to the increase in the resistance of the rubber and the reaction force magnitude for 2 ms test time are below 5% and the moment reaction is found to be higher in case of 12^0 angle of attack (AOA) which is 10%.
- It is also concluded that the rubber material with the 0.3 MPa has given the reaction force of low value and the acceleration in this case is slightly higher than the experiment. However the magnitude of the reaction force increases with the AOA and also the stiffness of the rubber offers resistance to the free flying motion.
- The location of the accelerometer for a slender body for higher angles of attack is preferable to place at the nose location of the body. However for the normal acceleration measurement the location can be chosen at the center of gravity location (C.G) or at equal distances from the C.G for calculating the moments.
- It is also concluded that the FSI is very much useful for the design of the force balance for impulse facilities to predict the force and moment coefficients nearly same as that of actual coefficients from the literature.

(c) Three dimensional finite element analysis and soft computing technique

- Three dimensional finite element analysis has been carried out on a hemispherical model and AGARD model with L/D ratio of 4.44, outer diameter 51 mm and 226 mm length. Forces of different magnitudes are applied at 30^0 AOA to the axis of the model

and a new soft computing methodology viz. NN and ANFIS based soft computing techniques are used for force prediction for the first time for impulse facilities.

- An optimum ANFIS model with two membership functions was implemented successfully for the prediction of unknown three dimensional force using the acceleration history obtained from the simulation.
- Three kinds of short duration of forces such as impulse, ramp and hat were used in the present analysis. Accurate recovery of all the three forces with optimized ANFIS structure has been obtained while training with the impulse force due to its universal approximation capability.
- Highest accuracy obtained in case of hemispherical model is 99.09 % for the recovery of ramp force of 20 N viz. However the minimum accuracy was found to be 91.74 % while recovering moment induced due to 30 N impulse force.
- The maximum accuracy in case of Model B is 99.56 % while prediction of X-component of 20 N hat and ramp force and minimum accuracy of 92.48 % while recovering the Z-component of moment for 30 N ramp and hat forces. It depends on the magnitude of the applied load.

(d) Shock tunnel test using three component accelerometer force balance

- The soft computing techniques such as neural network and ANFIS method can be used for the experimental force prediction, it has been implemented for the first time for the impulse experimental force prediction.
- A three component of accelerometer balance has been designed and fabricated to be used for force measurement on a hemispherical body under hypersonic flow of Mach 8. The accelerometer balance was calibrated using the impact hammer to find out the response of the system to the applied forces with help of the training of the neural network.
- It has been concluded that the shock tunnel performance was good for the force measurement and the tests conducted were having the same free stream conditions as set which are seen clearly from the pitot tests.
- The shock tunnel tests are conducted on the hemispherical model with 0^0, 15^0 angle of attack respectively. It is derived from the experimental acceleration history that with increase in the angle of attack the drag force increase and also the lift component adds to

the model since at angle of attacks the two components of forces acts on the model resulting drag and lift.

- Three dimensional force coefficients are analyzed using CFD, Newtonian theory (conventional method) and soft computing techniques. It is concluded that the CFD predictions in case of the drag coefficient are over predictive in nature because of the inviscid assumption which is observed from the results and also the lift components are under predictive.
- From the above results it is resolved that the ANFIS optimized modal is able to predicted with highest accuracy of 98.8 % for drag coefficient and the minimum accuracy of the 64 % in case of the lift coefficient.
- However, the average recovered shock tunnel experimental force is very much accurate using ANFIS method of prediction which was not done by any other prediction method for the impulse facilities so far.

7.2 Future Recommendations

Some of the improvements in the design of the calibration methods for the betterment of the accuracy of the force prediction are carried out using the non-intrusive type of force measurement and also by using the soft computing techniques. However there is lot of scope for further improvement in the hypersonic short duration test facilities some of which are listed below.

- Use of non-intrusive laser based force measurement techniques has been demonstrated for only single component force balance. Hence demonstration of the same for multi-component force balance needs to be evolved.
- The calibration of three component accelerometer balance based force measurement can be extended to the six component force balance.
- The stress wave force balance has been used for the single component force measurement in present studies. However the use of computational tools for design of multi-component stress wave force balance can be demonstrated.
- The one way FSI analysis has been carried out for the axisymmetric standard body and can be extended to two way FSI method which is more accurate.
- Laser based force measurements can also be compared with the piezofilm based strain measurement for step and impulse loads.

- ANFIS based force recovery strategy should be evolved for six component of force balance system.
- Applicability of such method can be tested in shock tunnel experiments.

REFERENCES

Abdel-Jawad, M. M., Mee, D. J., and Morgan, R. G. (2007). New calibration technique for multiple-component stress wave force balances. *Review of Scientific Instruments*, 78(6): 065101:1-7.

Abramchuk, G. A., Alekhin, V. A., Vashchenko, A. P., Sandulova, A. V., and Stepanov, G. V. (1977). Characteristics of semiconductor strain gauge resistors in elastic waves. *Strength of Materials*, 9(6): 771-773.

Anderson, J. D. (2005). Introduction to flight. Fifth edition, *McGraw-Hill*, Boston.

Anderson, K. F. (1997). The new current loop: NASA's successor to the Wheatstone bridge. *ISA Transactions*, 36(4): 351-356.

Azari, A., Poursina, M., and Poursina, D. (2014). Radial forging force prediction through MR, ANN, and ANFIS models. *Neural Computing & Applications*, 25(3-4): 849-858.

Beck, W. H., Eitelberg, G., Mclntyre, T. J., Baird, J. P., Lacey, J., and Simon, H. (1991). The High Enthalpy Shock Tunnel in Gottingen (HEG). *Proceedings of 18th International Symposium on Shock Waves*, Sendai, Japan: 677-683.

Benedetti, M., Bortoluzzi, D., Baglivo, L., and Vitale, S. (2011). An optimal two-input approach for impulse measurements in the nano N.s range produced by contact forces. *Mechanical Systems and Signal Processing*, 25: 1646-1660.

Bray, K. N. C. (1961). Evaluation of the hypersonic gun tunnel. *Proceedings of the ARS International Hypersonic Conference*.

Cappa, P. (1990). Limits of stability of microcomputer-controlled scanning systems for strain-gage data readings. *Experimental Mechanics*, 30(3): 300-302.

Carbonara, M. (1993). Aerodynamic force measurements in the VKI Longshot hypersonic facility, new trends in instrumentation for hypersonic research. *Ed. A. Boutier, NATO ASI Ser. E*, 224: 317–325.

Cayley, G. (1810). On aerial navigation. *William Nicholson.*

Chabannes, V., Pena, G., and Prudhomme, C. (2013). High-order fluid–structure interaction in 2D and 3D application to blood flow in arteries. *Journal of Computational and Applied Mathematics*, 246: 1-9.

Chen, Z., Khurgin, J., Rodriguez, P., Lorenzo, J., Trivedi, S., Jin, F. and Habersat, J.(2007). Absolute surface displacement measurement using pulsed photo electromotive-force laser vibrometer. *Conference on Lasers and Electro-Optics, 2007 (CLEO 2007), May, 6-11, 2007, Optical Society of America.*

Cus, F., Zuperl, U., Milfelner, M., and Mursec, B. (2006). An adaptive neuro-fuzzy inference system for modeling of end-milling. *Report Submitted to Production Engineering Institute, Mechanical Engineering University of Maribor, Maribor, Slovenia.*

Daniel, W.J.T., and Mee, D.J. (1995). Finite element modelling of a three-component force balance for hypersonic flows. *Computers and Structures*, 54(1): 35-48.

Dem'yan, M. L., Luchko, I. I., and Varshava, S. S. (2000). New types of resistance strain gauges made of semiconductor whiskers. *Materials Science*, 36(6): 910-915.

Espinosa, H.D., and Lee, S. (2006). A novel fluid structure interaction experiment to investigate deformation of structural elements subjected to impulsive loading. *Experimental Mechanics*, 46(6): 805-824.

Garelli, L., Paz, R.R., and Storti, M.A. (2010). Fluid–structure interaction study of the start-up of a rocket engine nozzle. *Computers and Fluids*, 39(7): 1208-1218.

Gerdroodbary, M.B., and Hosseinalipour, S.M. (2010). Numerical simulation of hypersonic flow over highly blunted cones with spike. *Acta Astronautica*, 67(1): 180-193.

Gregory, O. J., and Luo, Q. (2001). A self-compensated ceramic strain gage for use at elevated temperatures. *Sensors and Actuators A: Physical*, 88(3): 234-240.

Hannemann, K., Schramm, J. M., Laurence, S., and Karl, S. (2015). Shock tunnel free flight force measurements using a complex model configuration. *20th AIAA International Space Planes and Hypersonic Systems and Technologies Conference (Hypersonics 2015), 6 - 9 July 2015, Strathclyde University, Glasgow, Scotland.*

Holden, M.S. (1985). Experimental studies of the effects of axi-symmetric transition on the aerothermal characteristics of hypersonic blunted slender cones. *Proceedings of AIAA 23rd Aerospace Sciences Meeting, 5*, 0325.

Hornung, H., Sturtevant, B., B61anger, J., Sanderson, S., Brouillette, M., and Jenkins, M. (1991). Performance data for the new free piston shock tunnel T5 at GALCIT, *Proceedings of 18th International Symposium on Shock Waves*, Sendai, Japan: 603-610.

Itoh, K., Komuro, T., Sato, K., Tanno, H., and Ueda, S. (2001). Hypersonic aerodynamic research of HOPE using high enthalpy shock tunnel. *Proceedings Of 10th AIAA/NAL-NASDA-ISAS International Space Planes and Hypersonic Systems and Technologies Conference.*

Jang, J. S. R. (1993). ANFIS: adaptive-network-based fuzzy inference system. *Systems, Man and Cybernetics, IEEE Transactions*, 23(3): 665-685.

Jessen, C., and Grönig, H. (1989). A new principle for a short-duration six component balance. *Experiments in Fluids*, 8: 231-233.

Joarder, R., and Jagadeesh, G. (2004). A new free floating accelerometer balance system for force measurements in shock tunnels. *Shock Waves*, 13: 409–412.

Knapp, J., Altmann, E., Niemann, J., and Warner, K.D. (1998). Measurement of shock events by means of strain gauges and accelerometers. *Measurement*, 24(2): 87-96.

Kozub, Y. I., and Tinyakov, V. G. (1970). The use of semiconductor transducers for measuring deformations. *Strength of Materials*, 2(5): 490-492.

Kroyer, R. (2003). FSI analysis in supersonic fluid flow. *Computers and Structures,* 81(8): 755-764.

Kulite Semiconductor strain gage Manual, (2001). Kulite Semiconductor Products. Inc., One Willow Tree Road, Leonia, New Jersey, 7605.

Laurence, S.J., and Sebastian K. (2010). An improved visualization-based force-measurement technique for short-duration hypersonic facilities. *Experiments in Fluids* 48(6): 949-965.

Laurence, S., Schramm, J. M., and Hannemann, K. (2012). Force and moment measurements on a free-flying capsule model in a high-enthalpy shock tunnel. *28th Aerodynamic Measurement Technology, Ground Testing, and Flight Testing Conference* New Orleans, Louisiana.

Liu, Z.G., Liu, Y., and Lu, J. (2012). Numerical simulation of the fluid–structure interaction for an elastic cylinder subjected to tubular fluid flow. *Computers and Fluids,* 68: 192-202.

Loganathan, C., and Girija, K.V. (2013). Hybrid learning for adaptive neuro fuzzy inference system. *Research Inventy: International Journal of Engineering and Science,* 2(11): 06-13.

Lukasiewicz, J., Whitfield, J. D., and Jackson, R. (1961). Aerodynamic testing at Mach numbers from 15 to 20. *ARS Progress in Astronautics and Rocketry: Hypersonic Flow Research,* 7: 473-511.

Lyon, R.L., and Zable, J.L. (1973). Impact force source and impact force calibrator. *Experimental Mechanics,* 13(6): 257-264.

Mee, D.J. (2003). Dynamic calibration of force balances for impulse hypersonic facilities. *Shock Waves* 12: 443–455.

Menezes, V., Trivedi, S., and Kumar, A. (2011). An accelerometer balance for the measurement of roll, lift and drag on a lifting model in a shock tunnel. *Measurement Science and Technology,* 22(6), 067003:1-5.

Michler, C., Hulshoff, S.J., Vanbrummelen, E.H., and Deborst, R. (2004). A monolithic approach to fluid–structure interaction. *Computers and Fluids*, 33(5): 839-848.

Naumann, K. W., Ende, H., and Mathieu, G. (1991). Technique for aerodynamic force measurement within milliseconds in shock tunnel. *Shock Waves*, 1(3): 223-232.

Naumann, K. W., Ende, H., Mathieu, G., and George, A. (1993). Millisecond aerodynamic force measurement with side-jet model in the ISL shock tunnel. *AIAA*, 31(6): 1068-1074.

Nayak, K.C., Tripathy, R.K., Panda, S.R., and Sahoo, S.N. (2014). Prediction of cutting and feed forces for conventional milling process using adaptive neuro fuzzy inference system (ANFIS). *IAES International Journal of Artificial Intelligence* (IJ-AI), 3(1): 24-35.

Nilifard, R., and Ahmadikia, H. (2010). Supersonic flow over blunt body using direct simulation Monte Carlo method and Navier-Stokes equation. *Advanced Theory of Applied Mechanics*, 3(2): 75-87.

Odeen, S., and Lundberg, B. (1990). Prediction of impact force by impulse response method. *International Journal of Impact Engineering*, 11(2): 149-158.

Panda, S.S., Chakraborty, D., and Pal, S.K. (2008). Flank wear prediction in drilling using back propagation neural network and radial basis function network. *Applied Soft Computing*, 8(2): 858-871.

Porter, L. M., Paull, A., Mee, D. J., and Simmons, J. M. (1994). Shock tunnel measurements of hypervelocity blunted cone drag. *AIAA*, 32(12): 2476-2477.

Pratihar, D. K. (2007). Soft computing. Narosa Publishing House, Ltd.

Rapuc, M. (1993). Hermes measurement needs in hot facilities. In New Trends in Instrumentation for Hypersonic Research. *NATO ASI Series, Springer*, 224: 11-23.

Rath, S., Singh, A.P., Bhaskar, U., Krishna, B., Santra, BK., Rai, D., and Neogi, N. (2010). Artificial neural network modeling for prediction of roll force during plate rolling process. *Materials and Manufacturing Processes*, 25: 149-153.

Rizal, M., Ghani, J.A., Nuawi, M.Z., and Haron, C.H.C. (2013). Online tool wear prediction system in the turning process using an adaptive neuro-fuzzy inference system. *Applied Soft Computing*, 13(4): 1960-1968.

Robinson, M. J., Schramm, J. M., and Hannemann, K. (2011). Design and implementation of an internal stress wave force balance in a shock tunnel. *CEAS Space Journal*, 1: 45-57.

Robinson, M.J., Mee, D.J. and Paull, A. (2006). Scramjet lift, thrust and pitching moment characteristics measured in a shock tunnel, *Journal of Propulsion and Power*, 22(1): 85-95.

Robinson, M.J., Mee, D.J., Tsai, C.Y., and Bakos, R.J. (2004). Three-component force measurements on a large scramjet in a shock tunnel, *Journal of Spacecraft and Rockets*, 41(3): 416–425.

Roveda, R. (2009). Benchmark CFD study of spiked blunt body configurations. *AIAA* , 367.

Roychowdhury, A. P., Unnikrishnan, C., and Aerodynamics, R. D. (2013). Numerical simulation of hypersonic flow over blunt bodies, *IJIRSET*, 2(5): 1-10.

Sahoo, N., and Reddy, K.P.J. (2010). Force measurement techniques for hypersonic flows in shock tunnels. *International Journal of Hypersonics*, 1(1): 31-58.

Sahoo, N., Mahapatra, D. R., Jagadeesh, G., Gopalakrishnan, S., and Reddy, K. P. J. (2003). An accelerometer balance system for measurement of aerodynamic force coefficients over blunt bodies in a hypersonic shock tunnel. *Measurement Science and Technology*, 14(3): 260.

Sahoo, N., Mahapatra, D. R., Jagadeesh, G., Gopalakrishnan, S., and Reddy, K. P. J. (2007). Design and analysis of a flat accelerometer-based force balance system for

shock tunnel testing. *Measurement*, 40(1): 93-106.

Sahoo, N., Suryavamshi K, Reddy K.P.J. and Mee D.J. (2005). Dynamic force balances for short duration hypersonic testing facilities, *Experiments in Fluids*, 38: 606–614.

Saravanan, S., Jagadeesh, G., and Reddy, K.P.J. (2009). Aerodynamic force measurement using 3- component accelerometer force balance system in a hypersonic shock tunnel. *Shock Waves*, 18: 425-435.

Silton, S. I. (2011). Navier-Stokes Predictions of Aerodynamic Coefficients and Dynamic Derivatives of a 0.50-cal Projectile. *Proceedings of 29th Applied Aerodynamics Conference, AIAA*, Reston, VA, 3030.

Simmons, J. M., and Sanderson, S. R. (1991). Drag balance for hypervelocity impulse facilities. *AIAA*, 29(12): 2185-2191.

Smith, A.L., and Mee, D.J. (1996). Dynamic strain measurement using piezoelectric polymer film. *Journal of Strain Analysis for Engineering Design*, 31(6): 463–465.

Smith, A.L., Mee, D.J., Daniel, W.J.T., and Shimoda, T. (2001). Design, modelling and analysis of a six component force balance for hypervelocity wind tunnel testing. *Computers and Structures*, 79(11): 1077-1088.

Stalker, R. J. (1972). Development of a hypervelocity wind tunnel. *Aeronautical Journal*, 76(738): 374-384.

Stalker, R. J. (1988). Hypervelocity Aerodynamics in Australia. *Journal of the British Interplanetary Society*, 41: 611-618.

Stalker, R. J. (1989). Hypervelocity aerodynamics with chemical non-equilibrium. *Annual Review of Fluid Mechanics*, 21(1): 37-60.

Stalker, R.J., Paull, A., Mee, D.J., Morgan, R.G., and Jacobs, P.A. (2005). Scramjets and shock tunnels - The Queensland experience. *Progress in Aerospace Sciences*, 41: 471–513.

Storkmann, V., Olivier, H., and Gronig, H. (1998). Force measurement in hypersonic impulse facilities, *AIAA*, 36(3): 342–348.

Takeo, T., and Yoshinobu, K. (2004). Measurement of impulsive forces and crater formation in impulse discharge. *Journal of Material Processing Technology*, 149: 212-216.

Trivedi, S., and Menezes, V. (2011). A balance for measurement of yaw, lift and drag on a model in a hypersonic shock tunnel. *Proceedings of the World Congress on Engineering*, 3: 1-6.

Trivedi, S., and Menezes, V. (2012). Measurement of yaw, pitch and side-force on a lifting model in a hypersonic shock tunnel. *Measurement*, 45(7): 1755-1764.

Tuttle, S. L., and Simmons, J. M. (1992). Hypersonic drag measurements in free piston shock tunnels. *Proceedings of 11th Australasian Fluid Mechanics Conference*, Hobart.

Tuttle, S.L., Mee D.J., and Simmons, J.M. (1995). Drag measurement at Mach 5 using a stress wave force balance, *Experiments in Fluids*, 19(5): 336–341.

Vidal, R. J., 1956. Model instrumentation techniques for heat transfer and force measurements in a hypersonic shock tunnel. *Report submitted to Cornell aeronautical laboratory*, Report No. WADC TN: 56-315.

Wang, W. L., and Boyd, I. D. (2003). Hybrid DSMC-CFD simulations of hypersonic flow over sharp and blunted bodies. AIAA, 3644: 1-13.

Wang, Y.C., and Chen, Y.W. (2007). Application of piezoelectric PVDF film to the measurement of impulsive forces generated by cavitation bubble collapse near a solid boundary. *Experimental Thermal and Fluid Science*, 32: 403–414.

Wei, M., Bai, B., Sung, A.H., Liu, Q., Wang, J., and Cather, M.E. (2007). Predicting injection profiles using ANFIS. *Information Sciences*, 177(20): 4445-4461.

Yu, Li., Cheng, H., Zhan, Y. N., and Li, S. (2014). Study of parachute inflation process using fluid–structure interaction method. *Chinese Journal of Aeronautics*, 27(2): 272-279.

Yusaku, Fujii. (2009). Toward dynamic force calibration. *Measurement*, 42: 1039-1044.

Zadeh, L. A. (1998). Roles of soft computing and fuzzy logic in the conception, design and deployment of information/intelligent systems. *Computational Intelligence: Soft Computing and Fuzzy-Neuro Integration with Applications*, Springer Berlin Heidelberg, 1-9.

Zhang, J., Guo, L., Wu, H., Zhou, A., Hu, D., and Ren, J. (2014). The influence of wind shear on vibration of geometrically nonlinear wind turbine blade under fluid–structure interaction. *Ocean Engineering*, 84: 14-19.

Zhu, F., and Wu, Y. (2014). A rapid structural damage detection method using integrated ANFIS and interval modeling technique. *Applied Soft Computing*, 25: 473-484.

Zhu, H., Zhang, W., Feng, G., and Qi, X. (2014). Fluid–structure interaction computational analysis of flow field, shear stress distribution and deformation of three-limb pipe. *Engineering Failure Analysis*, 42: 252-262.

LIST OF PUBLICATIONS

Journal Papers

1. **Pallekonda Ramesh**, Divakar Bommana, Vinayak N. Kulkarni, N. Sahoo, and S. K. Dwivedy, Experimental assessment of non-contact type laser based force measurement technique for impulsive loading. International Journal of Structural Stability and Dynamics. Vol. 14, No. 4, 1450003(1-11), 2014.

2. **Pallekonda Ramesh**, Soumya R Nanda, Vinayak Kulkarni and Santosha Kumar Dwivedy, Design of artificial neuro-fuzzy inference system based methodology for prediction of short duration forces, Applied Soft Computing (Under Review).

3. **Pallekonda Ramesh**, Markhand Vyas, Vinayak Kulkarni and Santosha Kumar Dwivedy, Computational investigations for the design of multi component accelerometer force balances in hypersonic applications. (Under Preparation).

4. **Pallekonda Ramesh**, Kiran Joy Irimpan, Soumya R Nanda, Vinayak N. Kulkarni, Santosha K. Dwivedy, and Viren Menezes, Experimental and computational investigations of three component accelerometer balance with implementation of soft computing technique for force prediction. (Under Preparation).

Conference Papers

1. **Pallekonda Ramesh**, Vinayak Kulkarni, and S. K. Dwivedy, Calibration of single component accelerometer force balance and vibrometer balance using step load. ***29th*** International Symposium on Shock Waves, Madison, USA, July: 14-19, 2013.
2. **Pallekonda Ramesh**, Vinayak Kulkarni and S. K. Dwivedy, Design of various calibration methods for force measurement in impulse facilities, National Conference on Wind Tunnel Testing, Vikram Sarabhai Space Center, Thiruvananthapuram, August: 23-24, 2013.
3. **Pallekonda Ramesh**, Sreeja Bibin, Vinayak Kulkarni and S. K. Dwivedy, Computational methodology for design of accelerometer force balance, 3rd National Symposium on Shock Waves, IIT Bombay, India, February: 23-24, 2014.

4. **Pallekonda Ramesh,** Soumya R Nanda, Vinayak N. Kulkarni and S. K. Dwivedy, Fluid Structure Interaction (FSI) analysis of hypersonic cone with flare at different angles of attack and various Mach numbers. Presented at 12th International Conference on Vibration Problems (ICVOP-2015), IIT Guwahati, India, December: 14-17, 2015.

5. **Pallekonda Ramesh**, Vinayak N. Kulkarni, S. K. Dwivedy. Analysis of stress waves induce in brass rod under the impact loading condition. Accepted in the Fourth National Symposium on Shock Waves (NSSW-4), to be held in Karunya Insttute of Technology, Coimbatore, India, from February 25-26th 2016.